a Coriolis tutorial, Part 4:
wind-driven ocean circulation and the Sverdrup relation

James F. Price

Woods Hole Oceanographic Institution,
Woods Hole, Massachusetts, 02543
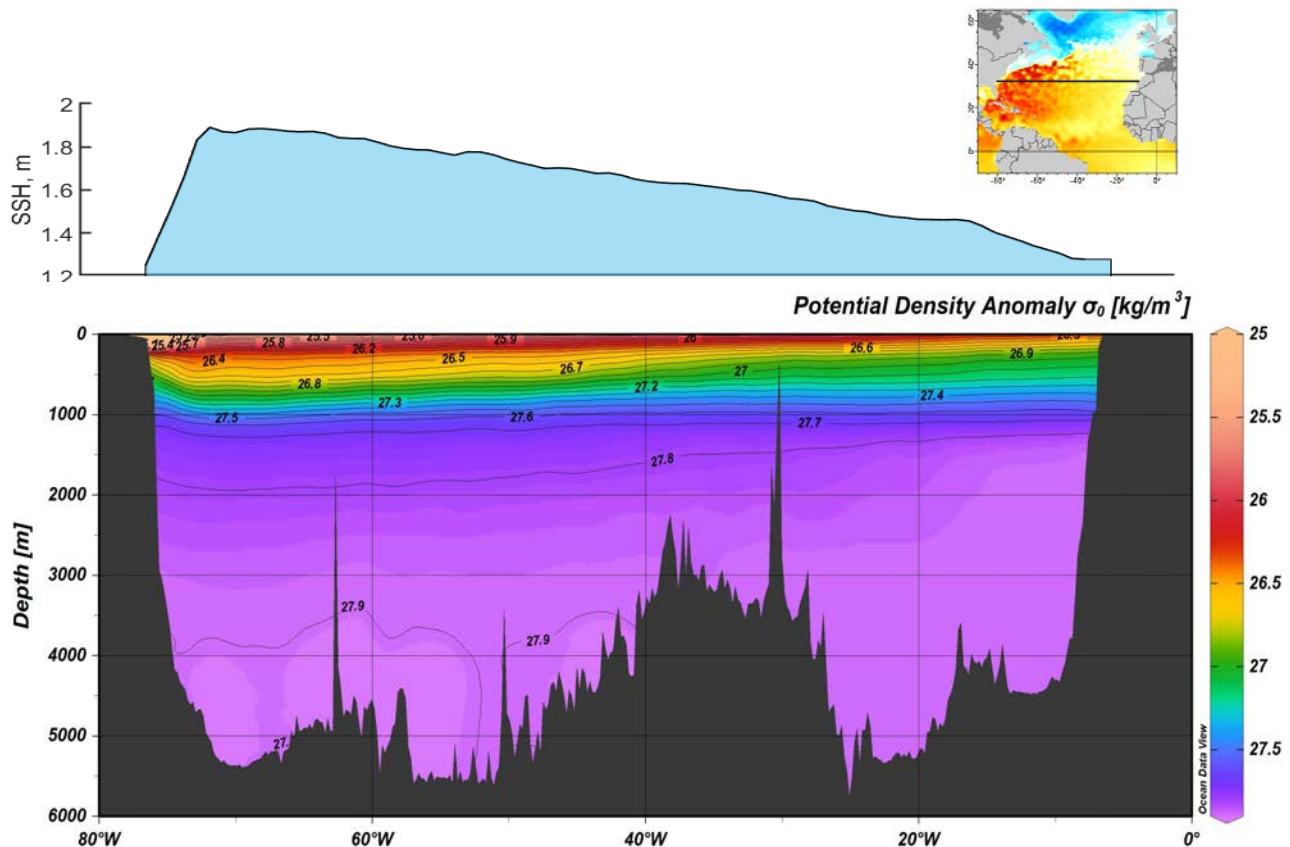https://www2.whoi.edu/staff/jprice/   jprice@whoi.edu

Figure 1: This section across the subtropical North Atlantic at 32 N shows the remarkable east-west asymmetry that is characteristic of wind-driven, upper ocean gyres. **(upper)** Sea surface height (SSH) from satellite altimetry, and **(lower)** potential density anomaly from *in situ* observations; both are averaged over several decades. Within a narrow western boundary region the SSH slope is positive and very large, and the inferred geostrophic current, the Gulf Stream, is northward and very fast. Over the interior of the basin, the SSH slope is negative and much smaller and the inferred geostrophic flow is southward and very slow. The associated baroclinic transport within the basin interior is consistent with the overlying, negative wind stress curl and the Sverdrup relation, a focus of this essay.

Abstract. This essay seeks to develop insight for several major features of the observed, upper ocean circulation, *e.g.,* western intensification of the major gyres and the geography of seasonal variability. A key element in this is understanding Sverdrup relation between meridional transport and the wind stress curl. To see how Sverdrup flow arises, shallow water models are solved for the circulation of a model ocean that is started from rest and driven by a specified wind stress: westerlies at mid-latitudes and easterlies in subpolar and tropical regions. This gives three regions of stress curl, negative over the subtropics, and positive over subpolar and tropical regions. The model used most extensively has just one active layer and makes the reduced gravity approximation. This is a minor extension of the model used in Parts 2 and 3 and is here dubbed 1l-rg. The dynamics of this model are baroclinic only. A second model includes three active layers, including a thick, active abyssal layer and a free sea surface and hence, 3l-fs. This more complete model includes the baroclinic dynamics of the 1l-rg model as well as fast, barotropic dynamics.

Baroclinic response in the 1l-rg solution. The developing baroclinic circulation can be described in terms of four stages. Stage 1 is the direct, local response to the imposed wind stress and includes inertia-gravity oscillations and Ekman transport within the upper, surface layer. The inertial-gravity oscillations die away after a couple of weeks with no evident lasting effect. The Ekman transport remains, and is very consequential for the long term ocean circulation. Ekman transport varies spatially on account of the latitudinal variation of wind stress and of the Coriolis parameter, f. The resulting divergence of Ekman transport modifies the thickness of the upper layer field and thus the mass field, the pressure field, and hence the circulation. Over the central subtropics, where wind stress curl is negative, the Ekman transport is convergent, which leads to a slowly thickening thermocline (about 30 meters per year in the central subtropics) and a high pressure in the upper ocean. This induces a nearly geostrophic zonal current which increases in step with the thickness field and dubbed the Stage 2 response. The amplitude is proportional to $1/f^2$ and so is much larger at lower latitudes. This local response to wind stress curl goes on for about three years (subtropical gyre) until the zonal thickness gradient balances the Ekman convergence and yields a steady state thickness and flow field. The circulation is then a baroclinic Sverdrup flow, dubbed Stage 3. The transition from Stage 2 to Stage 3 sweeps westward across the basin at the rate of a long baroclinic Rossby, $-\beta C^2/f^2 = -3$ km day^{-1} in the subtropics. Baroclinic Sverdrup flow thus occurs much sooner in the tropics (a few months) than in the subtropics (a few years) or the subpolar region (a few decades).

Even after the subtropical gyre reaches steady-state Sverdrup flow, the layer thickness continues to increase very slowly and uniformly (spatially) over the next several decades as the subtropical region absorbs water expelled from the subpolar region where the wind stress curl is positive and the upper layer becomes dramatically thinner. A basin-wide steady state, Stage 4, arises only after the subpolar gyre has also been swept by a slowly moving long baroclinic Rossby wave. Along the northern boundary of the 1l-rg model, that requires about 30 years.

The observed, basin-scale horizontal structure of the wind-driven ocean circulation, including western intensification and several of the qualitative differences between tropical, subtropical and subpolar gyres, have a plausible analog in solutions of the baroclinic shallow water model. In particular, the Sverdrup relation plus the observed pattern of wind stress curl provide a concise and convincing

explanation of the sense of the circulation over the North Atlantic: equatorward (southward) meridional flow in the subtropics of the North Atlantic, where the wind stress curl is negative, and the opposite signs in the tropical and subpolar regions. The Sverdrup relation is valid where the dominant terms of the potential vorticity balance are just two: the advection of planetary vorticity by a very slow meridional flow, and the curl of the wind stress. In practice, this holds in the interior of a basin, where the currents and friction are very weak, but not within zonal or meridional boundaries.

These experiments are carried out within a closed basin, and so the net transport through any given basin-wide zonal section must vanish in steady state. The meridional Sverdrup transport in the interior of the basin is balanced in this volumetric sense by a very intense western boundary current (wbc) having a width of order the baroclinic radius of deformation, O(100 km) in the subtropics. The baroclinic transport of a wbc reaches approximate steady state after the ocean interior to the east of the wbc has reached steady baroclinic Sverdrup flow, about three to five years in the subtropical gyre. The wbc thus follows the interior circulation, despite that it is far more energetic.

The meridional transport must vanish on zonal boundaries, and in the present model the affected zonal boundary regions are fairly wide, 500 - 1000 km in north-south extent. Within these wide zonal boundary regions, the meridional transport has the sign of the expected Sverdrup transport, but considerably reduced amplitude, going to zero on the boundary.

The annual cycle of wind stress is significant in most regions. To see the consequence, experiments are carried out with a zonal wind stress that includes a large, ±50%, annual cycle. The ocean's response is, in most respects, unimpressive, but this depends very much upon latitude. In the subtropical gyre, the resulting annual cycle of the baroclinic wbc transport is only about ±4% of the mean transport. The annual cycle of wbc transport is even smaller in the subpolar gyre, and somewhat greater though still not prominent in the tropical gyre. There is, however, an appreciable baroclinic response in the eastern half of the tropical gyre. There the annual cycle of upper ocean (baroclinic) zonal currents is about ±50% of the mean, or roughly proportional to the wind stress variation. This vigorous seasonal cycle of tropical zonal currents appears to be a mainly local response to the varying stress curl, here called the Stage 2 response, but includes a contribution from an annual period, eastern boundary Rossby wave as well.

A barotropic and then a baroclinic response, 3l-fs. What happens when the same start up experiment is carried out with the three layer, free surface model, 3l-fs? In one key respect the results are strikingly different from those described above — the circulation comes to a nearly steady, *barotropic* Sverdrup flow within just a few weeks, even at subpolar latitudes. The comparatively very short response time of the barotropic circulation is consistent with the very fast zonal propagation of barotropic long Rossby waves, about -1200 km day^{-1} at 30 N. The basin-scale pattern of the barotropic transport, including the western boundary currents and the zonal boundary regions, is very similar to that of the baroclinic Sverdrup flow found in the 1l-rg model solution. This barotropic Sverdrup transport is almost depth-independent (as barotropic usually implies) and occurs mainly within the thick abyssal layer. The amplitude of upper ocean currents and the associated SSH anomaly are thus quite small compared to the observed SSH.

Over the following several years a baroclinic adjustment occurs in the 3l-fs model solution in just the way it does in the 1l-rg solution. In the central subtropical gyre, a first mode, long baroclinic Rossby

wave arrives from the east after about three years. As it passes, the abyssal layer comes to rest, and the Sverdrup transport is thereafter confined to the two upper ocean layers, i.e., the Sverdrup transport is then baroclinic. After about another five years and the passage of a second mode wave, the Sverdrup transport is extinguished in the unforced, lower thermocline layer and thereafter is present only in the uppermost, wind-forced layer. The amplitude of the across-basin SSH anomaly is then fairly realistic, about 1 m across the subtropical gyre. This is more the result of a felicitous choice for the initial surface layer thickness, 250 m, than it is a genuine prediction of the vertical structure of the Sverdrup flow.

More on Fig. (1) These SSH data were processed and compiled thanks to the AVISO Project https://www.aviso.altimetry.fr and served by the NOAA ERDDAP web archive, https://coastwatch.pfeg.noaa.gov/erddap/griddap/, an invaluable source for a wide variety of oceanographic data. This is the AVISO Level 4 analysis, compiled from multiple satellite missions, and SSH is relative to a carefully mapped geoid. The lower panel is the grand average of potential density from *in situ* measurements extracted from the World Ocean Atlas 2018, http://www.nodc.noaa.gov/OC5/WOA18/pr_woa18.html. The very long-time averaging of these data has suppressed the large amplitude, time-dependent signal of mesoscale eddies that is very prominent in the synoptic data of, e.g., Fig.(1), Part 3. Notice that the tilt of the thermocline mirrors the tilt of SSH so that high SSH corresponds to a thick, low density upper layer. The result is a comparatively small horizontal gradient of hydrostatic pressure at depths below about 1200 m, which is suggestive of a reduced gravity approximation that will be utilized in many of the numerical experiments discussed here. This handsome presentation was made possible by Ocean Data View, https://odv.awi.de/

Contents

1 Earth's rotation has a profound influence on the large-scale, low frequency flows of the atmosphere and the ocean

This essay is the fourth in a five-part introduction to fluid dynamics on a rotating Earth. The broad goal of these essays is to help illuminate the effects of Earth's rotation, which include some of the most important and subtle phenomena of geophysical fluid dynamics. The first of these essays introduced the Coriolis force, the second examined geostrophic adjustment, and the third studied the phenomenon of westward propagation. These topics are about equally relevant for students of atmospheric and oceanic science.

1.1 The goal: Insight for the link between the winds and ocean circulation

The present essay continues this introduction to rotation effects, but now with a decidedly oceanic bent — large-scale, long-term mean upper ocean circulation — and especially the quasi-steady, horizontally rotating gyres that fill the subpolar and subtropical basins (Fig. 2). The broad goal is to learn how the upper ocean circulation is linked to the wind (Fig. 3) and the specific goal is to develop insight for four Observed properties:

O1: SSH anomaly of the gyres is correlated with the overlying wind stress curl,

O2: The gyres are strongly asymmetric east-to-west, implying a special direction,

O3: The subtropical and subpolar gyres are unresponsive to annually-varying wind, while the tropical ocean circulation varies significantly,

O4: The circulation of the subtropical gyre is somewhat surface intensified.

These are each elaborated and quantified in Sec. 2 by inspection of several kinds of remotely sensed data sets, especially SSH and wind stress and supplemented by some *in situ* and reanalysis data sets.
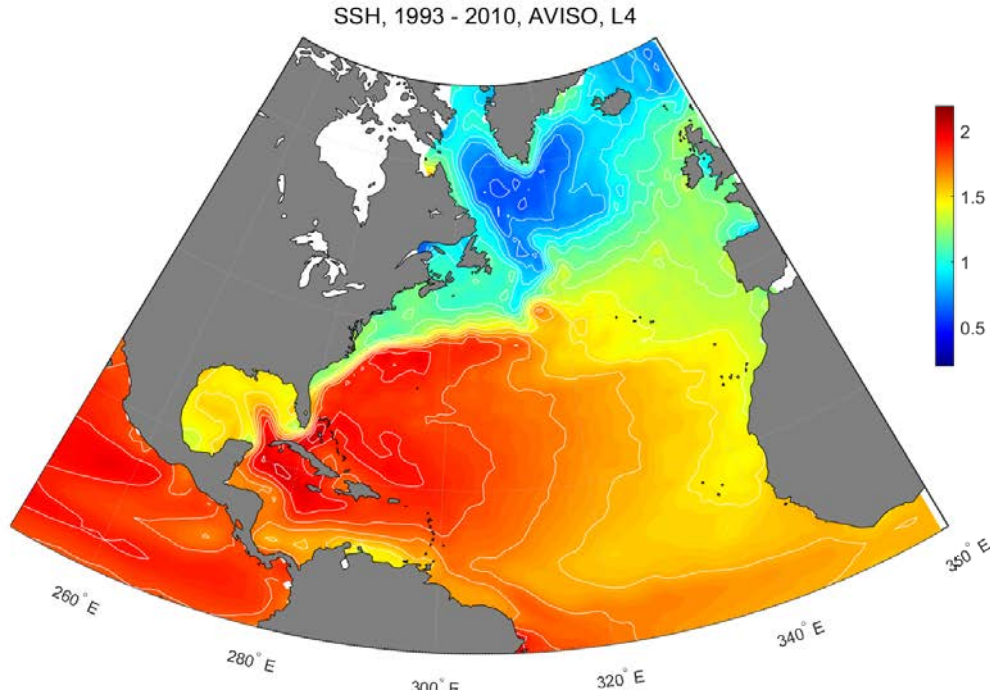
Figure 2: Sea surface height of the North Atlantic, averaged almost two decades of satellite altimetry compiled by the AVISO Project (this repeats Fig. 1 of Part 1). The color scale at right is in meters. Major features discussed here are an SSH high that fills the subtropical basin, and a SSH low in the subpolar basin. The inferred geostrophic current of the subtropical basin is a clock-wise turning gyre that is strongly asymmetric: very slow southward flow over most of the basin, and a fast north-northeastward flow in a very narrow western boundary current. The goal of this essay is to describe the connection between these circulation phenomena and the overlying wind stress. The centerpiece of this is the Sverdrup relation.

The conceptual centerpiece of this study is the **Sverdrup relation**,[1]

$$\int_{-d_o}^{0} v(z)\,dz \;=\; M^{Sv} \;\equiv\; \frac{1}{\rho_o \beta}\nabla\times\tau(x,y) \tag{1}$$

which is a highly distilled description of vorticity and volume conservation in a wind-driven ocean on a beta-plane. The left hand side is the meridional (north-south) component of volume transport per unit

---

[1]Sverdrup's pioneering paper that introduced the equivalent of Eqn. (1) is unfortunately not easily read or appreciated, but nevertheless: Sverdrup, H. U., 1947, 'Wind-driven currents in a baroclinic ocean, with application to the eastern Pacific', *Proc. Natl. Acad. Sci. U. S. A.*, **33**, 318-326, which is available online at http://www.pnas.org/content/33/11/318 The first model of a western-intensified, wind-driven gyre was by Stommel, H., 1948, and the time-dependent, gyre spin-up problem was discussed by Stommel, H., 1957, 'A survey of ocean current theory', *Deep Sea Res.*, **4**, 149-184. Be sure to see also Stommel's masterpiece, 'The Gulf Stream', 1966, Univ. of California Press. Time-dependence was treated in greater detail by Anderson, D. L. T. and Gill A. E., 1975, 'Spin-up of a stratified ocean with applications to upwelling', *Deep-Sea Research* **22**. The GFD texts noted in Part 1 each have very good discussion of the Sverdrup interior. Ch. 1 of Pedlosky, J.,1998, 'Ocean Circulation Theory', and Ch. 10 of Marshall, J. and R. A. Plumb, 2008, 'Atmosphere, Ocean and Climate Dynamics', and Ch. 14 of Vallis, G., 2006, 'Atmospheric and Oceanic Fluid Dynamics', are all highly recommended.

8

width and the righthand side is the curl of the wind stress, $\tau(x, y)$, a horizontal vector field that is here presumed to be known from observations (Fig. 3). The Sverdrup relation is one of the true bedrocks of ocean circulation theory; it has been repeatedly tested successfully against observations, and has been widely accepted for at least 50 years. The Sverdrup relation is also abstract to the point of being abstruse, and taken alone can not explain much of O1 - O4. For example, the Sverdrup relation is local in space (x, y) and so does not account for the striking asymmetry of the gyres (Fig. 1). The Sverdrup relation makes no reference to time or depth, and so neither can it explain O3 or O4.

1.2   Objectives and plan of this essay

The premise (and the promise) of this essay is that significant insight for the observations O1 - O4 will follow as we learn how the Sverdrup relation arises in a spin-up problem posed in a closed basin. A beta-plane approximation is used to represent the very important latitudinal variation of the Coriolis parameter, f. The objectives of this essay are then to:

  i) Solve for the stratification and currents from the start up to a steady state, and characterize the processes that shape the large scale response. The initial response to stress curl and the resulting divergence of Ekman transport is local, and includes a slow but steady increase of SSH over the subtropical gyre. The amplitude depend strongly upon latitude (relevant to O1).

  ii) Show that the low frequency beta effect eventually halts the local response, and the resulting steady state is then consistent with the Sverdrup relation. The time this takes varies greatly with latitude, being much faster at lower latitudes (relevant to O3).

  iii) Show that the Sverdrup relation holds over most of the interior of a model ocean basin and hence the sign of the wind stress curl determines the sense (clockwise or anti-clockwise) of wind-driven gyres (relevant to O1).

  iv) Observe that the Sverdrup relation necessarily fails near (most) solid boundaries and is supplanted by western or zonal boundary current dynamics (relevant to O2).

  v) Consider some of the processes that determine the depth of the upper ocean circulation, the d_o of Eqn. (1) (relevant to O4). Just to be clear at the outset, the depth of Sverdrup transport appears to be beyond the simple theory used here, but it is worthwhile to preview the issues involved in making a more complete theory/model.

    These are among the foundational problems of physical oceanography and have been addressed many times over, and from a variety of perspectives. This essay will work towards these objectives by an analysis of solutions from two shallow water (layered) models. The first model is familiar from Parts 2 and 3 — one active layer and pressure anomaly computed from the baroclinic density field assuming a
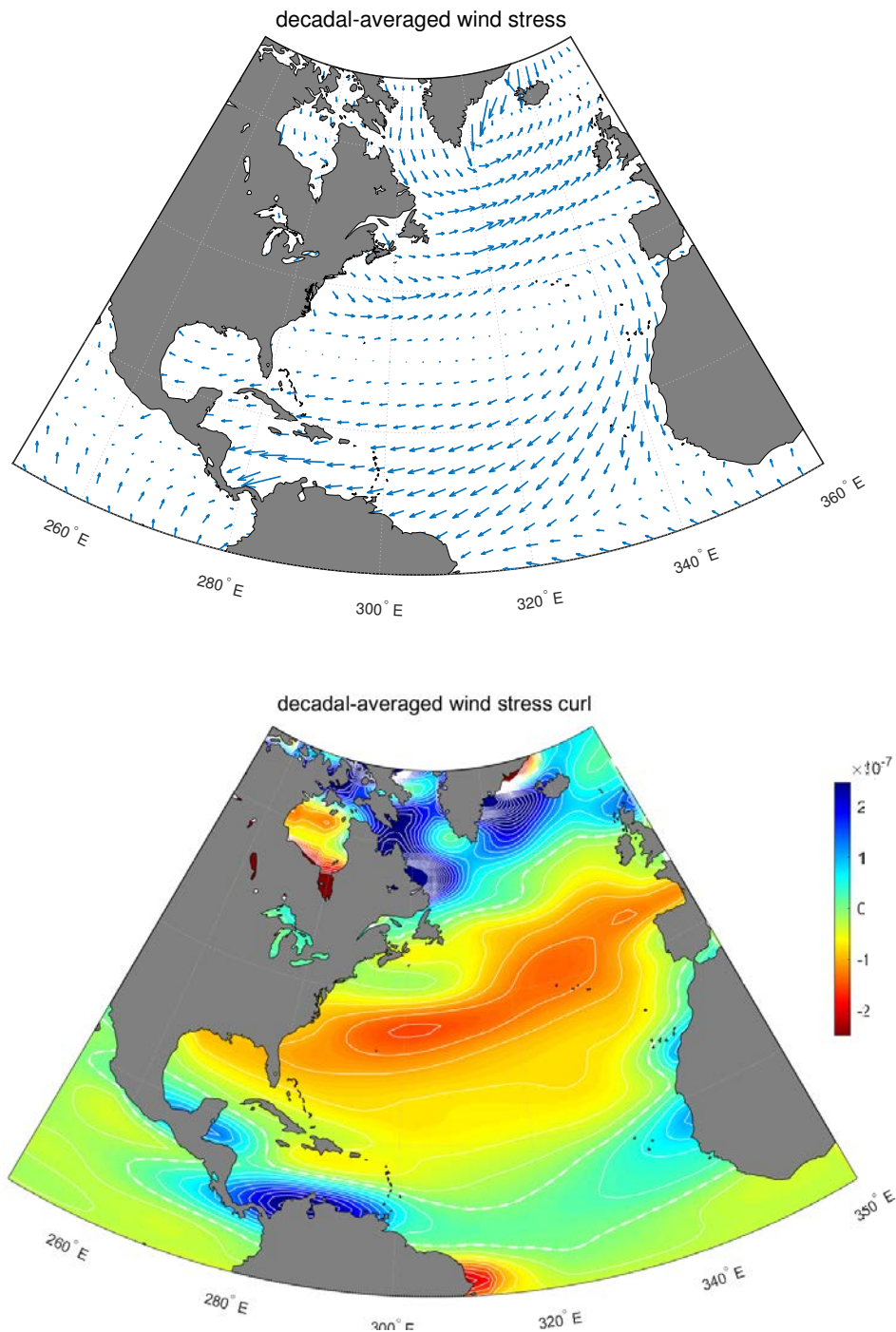
Figure 3: **(upper)** Wind stress computed from about ten years of NASA QuickSCAT scatterometry (1999 - 2009) and served by NOAA ERDDAP, https://coastwatch.pfeg.noaa.gov/erddap/griddap/ The largest magnitude of stress is 0.2 Pa east of Greenland. **(lower)** Wind stress curl, with a colorbar at right in units [Pa m^{-1}]. The heavy dashed contour is the zero. The basin-scale variation of wind stress curl includes a very extensive region of negative stress curl over the subtropics. There is positive stress curl over the subpolar region and within a narrow band over the tropics. There are pronounced, smaller spatial scale variations of stress and stress curl that are evidently associated with topography, e. g., around Greenland. Notice the similarity of the wind stress curl with the long-term average SSH of Fig. (1).

quiescent abyssal ocean. This is dubbed the 1l-rg model (Sec. 4), and can be thought of as a baroclinic only model. This 1l-rg model configuration is comparatively simple and economical and is appropriate to the first three objectives of this essay. A second model has three active layers and a free (moving) sea surface and dubbed 3l-fs. This model includes the baroclinic dynamics of the first model, as well as a very fast barotropic response that makes this model somewhat burdensome computationally. This model can help us understand some aspects of depth-dependence, but not all. For both models the shallow water model equations are extended to include wind forcing and dissipation. These new features are described in Section 4, which may be skipped by readers not interested in the fine details (but who should nevertheless take a look at the wind stress field in Sec. 4.3). The experiments are started from a state of rest and continue until the circulation reaches a basin-wide steady state, requiring about 30 years of ocean time (and a few hours (1l-rg) or a few days (3l-fs) of computer time on an ordinary personal workstation). The transient baroclinic circulation is described in Section 5 in terms of four overlapping stages, and e.g., Stage 3 begins with the onset of baroclinic Sverdrup flow. The steady circulation varies a great deal over the basin. Over the majority of the basin, the steady potential vorticity balance is that of the Sverdrup relation. However, near the western boundary, the balance includes a significant torque due to drag on an energetic western boundary current, discussed in Section 6. Section 7 considers several experiments with other wind fields including one with an annual cycle, especially relevant to study of the annual variation of tropical ocean circulation noted in O3 above. Section 8 describes the solutions from the free surface model, 3l-fs, that includes a barotropic response. You could say that this second model solution changes everything, or, you could equally well argue that it changes almost nothing. Closing remarks are in Section 9, and links to the model code and a few homework problems are in Section 10.

1.3   About this essay

This essay has grown out of 'a Coriolis tutorial' that was first published online in 2002. It has been revised many times since then, and future revisions are likely (especially in response to questions and comments, which are encouraged). The most recent update of this essay will be posted on the Education Projects page of https://www2.whoi.edu/staff/jprice/

2 Worldwide, there are seven major gyres

The world ocean includes seven, major upper ocean gyres - five in the subtropics that are relative highs of SSH, and two in subpolar regions, both lows, Table 1 and Fig. (4).

2.1 O1, The SSH signature of the major upper ocean gyres is well correlated with the wind stress curl

Evidence that these gyres are wind-driven is the striking visual correlation between the large scale distributions of SSH anomaly and the wind stress curl over especially the North Atlantic ocean (Figs. 1 and 2), and also worldwide (Figs. 3 and 4). The North Atlantic subtropical high of SSH underlies the extensive region of negative stress curl that arises mainly from meridional shear along the southern side of the westerly wind belt and the easterly trade winds. Notice that the boundary between the subpolar and subtropical gyres as seen in SSH trends poleward with east distance, as does the axis of the westerly winds and thus the zero of wind stress curl, cf. Fig. (4). The subpolar low of SSH underlies the region of positive stress curl along the north side of the westerly wind belt. A very similar pattern holds as well in the North Pacific and thus the correlation between SSH and wind stress curl is negative.

The southern hemisphere oceans also display such a correlation, but the sign is reversed, e.g., high SSH in the subtropical South Pacific underlies positive wind stress stress curl and so on. This implies that the link between SSH and wind stress curl is going to involve mainly f, the Coriolis parameter (which, of course, changes sign between the hemispheres), rather than β, which does not.[2] Results coming below indicate that this correlation of SSH with wind stress curl is not merely coincidental, but neither is it the most fundamental and important link between wind stress and circulation which is instead given by the Sverdrup relation, Eqn. (1), which, notice, involves β but not f.

These seven gyres have some very important features in common, especially their relationship to the overlying wind stress (cf. Fig. 4) of the westerly wind belts (eastward wind and wind stress that extend across the entirety of ocean basins and, indeed, encircle both hemispheres. The gyres are also unique in that the shape of their respective basins and sea floor topography vary enormously from one to the next. There is also a very important effect in the Atlantic and even more the North Atlantic, associated with the global-scale thermohaline circulation, about which more later.

---

[2]You must be thinking .... hmmmm .... what's it do right on the equator? If this SSH/stress curl relationship is not possible on or very near the equator (from symmetry), then perhaps the wind stress (rather then the wind stress curl) is relevant. What can you discern from inspection of Fig. 3, upper, and Fig. 4, upper ?

decadal-averaged SSH

decadal-averaged wind stress curl
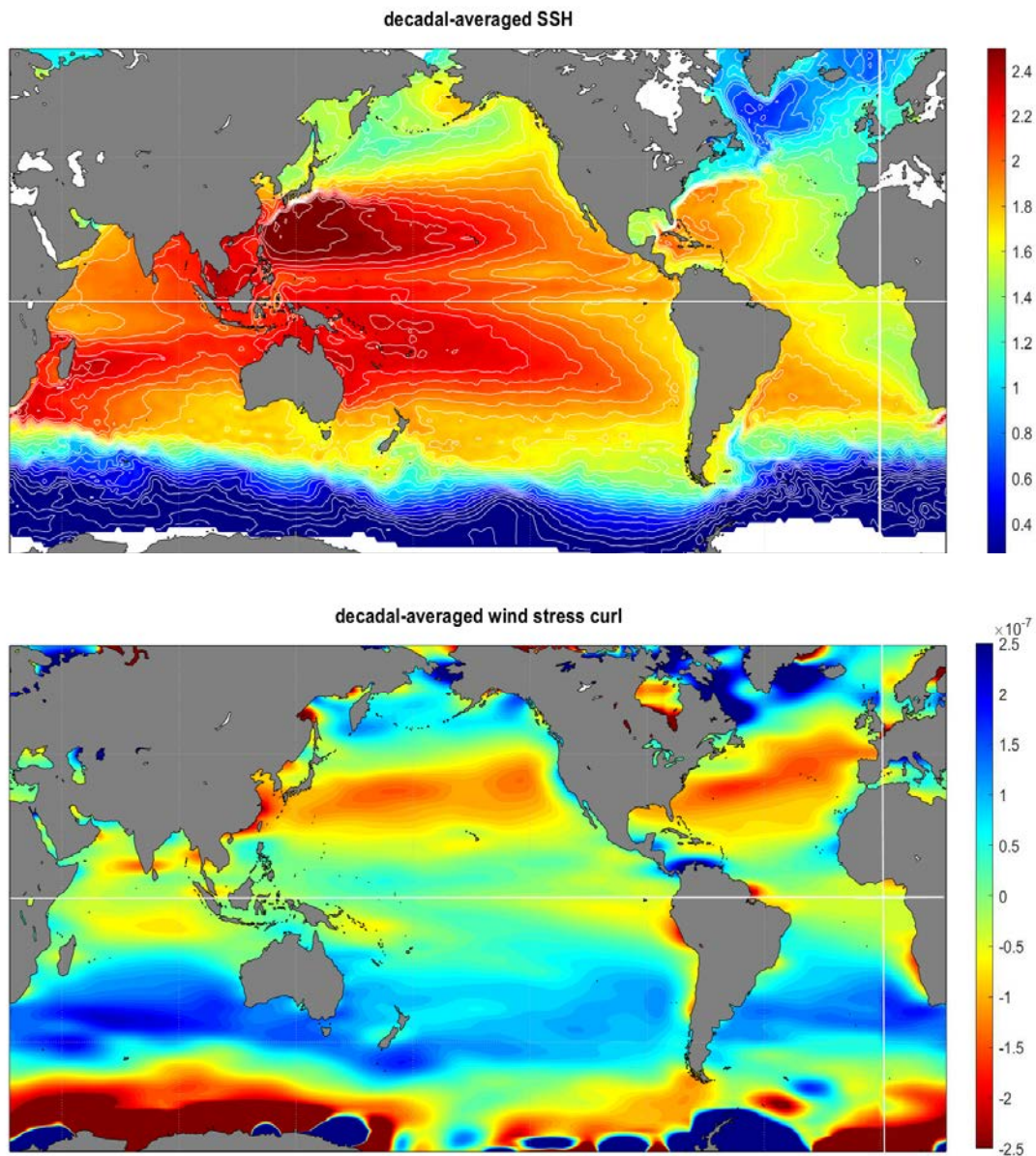
Figure 4: **(upper)** Time mean sea surface height relative to a geoid (absolute SSH) computed over almost two decades of satellite altimetric measurement. These altimeter data were compiled and processed by the AVISO project and served by the NOAA ERDDAP web page. The colorbar at right is in meters. Seven major upper ocean gyres are evident here as regional highs or lows of SSH. **(lower)** Time mean of the wind stress curl computed over about 10 years of satellite scatterometry by NASA QuickSCAT SeaWinds and served by NOAA ERDDAP. The colorbar at right is in Pa m^{-1}.

2.2 O2, Upper ocean gyres are markedly asymmetric east to west

SSH sampled along 32 N across the North Atlantic subtropical gyre shows two distinctly different regions of SSH zonal slope, $\partial\eta/\partial x$ (Fig. 6, upper). Going from the western boundary toward the east,

Basin/Gyre	f	$\nabla \times \tau$	SSH	N^{Sv}	WBC	WBC sense
North Pacific subpolar	+	+	L	30	Oyashio	equatorward
North Atlantic subpolar	+	+	L	25	East Greenland - Labrador	equatorward
North Pacific subtropical	+	-	H	-55	Kuroshio	poleward
North Atlantic subtropical	+	-	H	-30	Gulf Stream	poleward
South Pacific subtropical	-	+	H	55	East Australian	poleward
South Atlantic subtropical	-	+	H	25	Brazil	poleward
South Indian subtropical	-	+	H	40	Agulhas - Mozambique	poleward

Table 1: The seven major semi-permanent gyres and their western boundary currents. The first three entries are sign only. The Sverdrup volume transport, N^{Sv}, in Sverdrups, has been estimated from long-term average wind stress curl that was integrated across the basin at the central latitude of the gyre as seen in SSH (Sec. 1.2). The sign is the usual, positive north.

there is a narrow region adjacent to the western boundary of width L_{wb} that is O(100 km) within which the SSH increases eastward to a maximum $\delta\eta \approx 1$ m. The inferred geostrophic current in this western boundary current, the Gulf Stream, is poleward (northward) and swift, $U_{wb} \approx g\delta\eta/(L_{wb}f)$ is O(1 m sec^{-1}). To the east, there is a broad interior region, essentially all the rest of the basin, width $L_i \approx 7000$ km, over which there is a gradual decrease of η to approx. zero on the eastern boundary. The inferred geostrophic current in the interior is equatorward (southward) and very slow compared to the the western boundary current, $U_i \approx U_{wb}L_{wb}/L_i$ is O(0.01 m sec^{-1}) when averaged over zonal scales of O(1000 km). This slow southward flow of the interior is consistent with Sverdrup transport, about which much more below. A similar structure of rapid western boundary current and very slow interior flow is found also in the subpolar gyre of the North Atlantic, though with the sense of the SSH anomaly and the circulation reversed, and in the other five gyres (Fig. 7).[3] From this brief inspection, it is evident that the east-west asymmetry of upper ocean circulation, often called western intensification, is very pronounced,

$$\frac{L_i}{L_{wb}} \approx \frac{U_{wb}}{U_i} \text{ is } O(100).$$

---

[3]If you look carefully you will notice that the expected poleward-flowing, western boundary current of the South Pacific subtropical gyre, the East Australian Current, seems to be missing from Fig. (7). This is evidently an artifact of the heavy time averaging inflicted upon these data. The East Australian Current is readily apparent in SSH data sampled at a higher resolution, 1/4 degree vs. 1 degree used here, and omitting decadal time-averaging.

decadal-averaged wind stress
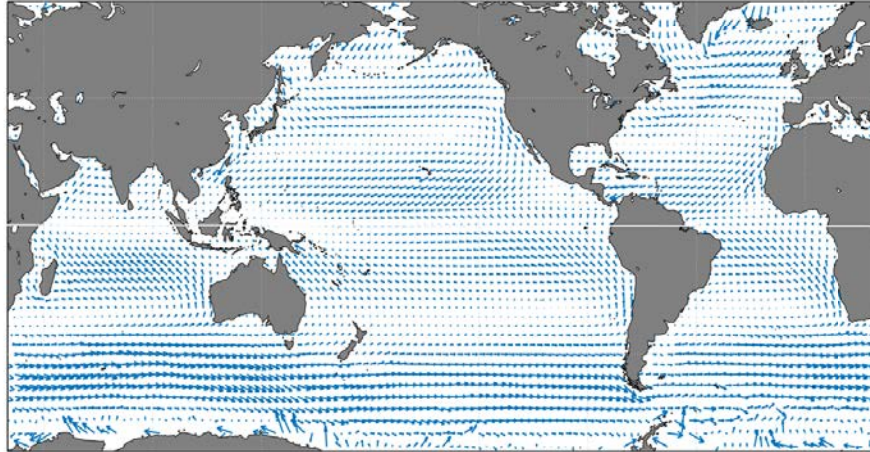
decadal-average east wind stress
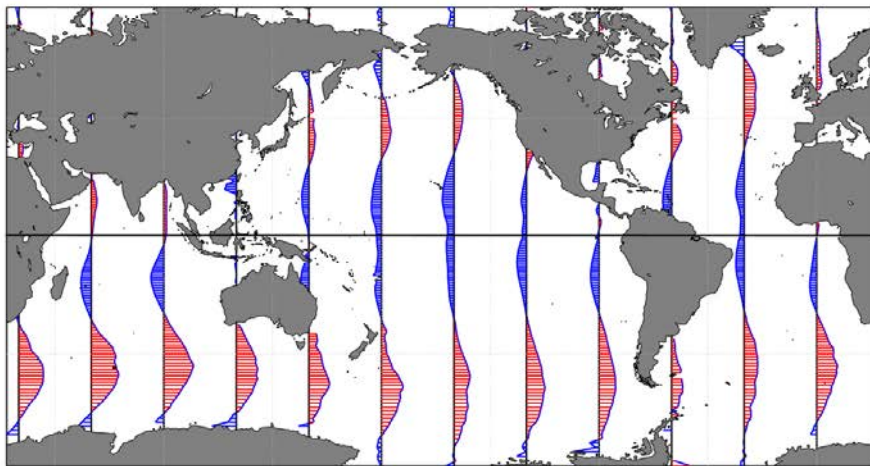
Figure 5: **(upper)** Time mean of the wind stress computed over about 10 years of satellite scatterometry measurement by NASA QuickSCAT SeaWinds and served from the NOAA ERDDAP web page. The largest magnitude of stress is about 0.25 Pa in the Southern Ocean west of Australia. **(lower)** Time mean of the east component of wind stress. East going stress (associated with westerly wind) is in red, and west going stress (easterly wind) is in blue. The largest scale of variability in the wind stress curl field comes from the meridional shear between the westerly winds (eastward stress) and the easterly trade winds (westward stress) and on the poleward side, the subpolar easterlies.
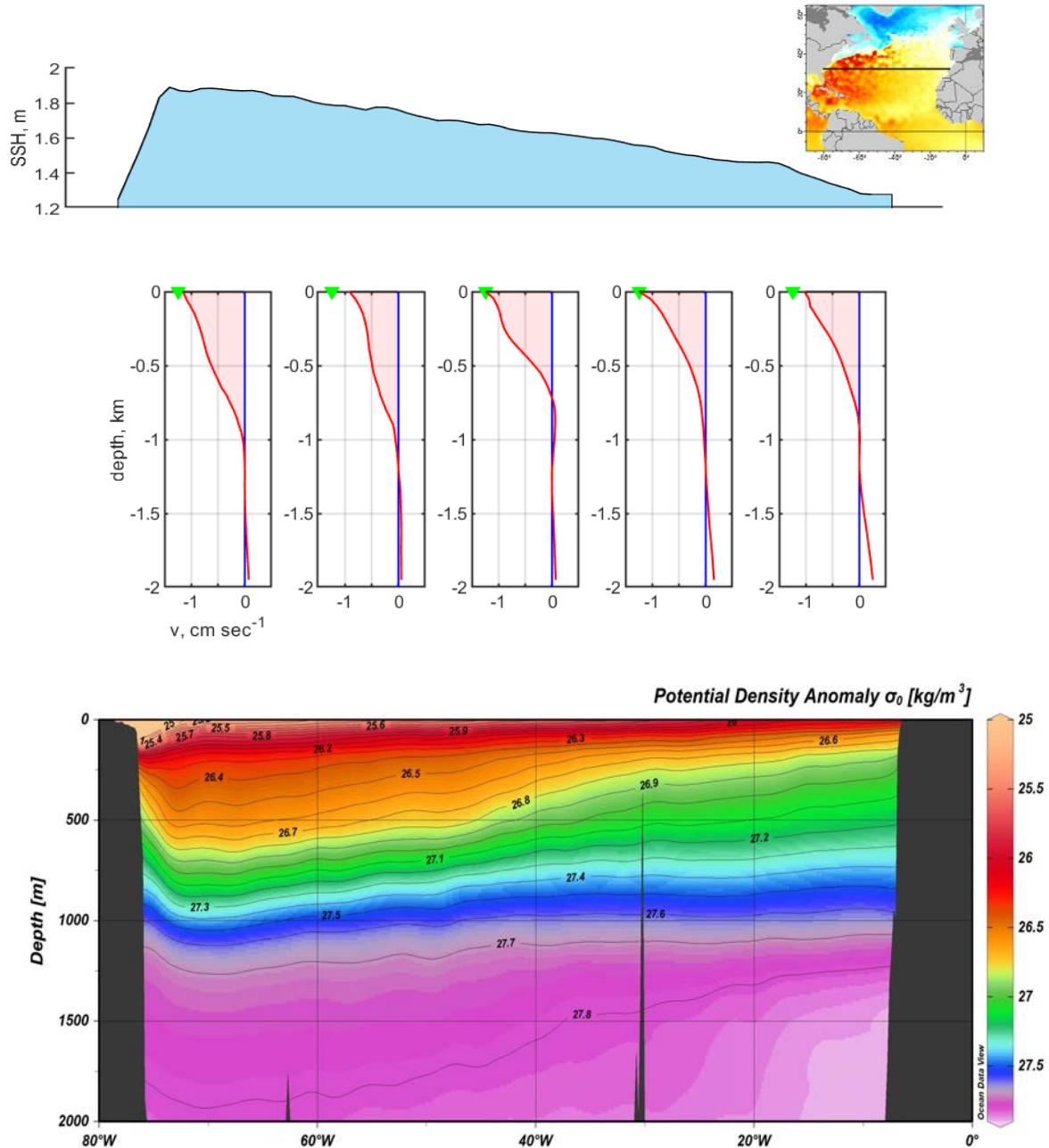
Figure 6: This section across the subtropical North Atlantic at 32 N shows the remarkable east-west asymmetry that is characteristic of wind-driven, upper ocean gyres. **(upper)** Sea surface height (SSH) from long-term averaged satellite altimetry as in Fig. (1). **(middle)** Profiles of the meridional geostrophic current referenced to 1200 m depth. These are lined up with the density section; the westernmost profile does not include the western boundary current. **(lower)** Potential density from *in situ* observations and averaged over several decades, as in Fig. (1), but here the upper 2000 m only. The density data were extracted from the World Ocean Atlas 2018, https://www.ncei.noaa.gov/products/world-ocean-atlas and displayed thanks to Ocean Data View, https://odv.awi.de

time mean SSH across the seven major gyres

Legend:
- strop N Pac, 32 N
- strop N Atl, 32 N
- strop S Ind, 30 S
- strop S Pac, 30 S
- strop S Atl, 30 S
- spolar N Pac, 40 N
- spolar N Atl, 55 N
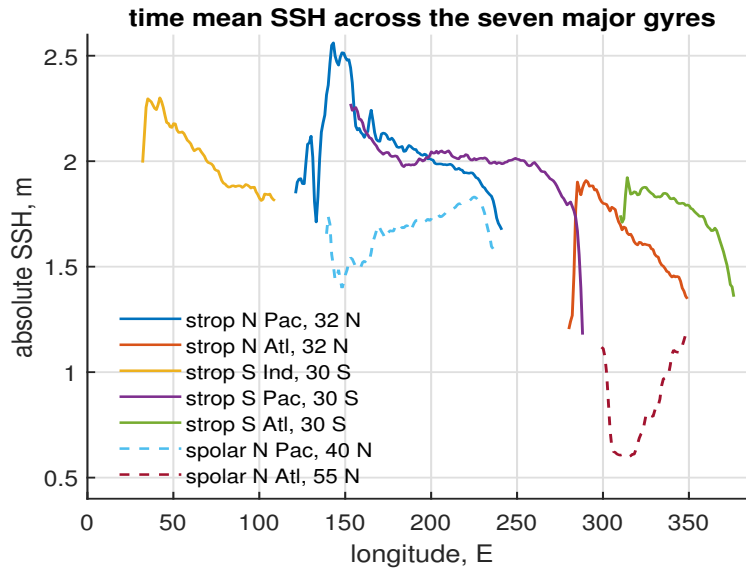
Figure 7: A longitudinal slice through each of the seven major (semi-permanent) upper ocean gyres, at the latitude noted in the legend. These sections go from coast to coast. The five subtropical gyres (solid lines) are relative highs of SSH that fill their respective basins, and have well-defined, narrow western boundary currents. The two subpolar gyres (dashed lines) are relative lows of SSH, also with narrow western boundary currents. Notice the marked dip in SSH near the eastern boundary of especially the subtropical South Pacific and South Atlantic gyres, the signature of major coastal upwelling regions.

2.3   O3, Subtropical and subpolar gyres are quasi-steady annually, while tropical ocean circulation shows significant seasonal variation

The subtropical gyre is always present in the sense that every basin-wide snapshot of SSH (examples in Part 3) and every across-basin hydrographic section will show an easily recognizable, poleward-flowing Gulf Stream near the western boundary and an equatorward Sverdrup flow over most of the rest of the basin. Said a little differently, the subtropical gyre is clearly evident not only in a long-term average, but also instantaneously, despite that there are always significant, time-dependent perturbations due to mesoscale eddies.[4] These comments hold just as well for the subpolar gyre.

Minimal seasonal variation of the subtropics and subpolar regions.   One might reasonably expect

---

[4]Mesoscale eddies are ubiquitous, and impose large amplitude, but comparatively short time (periods of several months) and space (several hundred kilometers) scale variations on the gyre-scale SSH and currents, Fig. (1), Part 3. Thus the near-instantaneous (time and space) meridional geostrophic current in the basin interior is just about as likely to be northward as southward. The very smooth, almost linear slope of interior SSH seen in Fig.(2), upper, arises only upon long-term (decadal) averaging. Similarly, any single estimate of the instantaneous Gulf Stream transport may vary by $\pm 15\%$ around the long term mean due to superimposed, apparently random mesoscale eddy variability; Rossby, T, C. Flagg and K. Donohue, 2010, 'On the variability of Gulf Stream transport from seasonal to decadal', *J. Mar. Res., 68,* 503-522.

seasonal east wind stress, 30 W, Atlantic
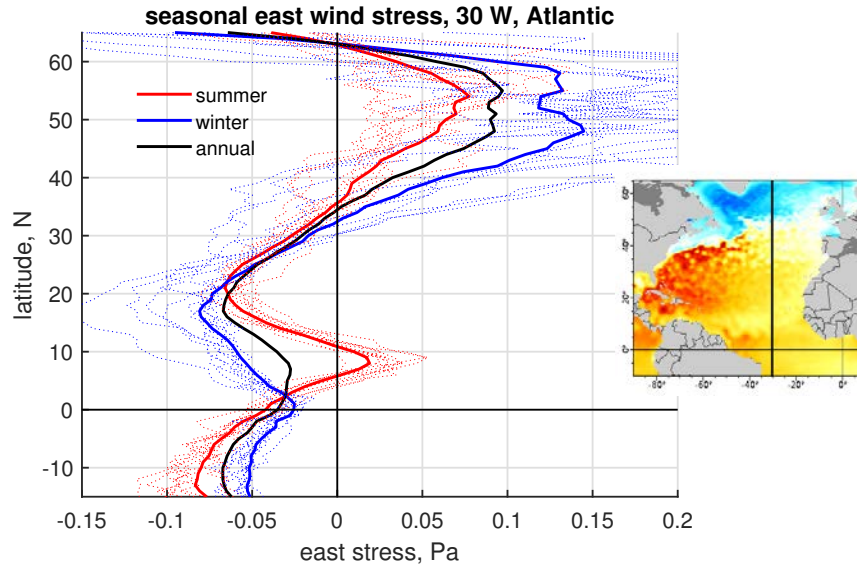
Figure 8: The east component of wind stress sampled along 30 W of the North Atlantic. Data are from a decade of scatterometry observation, QuikSCAT SeaWinds, served by the NOAA ERDDAP web page. The heavy red and blue lines are the summer and winter composite averages, and the thinner dashed lines are the individual monthly estimates. At mid-latitudes, the seasonal cycle is mainly a pronounced strengthening of the westerlies in winter, along with a very substantial increase in monthly variability (storminess). At tropical latitudes, the biggest feature is a shift in latitude of the near-equatorial easterly minimum (the doldrums) — northward during northern hemisphere summer and returning to the equator during winter. The result is a fairly substantial annual cycle of wind stress and wind stress curl in the lower subtropics.

that the upper ocean circulation would show a significant seasonal variation (i.e., an annual cycle) since the wind stress and the wind stress curl that are the ultimate source of the circulation vary quite a lot with season, in some regions up to ±50% (Figs. 8 and 9). However, the systematic, seasonal (annual) variation of the subtropical gyre, represented here by the seasonal average zonal profile of SSH (Fig. 10) or by the Gulf Stream transport is quite small, only about 5 to 10% of the time-mean.[4] The same comments hold for the subpolar gyre. This almost complete *absence* of significant seasonal variation in the subtropical and subpolar gyres indicates that the response time of these gyres to a changing wind stress must be considerably longer than a season.

Pronounced seasonal variation of the tropical ocean circulation. The time-mean and the seasonal variation of the tropical Atlantic circulation (within about 15 degrees of the equator) is markedly different in character from the subtropical and subpolar circulation described above. The dominant features of the tropical North Atlantic SSH are several comparatively narrow, zonally elongated ridges and troughs (just barely evident in Fig. (1), which is scaled appropriately for the entire North Atlantic; cf., Fig. 11). The magnitude of the near-surface current associated with these tropical ocean features is comparable to that found in the subtropical and subpolar gyres, though the SSH amplitude is considerably less, typically only about 0.1 m, consistent with geostrophy at low latitudes. The associated, zonal geostrophic currents

18
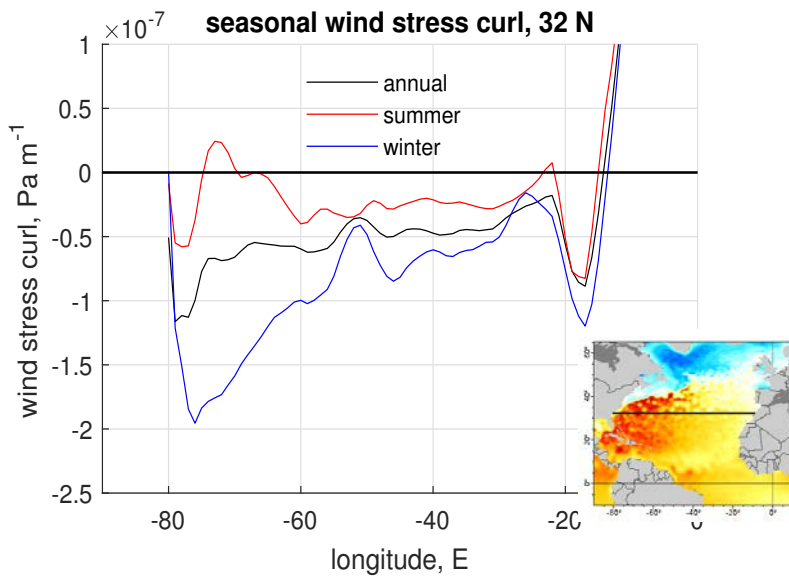
Figure 9: Longitudinal profile of wind stress curl along 32 N, as in Fig. (10) above. The black line is the annual mean, and the red and blue lines are the mean for summer and winter respectively. Notice that the wintertime curl is considerably greater in magnitude (more negative) than is the summertime curl. This wind stress data was downloaded from the SODA3 reanalysis that is archived on the NOAA ERDDAP web site.

have alternate signs: between about 25 N and 15 N there is a rather diffuse, westward flowing North Equatorial Current (NEC), essentially the southern part of the subtropical gyre, a little farther south between about 12 N and 5 N there is an eastward flowing North Equatorial Countercurrent (NECC), and still farther south, a northwestward flowing South Equatorial Current (SEC) that crosses the equator from south to north. The connection of these zonal currents with a western boundary current and with a gyre-like circulation is not clear from observations.[5]

In marked contrast to the quasi-steady subtropical and subpolar gyres noted above, these tropical ocean circulation features exhibit systematic, large amplitude seasonality: the North Equatorial Current

---

[5]There is a significant, northward-flowing western boundary current evident in Fig. 2 that crosses the equator and continues northwestward along the coast of South America. This North Brazil Current is the shallow side of the the global-scale, overturning circulation that imports warm South Atlantic water into the North Atlantic basin and returns cold water at great depth. The meandering North Brazil Current frequently sheds large (several hundred kilometer diameter) eddies that transport a significant part of the warm water flow. The presence of the strong and highly variable North Brazil Current makes it difficult to discern a relationship between a western boundary current and the mainly zonal currents to the east. A concise discussion of equatorial ocean circulation including the annual variability of winds and currents is by Philander, S. G., 2001, 'Atlantic ocean equatorial currents', Academic Press, doi:10.1006/rwos.2001.0361. An excellent depiction of surface currents generally is provided by http://oceancurrents.rsmas.miami.edu/atlantic/north-brazil.html

SSH, seasonal averages, 32 N and 55 N, North Atlantic
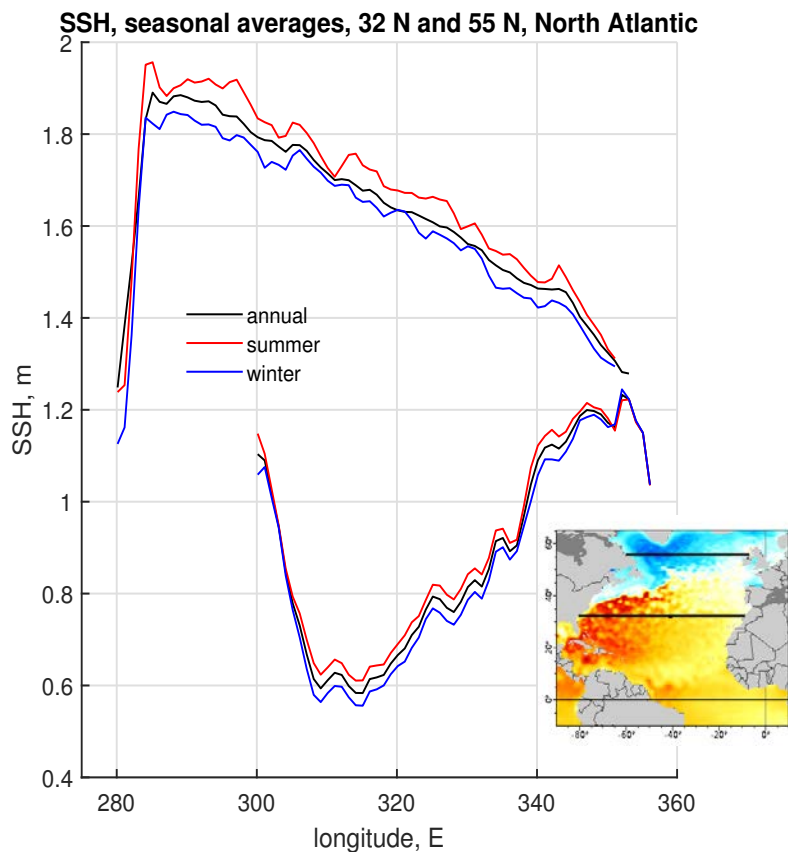
Figure 10: Longitudinal profile of decadal-averaged absolute SSH across the subtropical North Atlantic at 32 N (n.b., the upper set of curves) and at 55 N (the lower set of curves). Data are from the AVISO project via ERDDAP, and span the years 1992-2012. The black line is the annual mean, and the red and blue lines are the mean for summer and winter respectively. Note that in both gyres, the summertime SSH is slightly higher than the wintertime SSH, but the zonal slope of SSH is essentially unchanged from summer to winter. (For a little more on this, see homework problem 3 of Sec. 9.2)

and the South Equatorial Current are strongest in summer and disappear almost completely in winter, while the North Equatorial Counter Current fluctuates annually by about ±40% of its mean (Fig. 11). (A more compelling view of this annual variability is available by following the links to animations noted in the caption of Fig. 2, and see also the references in footnote 5.) A time-mean can always be defined, however the seasonal variability of these near-equatorial currents is more impressive and perhaps more significant than is the mean. This marked difference between the tropics and higher latitudes is emblematic of a very significant latitudinal dependence of the ocean's response to a changing wind stress, something that will be encountered at several turns in this essay. The most dramatic example of this is the monsoonal variation of circulation in the Arabian Sea, discussed at some depth in Part 5: on the seasonally-varying Arabian Sea.

seasonal SSH, 30 W, North Atlantic
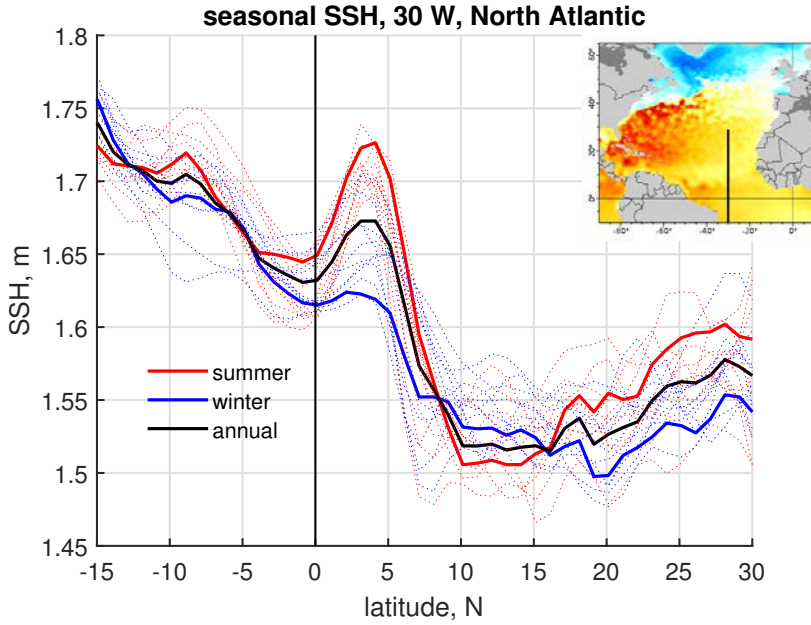
Figure 11: The summer and winter seasonal averages of SSH over 20 years of satellite altimetry along 30 W in the tropical North Atlantic. These SSH data were compiled by the AVISO project and served by NOAA's ERDDAP web page. Notice the large summer to winter change in the ridge near 7 N which supports the eastward flowing NECC on its north side during summer, and the westward flowing SEC on the south side. More subtle, but also significant, is the summer maximum of the northward slope of SSH between about 15 N and 25 N. This supports the westward flowing NEC.

2.4 O4, The geostrophic flow of the subtropical gyre is somewhat surface intensified

The SSH field gives us a good sense of the near-surface geostrophic flow, and the density section of Fig. (3) together with the thermal wind relation,

$$\frac{\partial v}{\partial z} = -\frac{g}{f\rho_o}\frac{\partial \rho}{\partial x}, \tag{2}$$

provides an opportunity to estimate the vertical extent of the underlying geostrophic flow (Fig. 6). Thermal wind may be integrated upward from a depth d_o,

$$v(z) = -\frac{g}{f\rho_o}\int_{-d_o}^{z}\frac{\partial \rho}{\partial x}dz + v(d_o). \tag{3}$$

The integration constant $v(d_o)$ may be evaluated in a variety of ways. The classic method is to set $v(d_o) = 0$ at a depth where the horizontal density gradient vanishes (isopycnals are level) and hence the thermal wind also vanishes. The velocity at that depth is then either barotropic, which is possible but not common, or the velocity vanishes, and d_o is said to be the 'depth of no motion'. Inspection of Fig. (6),

21

lower, suggests that $d_o = 1200$ m is a plausible guess for most of the interior of the subtropical gyre and yields the profiles of Fig. (6), upper. The long-term average SSH (Fig. 2) may also be used to make an independent estimate of the near-surface geostrophic current, and yields -1.2 cm sec^{-1}, averaged over the interior of the basin, -65 E to -10 E. This is (remarkably) consistent with the near-surface values of the thermal wind profiles, -1.1 to -1.4 cm sec^{-1}, suggesting that a depth of no motion at around 1200 m is indeed appropriate, on average, for the interior portion of this section. Hence, these current profiles may be regarded as absolute. It is important to note that there is no claim to know *why* $d_0 = 1200$ m in this instance, and hence there is no basis to argue that the same d_o will be appropriate for any other region, including the western boundary current region of this section.

A second characterization of meridional currents is available from the Simple Ocean Data Assimilation version 3, SODA3,[6] an ocean reanalysis run for the years 1985 to 2015 (Fig. 12). The reanalysis data were sampled along 32 N, and then time-averaged over two decades (Fig. 12). Reanalysis is a complex process (name notwithstanding) that uses extensive oceanic and atmospheric data sets (all available hydrographic data, satellite-observed SST, wind stress from scatterometry and air-sea heat exchange from other reanalyses) to continually update an Ocean General Circulation Model (OGCM). The aim is to produce a dynamically consistent solution including four-dimensional temperature, salinity and currents at high spatial and temporal resolution. The resulting SODA3 currents are absolute, and so there is no need to fuss with a level of no motion. As well, the OGCM includes a wind-forced Ekman layer within the upper 50 m, roughly.

These current profiles are used to investigate volume transport in a later section 1.2.1, but for now the aim is to define the depth scale (vertical extent) of the subtropical gyre circulation. There is very weak (or vanishing) meridional flow at depths of ≈ 1200 m, as expected from the nearly flat isopycnals around that depth. The meridional geostrophic current becomes more southerly approaching the surface, and has a near-surface value of about -1.3 cm sec^{-1} on average across this section. The profiles are quasi-linear in depth, and so a plausible measure of the vertical extent (i.e., the depth scale) is the half amplitude, $d_{1/2} \approx 500$ m on the western side of the section, and somewhat less, about 300 m on the eastern side. This eastward shoaling of the current is significant, but if you had to pick a single number, then

$$d_{1/2} \approx 400 \text{ m}$$

is about right for the subtropical gyre. The meridional current of the subtropical gyre interior is significantly surface-intensified in as much as it occupies only about the shallowest 10% of the water column. This will be termed the 'upper ocean', and is the part of the water column that is kept in motion by the direct and indirect effects of the overlying wind field.[7] Notice that the upper ocean so defined is roughly coincident with the main thermocline. It is, of course, very helpful to have a number in mind for

---

[6]Carton, J. A., G. A. Chepurin and L. Chen, 2018. SODA3: A new ocean climate reanalysis. *J. Clim.*, Vol. 31, 6967-6983.

[7]In the deep, cold 'abyssal' ocean below the main thermocline, the horizontal and vertical density gradients are much smaller and the inferred circulation is comparably very slow. Abyssal ocean circulation also owes, ultimately, to interaction with the atmosphere, including heat and fresh water exchanges that are excluded from this study. It also has a truly global extent, rather than merely basin-wide.

SODA3 mean v(z), 32 N interior, N Atlantic
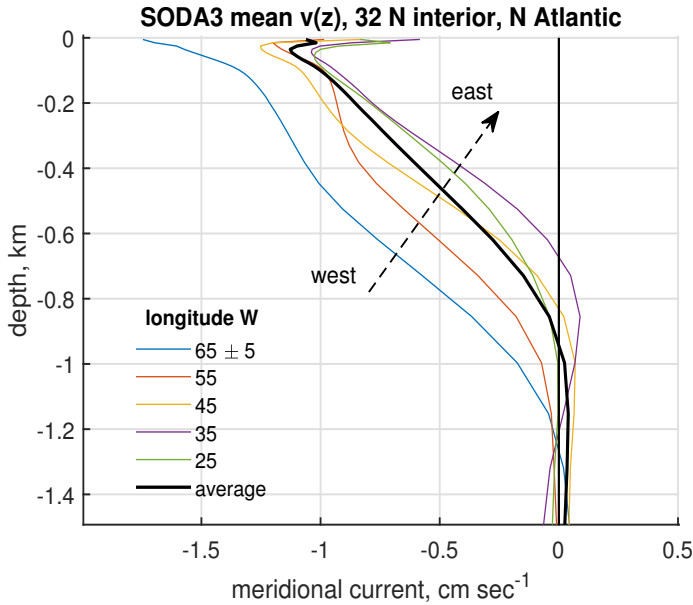
Figure 12: Profiles of long time-averaged meridional current from the SODA3 reanalysis sampled along 32 N in the subtropical North Atlantic. These data were downloaded from the NOAA ERDDAP server. Profiles are plotted every 10 deg of longitude from 65 W to 25 W. These profiles include an Ekman current in the shallowest ≈ 50 m, which is not present in the thermal-wind inferred profiles of Fig. (6), upper. Otherwise, these are very similar to thermal wind profiles computed from time-averaged density field data. Notice that the half-amplitude thickness of the current decreases from west to east, roughly 500 m to 300 m.

the depth (vertical extent) of the wind-driven circulation, but it is also very important to know why, i.e., what it depends upon and how it might vary from one region to the next.

2.5 Appendix: Notable phenomena that are not addressed here

Eastern boundary upwelling. One significant feature of the zonal SSH profiles that will not be treated here but that deserves much more than a passing mention is the pronounced low of SSH close to the eastern boundary of four of the subtropical gyres (the exception being the South Indian Ocean gyre). This low SSH is especially prominent in the subtropical gyres of the South Pacific and the South Atlantic. These SSH eastern boundary lows are the signature of two of the ocean's most important coastal upwelling regions, often named for their associated upper ocean current, the equatorward Humboldt Current off of Chile and Peru, and the equatorward Benguela Current off of South Africa and Namibia. These Eastern Boundary Upwelling (EBU) regions extend for hundreds of kilometers along the coast, and are marked by SST that is much cooler than is found in the interior offshore, as well as an uplifted thermocline. This is the consequence of a more or less persistent upward-going, vertical flow (or upwelling) of subsurface waters into the near surface, as much as 5 to 10 m day^{-1} or O(50) times the rate of typical open ocean Ekman suction. Thermocline water is high in nutrients that fuels very intense biological productivity in EBU regions, an order of magnitude greater than is typical of the open ocean. The proximate cause of EBU upwelling is alongshore, equatorward winds (Fig. 3) that produce a divergent Ekman transport next to the coast, and is strengthened by negative stress curl offshore (southern hemisphere). The direction and amplitude of the prevailing wind stress is the most important cause of an EBU, but it is also significant that they are found along the eastern boundaries of subtropical gyres where

cool, nutrient rich thermocline water is unusually close to the sea surface.

North Indian Ocean. The only large ocean basin that is missing from Table 1 is the North Indian Ocean. The long-term mean wind stress and wind stress curl over this basin are somewhat smaller than are found over other ocean basins. Given this, and the low (tropical) latitude of this ocean basin, it is not surprising that the time-mean SSH does not show an obvious, gyre-like structure.

What the North Indian Ocean may lack in a time-mean circulation it more than makes up with very strong seasonal circulation that is associated with seasonally reversing, or monsoonal, winds that are very different from the mainly zonal winds that drive midlatitude circulations. The summertime, Southwest monsoon winds of the Arabian Sea include what are typically quite strong southwesterly winds along the coast of Somalia and Oman. The ocean circulation responds vigorously to the onset of Southwest Monsoon winds, within a month, with a strong flow to the northeast along the coast of Somalia. This Somali Current has surface current speeds in excess of 2 m sec^{-1}, a depth (thickness) of about 250 m, and a transport of roughly 30 Sv, which is comparable to that of some semi-permanent western boundary currents. This monsoon response is examined in some depth in Part 5, where the conclusion is that the summertime circulation of the Arabian Sea is not unlike that of the subtropical North Atlantic, including that its amplitude is approximately consistent with the Sverdrup relation.

3 A review of the low frequency beta effect and the Sverdrup relation

In Part 3 and here, the northward increase of f

$$f = 2\Omega \sin\left(latitude\right) \tag{4}$$

is represented by the β-plane approximation, a linear expansion of f around a central latitude,

$$\beta - \text{plane approximation}: \quad f_1 = f_o + \beta(y - y_o), \tag{5}$$

with y the north coordinate and $R_e = 6360$ km the Earth's mean radius. The coefficient

$$\beta = (2\Omega/R_e)\cos\left(lat_o\right) \tag{6}$$

is constant for a specific model. For this study, $lat_o = 30^o$ N and hence $f_o = 7.29 \times 10^{-5}$ sec^{-1}, and $\beta = 1.98 \times 10^{-11}$ sec^{-1} m^{-1}.
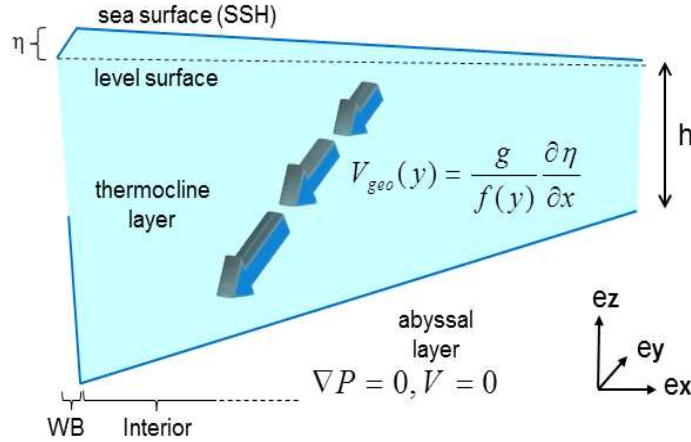
Figure 13: A schematic cross section of the North Atlantic subtropical thermocline, sliced east-west and viewed looking toward the north as in Fig. (6). The upper ocean (thermocline and above) is modeled as a single active layer. The tilt of the thermocline compensates the tilted sea surface so that the horizontal pressure gradient and velocity are vanishingly small in the very thick abyssal layer. The comparatively narrow western boundary region is noted at lower left, and the much wider interior region is all of the rest. The meridional geostrophic current in the interior is equatorward. The three bold arrows are meant to depict the geostrophic current amplitude at three latitudes and increase toward the equator, simply because because f decreases toward the equator. A meridional geostrophic current is thus divergent, $\partial v_{geo}/\partial y > 0$, which is here said to be the beta effect. In this example of equatorward flow, the resulting layer thickness tendency due to the beta effect alone is thus $\partial h/\partial t < 0$, i.e., thinning.

3.1   Balanced meridional motion is divergent horizontally

A beta-plane approximation is sufficient to reveal one of the most important consequences of the northward variation of f, that balanced meridional motion is divergent horizontally. To see how this arises, consider a vertically integrated continuity equation, or thickness balance, for a single layer (as in a reduced gravity, shallow water model, Part 2),

$$\frac{\partial h}{\partial t} = -(\frac{\partial hu}{\partial x} + \frac{\partial hv}{\partial y}). \tag{7}$$

Geostrophy for this model is just

$$-fv = -\frac{1}{\rho_o}\frac{\partial P}{\partial x} \quad \text{and} \quad fu = -\frac{1}{\rho_o}\frac{\partial P}{\partial y}. \tag{8}$$

Now substitute the geostrophic velocity components Eq. (8) and $f(y)$ from (5), to find

$$\boxed{\frac{\partial h_{geo}}{\partial t} = \frac{\beta h}{f}v_{geo}} \tag{9}$$

25

on the assumption that $\partial^2 P/\partial x \partial y = \partial^2 P/\partial y \partial x$. The subscript *geo* on the left side is just to emphasize that this is the geostrophic contribution only. This thickness tendency is due to the horizontal divergence of a balanced meridional velocity in the presence of a northward increase of f, here said to be the low frequency beta effect (to distinguish from the high frequency beta-effect on inertia-gravity waves noted Part 3).[8] In the example of Fig. (13), a balanced (geostrophic) current is presumed to be southerly, and thus increases in the direction of flow on account of the decrease of f toward the equator. The resulting horizontal divergence $\partial v/\partial y > 0$. Absent some other effect, the layer thickness in this example must then decrease, $\partial h/\partial t < 0$. It is easy to show that if the balanced current is instead poleward, then $\partial v/\partial y < 0$ and the layer will thicken on account of a beta-induced convergence of the horizontal velocity.

Exactly the same thing will happen if there is an applied wind stress and an Ekman current,

$$\boxed{fhu_{Ek} = \frac{1}{\rho_o}\tau_y \quad \text{and} \quad fhv_{Ek} = -\frac{1}{\rho_o}\tau_y} \tag{10}$$

Substituting these into the thickness balance yields

$$\frac{\partial h_{Ek}}{\partial t} = \frac{1}{\rho_o}\left(\frac{1}{f}\frac{\partial \tau_y}{\partial x} - \frac{\partial}{\partial y}(\frac{\tau_x}{f})\right). \tag{11}$$

Expanding the derivative on the rightmost term brings out a term that involves beta,

$$\frac{\partial h_{Ek}}{\partial t} = \frac{\beta h}{f}v_{Ek} + \frac{1}{\rho_o f}\left(\frac{\partial \tau_y}{\partial x} - \frac{\partial \tau_x}{\partial y}\right). \tag{12}$$

The wind stress field may (usually will) have some curl, while the pressure gradient field can not.

The geostrophic and Ekman velocities appear in parallel forms here and so it is useful to define their sum to be the balanced velocity,[9]

$$v_{bal} = v_{geo} + v_{Ek} \tag{13}$$

and the sum of (9) and (12) is the corresponding thickness balance,

$$\boxed{\frac{\partial h_{bal}}{\partial t} = \frac{\beta h}{f}v_{bal} + \frac{1}{\rho_o f}\left(\frac{\partial \tau_y}{\partial x} - \frac{\partial \tau_x}{\partial y}\right)} \tag{14}$$

The thickness equation (14) has three modes by which is meant notable two term balances. The first and third terms define a forced, time-dependent balance in which the Ekman convergence associated with

---

[8]There does not appear to be a wide consensus on the meaning of the phrase 'beta effect'. Many authors, including the Glossary of the American Meteorological Society, use the term to signify anything that happens on a beta plane that would not have happened on an otherwise similar f-plane. By that usage, the divergence of balanced meridional flow would be *a* beta effect.

[9]This use of 'balanced' is evidently not conventional. A balanced velocity is usually meant to indicate a steady, vortical flow in which geostrophy is modified by centrifugal force.

wind stress curl thickens or thins the surface layer locally. This is a very important process insofar as it changes the mass field and thus the pressure field, and will figure prominently in discussion of the Stage 2 response of Sec. 4.2.1. The first and second terms define a time-dependent, free (unforced) balance that describes the mechanism of westward propagation, and the second and third terms define a forced, steady flow which is Sverdrup balance, albeit in a one layer model.

3.1.1   Free, time-dependent motions propagate westward

The mechanism of westward propagation may be understood as the second mode noted above, the balance between time-dependence and the beta effect. To see this, rewrite the beta term using the geostrophic velocity, to find a first order wave/advection equation (Sec. 10.2, Problem 2),

$$\frac{\partial h_{geo}}{\partial t} \;=\; \beta R_d^2 \frac{\partial h}{\partial x},\tag{15}$$

where

$$R_d \;=\; \frac{\sqrt{g'h}}{f} \;=\; \frac{C}{f}$$

is the radius of deformation. C is the gravity wave speed; in the subtropics, $C \approx 3$ m sec^{-1}, and at 30° N, $R_d \approx 40$ km. Eqn. (18) is appropriate for free motions, e.g., elementary waves $h(x,t) \propto sin(kx - \omega t)$, and so may be characterized by a dispersion relation that connects the wavenumber, $k = 2\pi/\lambda$, and the frequency, ω,

$$\omega \;=\; -k\beta R_d^2.\tag{16}$$

This is the long wave limit of baroclinic Rossby waves (Part 3, Sec. 2.3). In this limit, phase and group speeds are equal to the long Rossby wave speed,

$$\boxed{C_{longRo} \;=\; \frac{\omega}{k} \;=\; \frac{\partial \omega}{\partial k} \;=\; -\beta R_d^2 \;\leq\; 0.}\tag{17}$$

C_{longRo} is independent of k and ω, and so this propagation is nondispersive and westward. Eqn. (15) is thus a first order wave/advection equation,

$$\boxed{\frac{\partial h_{geo}}{\partial t} \;=\; -C_{longRo}\frac{\partial h}{\partial x}}\tag{18}$$

C_{longRo} varies quite a lot with f, but at a fixed site, C_{longRo} is equivalent to a constant, westward advection velocity. Using values from 30° N, $C_{longRo} \approx -3$ km day^{-1}, which is consistent with the observed propagation of mesoscale eddies discussed in Part 3.

What is most important is that all free (unforced) large scale ($\lambda >> R_d$), low frequency ($\omega << f$) phenomena will propagate westward, regardless of planform. If there are indeed no small horizontal

scales involved (and so no dispersion), then the planform will be conserved and will appear to be shifted steadily westward, as if by advection, at the constant rate, C_{longRo}. It seems appropriate to call such westward propagating phenomena 'Rossby waves', even if they may look nothing at all like an elementary wave. An appreciation for this generalized Rossby wave propagation is a key concept needed to understand the response of an ocean circulation to a transient wind. (For a little more on this see Homework problem 2, Sec. 10.2.)

3.1.2 Forced, steady meridional motion is Sverdrup flow

The third mode of (14) is forced, steady motion,

$$
hv_{bal} = \frac{1}{\beta\rho_o}\left(\frac{\partial\tau_y}{\partial x} - \frac{\partial\tau_x}{\partial y}\right) \tag{19}
$$

or in a more streamlined notation,

$$
M_{bal}^y = \frac{1}{\rho_o\beta}\nabla\times\tau,
$$

which is none other than the Sverdrup relation for this single layer model in which

$$
M_{bal}^y = h(v_{geo} + v_{Ek}) = M_{geo}^y + M_{Ek}^y.
$$

Thus the mechanism behind the Sverdrup relation can be viewed as the mass (volume) balance between the beta-induced divergence of a balanced meridional current (geostrophic plus Ekman) and the wind stress curl component of Ekman transport divergence. To say it a little differently, if there is a steady state in the presence of a wind stress curl, then a beta effect acting upon a meridional transport will be implied. The sense and the magnitude of this meridional transport is given by the Sverdrup relation. In the single layer model considered here, the Sverdrup transport is, by default, present entirely within the single active layer, which is also the Ekman layer. Surprisingly, this is also a plausible outcome in a much more capable model of Sec. 6, though not necessarily what is in the ocean.

There is yet another way to see the Sverdrup relation that combines the previous two descriptions of modes. It has been empahsized that every large scale zonal gradient of thickness should have a tendency to propagate westward. Mesoscale eddies conform to this notion — why not same for the basin-scale meridional gradient seen in Fig. 1? If the gyre was a free motion, it would certainly propagate westward, and the result at a given site would be a thinning of the upper ocean layer as given by Eqn. (15). However, the basin scale flow i.e., the gyre, is subject also to wind stress curl, which will tend to thicken the upper ocean layer, Eqn. (11). If these two tendencies just offset one another, then

$$
\frac{\partial h_{geo}}{\partial t} + \frac{\partial h_{Ek}}{\partial t} = 0,
$$
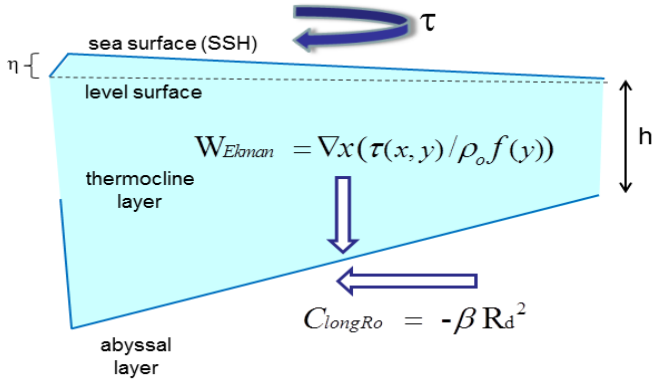
Figure 14: A schematic cross section of the North Atlantic subtropical thermocline, sliced east-west and viewed looking toward the north as in Fig. (6). The beta effect acting upon the associated meridional geostrophic current will produce a westward translation of the thickness gradient at a rate $-C_{longRo}$ and thus a thinning of the layer. The wind stress over the subtropical gyre produces an Ekman transport that is convergent and that would tend to thicken the thermocline layer. The Sverdrup relation may be viewed as a steady balance between this positive thickness tendency and the negative thickness tendency associated with the beta effect and westward propagation.

or using (11) and (15),

$$C_{longRo}\frac{\partial h}{\partial x} = \frac{1}{\rho_o}\left(\frac{1}{f}\frac{\partial \tau_y}{\partial x} - \frac{\partial}{\partial y}\left(\frac{\tau_x}{f}\right)\right).$$

This can be rearranged a little to find the geostrophic form of the Sverdrup relation,

$$M^y_{geo} = \frac{1}{\rho_o\beta}\nabla \times \frac{\tau}{f} \tag{20}$$

in which the curl operates on wind stress divided by $f(y)$.

The large scale thickness field of the subtropical gyre interior may thus be viewed as an arrested, long Rossby wave. The westward translation expected from the β-effect and the first order wave equation is balanced by a wind stress-induced convergence of the Ekman transport. Wind-driven gyres and mesoscale eddies are closely related in as much as they have the same β-effect acting upon meridional flows (this seems obviously true), the difference is that wind stress does not vary appreciably on the horizontal scale of a mesoscale eddy and hence the westward propagation of eddies.

3.2 Depth dependence of Sverdrup flow

The depth dependence of the circulation is, of course, very important, but not something that will be treated here well enough to develop much insight. It is helpful to consider briefly what amounts to the complement of a single-layered model, a three-dimensional system that is presumed to be quasi-steady, linear and inviscid and that admits depth-dependence. The three dimensional velocity components of this

system are u, v, and w, and e.g., u is $u(x, y, z)$ (note that this holds for the present section only). The three dimensional density, continuity and momentum equations of this system are

$$\left[\frac{\partial \rho}{\partial t}\right] = -w\frac{\partial \rho}{\partial z} + \left[A\frac{\partial^2 \rho}{\partial z^2}\right] \tag{21}$$

$$0 = \frac{\partial u}{\partial x} + \frac{\partial v}{\partial y} + \frac{\partial w}{\partial z}, \tag{22}$$

$$0 = -fv - \frac{1}{\rho_o}\frac{\partial p}{\partial x} + \frac{1}{\rho_o}\frac{\partial \tau^x}{\partial z}, \tag{23}$$

$$0 = fu - \frac{1}{\rho_o}\frac{\partial p}{\partial y} + \frac{1}{\rho_o}\frac{\partial \tau^y}{\partial z}, \tag{24}$$

$$0 = \frac{\partial p}{\partial z} + g\rho. \tag{25}$$

The Coriolis parameter f is $f(y)$ via the β-plane approximation, Eqn. (5), which is crucially important in what follows. There are two steady forces recognized here, the horizontal gradient of the hydrostatic pressure, p,

$$p(x, y, z) = \int_{-z}^{\eta(x,y)} g\,\rho(x, y, z)\,dz,$$

which, like the velocity components, is regarded as an unknown. A second important force is the vertical gradient of a turbulent momentum flux,

$$\tau^x(x, y, z) = \rho_o < u'(x, y, z, t)w'(x, y, z, t) >$$

where the brackets $<\quad>$ indicate a time average over tens of minutes. The small scale, three-dimensional motions u', w' that propagate a turbulent momentum flux are outside the scope of a large scale circulation model. The surface value, $\tau_o = \tau(x, y, z = 0)$, is presumed to be known from observations of wind over the oceans, i.e., τ_o is said to be the wind stress (Fig. 3).

Given that the momentum balances are steady and linear, the right hand side of (23) and (25) may be written in terms of geostrophic and Ekman velocity components, say for the meridional component,

$$v_{geo} = \frac{1}{\rho_o f}\frac{\partial p}{\partial x} \quad \text{and} \quad v_{Ek} = -\frac{1}{\rho_o f}\frac{\partial \tau^x}{\partial z}$$

with no loss of generality, and define the sum to be the balanced velocity,

$$v_{bal} = v_{geo} + v_{Ek},$$

30

just as before. The meridional transports associated with these velocities are

$$M_{bal}^y = M_{geo}^y + M_{Ek}^y \tag{26}$$

where

$$M_{geo}^y = \int_{-d_{geo}}^0 v_{geo} dz \quad \text{and} \quad M_{Ek}^y = \int_{-d_{Ek}}^0 v_{Ek} dz = -\frac{1}{\rho_o}\frac{\tau_o^x}{f}. \tag{27}$$

The lower limit of depth in these transport integrals is significant. The geostrophic velocity of the major, upper ocean gyres is appreciable down to the depth of the lower main thermocline, d_{geo} is O(1000 m), and geostrophic currents associated with the global-scale overturning circulation extend over the full depth water column, noted in the discussion of Fig. (1). The Ekman velocity will be significant within an upper ocean surface layer that is mixed by the turbulent stress imposed at the surface by the wind. In density-stratified regions, such as the subtropical gyre, this Ekman layer may be as deep as the top of the seasonal thermocline, d_{Ek} is O(100 m), and hence almost always much less than d_{geo}. This important effect of stratification is something to come back to when it is time to consider what is missing from a shallow water model (Sec. 8.3).

Vorticity balance. Assuming that the wind stress on the sea surface is given, then the Ekman transport is also known. The geostrophic transport remains completely unconstrained, however, and so we can not go any further with momentum balance and continuity alone. To find out what can be learned about this system, it is very helpful to form the vorticity balance: take the partial x derivative of (25) and subtract the y derivative of (23); then eliminate the horizontal divergence $\partial u/\partial x + \partial v/\partial y$ using the continuity equation (22). This eliminates the unknown pressure and yields the steady, linear vorticity balance,

$$\beta v_{bal} = f\frac{\partial w}{\partial z} + \frac{1}{\rho_o}\frac{\partial}{\partial z}\left(\frac{\partial \tau^y}{\partial x} - \frac{\partial \tau^x}{\partial y}\right), \tag{28}$$

that holds at all z where (23) - (22) are valid. The detailed depth-dependence of w and of the wind stress-induced momentum flux are not knowable within this system alone, but some relevant boundary values are known; depth-integrate (28) from some depth $z = -d$ up to the sea surface where the wind stress is presumed known, τ_o , and the vertical velocity must vanish, *to wit*, the depth integral of (28) is

$$\beta \int_{-d}^0 v_{bal} dz = -fw(-d) + \frac{1}{\rho_o}\left(\frac{\partial \tau^y}{\partial x} - \frac{\partial \tau^x}{\partial y}\right)\Big|_{-d}^0. \tag{29}$$

If d is deeper than the depth of the surface layer (Ekman layer), then $\tau(-d) = 0$ and all of the wind stress is absorbed within the volume of the integral and so

$$\beta \int_{-d}^0 v_{bal} dz = -fw(-d) + \frac{1}{\rho_o}\left(\frac{\partial \tau_o^y}{\partial x} - \frac{\partial \tau_o^x}{\partial y}\right). \tag{30}$$

Rewriting this using symbols already introduced,

$$\boxed{\beta M_{-d}^y = -fw(-d) + \frac{1}{\rho_o}\nabla \times \tau_\mathbf{o}} \tag{31}$$

31

(and run out of space for subscripts, and so M_{bal} will be understood.) This is very close to the classic Sverdrup relation (1), but includes the vortex stretching effect of the vertical velocity at $z = -d$, $fw(-d)$. With this term included, (31) is as general as Eqns. (23) - (22), and M^y_{-d} of (31) is the balanced meridional transport above $z = -d$ regardless of what the ultimate cause may be, i.e., whether wind-driven locally in the Sverdrup sense or a geostrophic flow associated with the global-scale overturning circulation.

About vertical velocity, w(z). The depth-integrated vorticity equation (31) is not closed as there are two unknowns, the transport M^y_{-d} that we seek, and the vortex stretching term, $fw(-d)$, at the base of the control volume. To estimate the transport requires some form of $w(z)$.

In theories of small scale, three-dimensional motions, e.g., short wind waves on the sea surface, the vertical velocity is treated exactly on par with the horizontal velocity. However, in large scale circulation models, which deal only with low frequency motions, the vertical velocity is treated very differently. The vertical momentum balance is hydrostatic, Eqn. (22), to a very high approximation, and hence $\partial w/\partial t$ is inaccessible, effectively. Instead, $\partial w/\partial z$ is computed diagnostically from the divergence of the horizontal velocity on the basis that the motion is non-divergent in three dimensions. In a somewhat similar way it is not possible to observe the large scale, low frequency vertical velocity in any kind of widely used field measurement as it is simply too small; a very significant vertical velocity is a mere 10 m year^{-1}. A diagnostic computation via the observed horizontal velocity is also problematic given the very small values of horizontal convergence compared with estimation errors. The saving grace in all of this is that we can claim to know the boundary values of the vertical velocity at the sea surface, $w(z = 0) = 0$, as already noted, and at the sea floor, $w(z = -b) = 0$, with b the depth of a presumably flat sea floor.

The model experiments discussed in Secs. 3 and 6 indicate two possible forms for $w(z)$ and d discussed briefly. The point is to show that a very wide range of velocity profiles can be consistent with Sverdrup transport. First, rearrange Eq. (28) to solve for fw, and integrate from the surface downward,

$$fw(z) = \beta \int_0^z v_{bal}\, dz + \frac{1}{\rho_o}\left(\frac{\partial \tau_o^y}{\partial x} - \frac{\partial \tau_o^x}{\partial y}\right) - \frac{1}{\rho_o}\left(\frac{\partial \tau^y(z)}{\partial x} - \frac{\partial \tau^x(z)}{\partial y}\right). \tag{32}$$

For this purpose, imagine a thick surface layer and specify that the depth-dependence of $\tau(z)$ is a linear decrease from the surface value to zero at the depth of the surface layer, $z = z_{Ek} = -0.2$. This linear decrease is equivalent to a constant wind stress acceleration within the surface layer. Assume that the local wind stress is zero, and that the wind stress field has negative curl. This will cause a converging Ekman transport and a downward vertical velocity (the blue line of Fig. (15 left)), often called Ekman pumping, that is zero at the sea surface and has a maximum at the base of the Ekman layer, $z = -0.2$. At depths below the surface layer, there is no additional divergence due to the Ekman transport, and hence the vertical velocity due solely to the wind stress curl is constant down to the sea floor. In order that w vanish at the sea floor, some additional source of divergence and thus another contribution to the vertical velocity is required — the beta effect acting upon a balanced meridional current (geostrophic only below the Ekman layer). Assuming that the vertical velocity due to Ekman pumping is downward (negative)
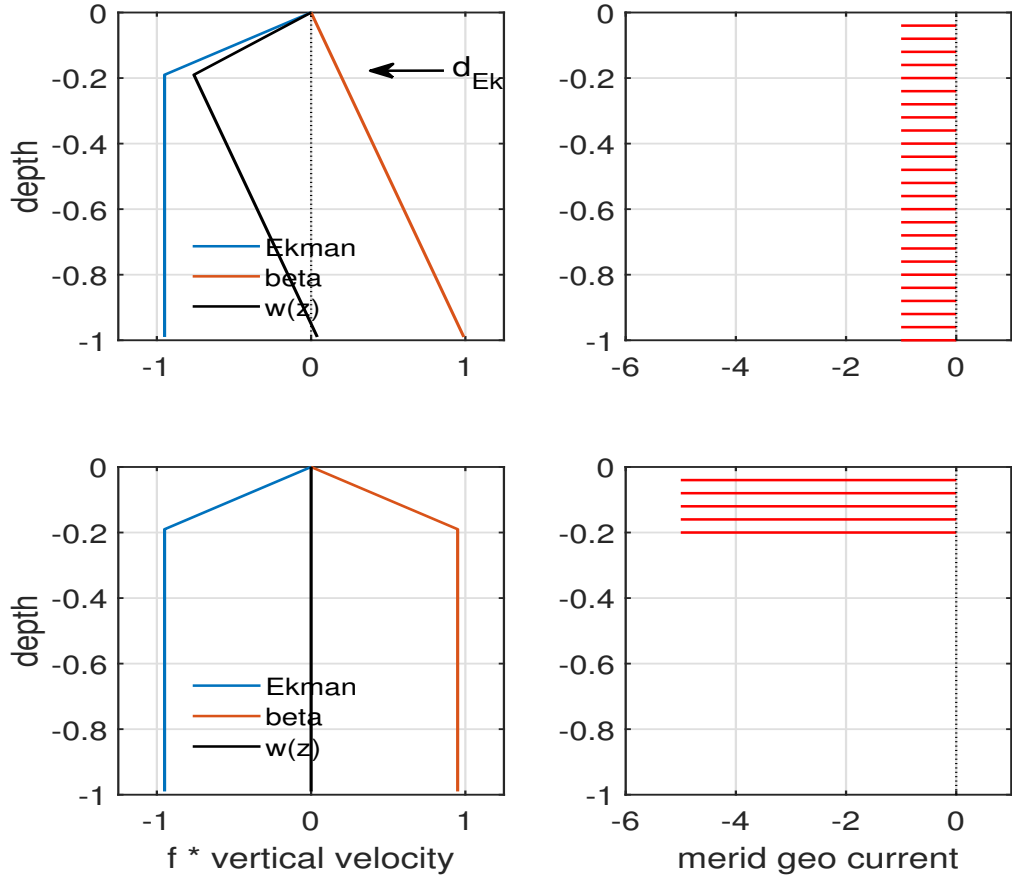
Figure 15: Schematic vertical velocity and gesotrophic velocity profiles that will be encountered in upcoming model experiments. In both cases the depth of the Ekman layer is taken to be $-d_{Ek}$ = -0.2, and the presumed flat sea floor is at $z = -1$. The Ekman transport is presumed to vanish. The vertical velocity associated with wind stress curl is the blue line, which vanishes at the sea surface. In these examples the Ekman-induced vertical velocity is downward, as in the subtropical gyre, and hence the balanced (geostrophic) current must be southward. (**upper**) Barotropic Sverdrup transport. Assuming a geostrophic current that is uniform with depth (sketched at right), the vertical velocity associated with the beta effect is the red line, which vanishes at the sea surface. The sum of the Ekman and the beta-induced vertical velocity is $w(z)$, the black line, which must vanish at the sea surface and at the sea floor. This determines the amplitude of the geostrophic current, -1 in this case. (**lower**) Baroclinic and surface-trapped Sverdrup transport. In this example, the geostrophic current is confined to the surface layer. In this case, w vanishes throughout the water column, and the geostrophic current has an amplitude of -5.

then the countervailing vertical velocity due to the beta effect must be upwards (positive) requiring that $\partial v/\partial y > 0$ and thus a southward flow (Fig. 13). Just how that southward (Sverdrup) flow is distributed in the water column is the issue. Inspection of field data in Sec. 1.1.2 led to the purely empirical result $w(d_o) = 0$ at $d_o = 1200$, and here are two other extreme possibilities that will rise in model experiments to come. For this purpose, assume that $f = \beta = 1$ and that the water column has a thickness of 1. Just for illustration, assume that the wind stress curl yields a vertical velocity $w(-0.2) = -1$. In order to satisfy the sea floor boundary condition, the beta term integrated down to the sea floor must then be the opposite, $+1$.

Barotropic Sverdrup transport, d $=$ b. One possibility is that the balanced current could be uniform with depth and with an amplitude -1, Fig. (15, upper). In that case $d = b$, and the transport integral over the full water column is given by the Sverdrup relation. While the vertical velocity will tehn vanish at the sea floor, at most depths above the sea floor w will be non zero. The velocity may be almost exactly geostrophic and the transport very accurately Sverdrupian, and yet the system will not be in a true steady state since the density will still be evolving, albeit slowly, on account of vertical advection, Eqn. (21). This is what we will find at short times (weeks to months) in experiments with a three layer model that includes an active lower layer and a free sea surface (Section 6). Hence, barotropic Sverdrup transport is quite possible, though it is not observed in the long-term averages of ocean field data.

Surface-trapped, baroclinic Sverdrup transport, d $=$ d$_{\text{Ek}}$. Another possibility consistent with the Sverdrup relation is that the balanced current could be baroclinic and confined to the surface layer. In that event, the current must have an amplitude of -5. This configuration yields a vertical velocity that is zero throughout the water column and so could be literally steady. This surface-trapped Sverdrup regime occurs by default in the single layer model as noted in Sec. 1.5.2, and it also arises in the solution of the three-layer model at very long times (decades after startup, Sec. 6). Interesting though it is, this surface trapped solution is not consistent with the inferred depth scale from field observations, since it is edthat d_{Ek} is O(100) m, and considerably less than the roughly 500 m inferred from field data (Sec. 1.1.2).

3.3   The Sverdrup relation is valid widely, but not everywhere

The limitations of the Sverdrup relation are emphasized in much of what follows, but there should be no doubt of its utility — given only the Sverdrup relation and the curl of the wind stress, one can predict meridional transport that is in accord with some of the major features of the upper ocean circulation. Notably, the meridional transport expected from a negative stress curl (clockwise rotating wind stress as occurs over the subtropics of the North Atlantic, Fig. 3) will be accompanied by a high of SSH and southward meridional flow, as indeed does occur, and evident from Figs. 1 and 2. A counterclockwise wind field and thus positive stress curl is expected to produce northward meridional flow and a low of SSH, which is consistent with observations of the subpolar basin (Fig. 2).

An informal, semi-quantitative test of the Sverdrup relation may be made using the absolute current profiles of Fig. (4) together with a more detailed look at the wind stress curl along 32 N (Fig. 9). The current profiles have a transport per unit width

$$M^y = \int_{-d_o}^{0} v\, dz$$

of from -5 to -3 m^2 sec^{-1}, with larger values toward the western side of the basin. The annual average wind stress curl is about $\nabla \times \tau = -1.0$ to -0.5×10^{-7} N m^{-2}, and again with larger values to the west (Fig. 9). The expected Sverdrup transport is thus about -5.1 to -2.5 m^2 sec^{-1}, which is roughly consistent with the observed, upper ocean meridional transport. It appears that

$$M^y \approx M^{Sv}$$

regionally, across the center of the North Atlantic subtropical gyre.

The basin-wide volume transport will often be of special interest,

$$N^y = \int_{basin} \int_{-d_o}^{0} v\, dz\, dx \approx -28 \text{ Sv},$$

and of course it is southward. The very widely used (though non-SI) unit of volume transport is (what else?) the Sverdrup, 1 Sv = 10^6 m^3 sec^{-1}. The basin-wide Sverdrup transport estimated from the long term averaged wind stress curl at this latitude is similar,

$$N^{Sv} = \frac{1}{\rho_o \beta} \int_{basin} \nabla \times \tau \ dx \approx -30 \text{ Sv}.$$

(This comparison ignores the contribution of Ekman transport to the Sverdrup transport which is very small at this latitude, but not everywhere. More on this below.) From this generally favorable comparison of observed (geostrophic) and Sverdrup transports, both basin-wide and regionally, we can be fairly confident that the Sverdrup relation plus the known wind stress curl gives a good account of the meridional, upper ocean transport in the interior part of the North Atlantic subtropical gyre. Notice that to evaluate the observed transport required the specification of the lower limit of Sverdrup flow, here $d_o \approx 1200$ m.

Modern observational methods and analyses have made it possible to make very detailed, quantitative tests of the Sverdrup relation over almost the entire, global ocean.[10] In a nutshell, these studies concur that the Sverdrup relation is reasonably accurate (to within about 25%) over most of the interior of the North Atlantic and North Pacific subtropical gyres, provided that winds and currents are

---

[10]Three excellent, observation-based studies of the Sverdrup relation are by Gray, A. R. and Riser, S. C., 2014, 'A global analysis of Sverdrup balance using absolute geostrophic velocities from Argo', *J. Phys. Oceanogr.*, 1213-1229, doi: 10.1175/JPO-D-12-0206.1, and by Wunsch, C., 2011, 'The decadal mean ocean circulation and Sverdrup balance', *J. Mar. Res.*, **69**, 417-434. online at dspace.mit.edu/openaccess-disseminate/1721.1/74048 and by Thomas, M. D. et al., 2014, 'Spatial and temporal scales of Sverdrup balance', *J. Phys. Oceanogr.*, **44**, 2644-2660. doi: 10.1175/JPO-D-13-0192.1

averaged over multi year periods and over horizontal scales of O(500 km) or greater, as done above. The Sverdrup relation is not valid near western boundary currents (wbc), which is no surprise, nor is it valid in the northeastward extension of the subtropical wbc (Gulf Stream) into the subpolar basin (North Atlantic Current). The subpolar gyres of the North Pacific and North Atlantic have the expected sense of the circulation (counterclockwise), but there is a poor correlation between the magnitude of the Sverdrup transport and the observed meridional transport. The difference is especially marked in the northerly half of the North Pacific subpolar gyre, where the observed meridional transport is considerably less than the expected Sverdrup transport.

4   Shallow water models of wind-driven circulation

The shallow water model introduced in Part 2 can be made into a useful tool for studying some important facets of the wind-driven circulation by 1) defining an appropriate domain and boundary conditions, 2) adding a new term that represents wind forcing, and 3) including a very simple form of dissipation. A straightforward extension to multiple layers including an active sea surface is also described.

4.1   Boundary conditions for a closed basin

The ocean domain is taken to be a square basin with sides of length $2L$ centered on 30 ^{o}N. Rotation is treated by a β-plane approximation and the basin size is then chosen so that the southern boundary will correspond to the equator, $f = 0$. Given $\beta(30^o)$, this requires $L = 3600$ km. The resulting basin width, $2L = 7200$ km, is roughly comparable to the average width of the North Atlantic Ocean, but is only about half the width of the mighty Pacific Ocean. The intention is to model a circulation that is self-contained within this basin, and so the boundaries are made impermeable by setting the normal component of velocity to zero,

$$\mathbf{V} \cdot \mathbf{n} = 0, \tag{33}$$

on all of the boundaries.

What this formulation ignores is that the southern and northern boundaries of the real North Atlantic basin are, of course, open, and there is a significant poleward flow of warm water from the southern hemisphere into and through the North Atlantic basin. In the equatorial region this occurs largely within a western boundary current, usually called the North Brazil Current (Fig. 2 and footnote 5). Within the subtropical gyre this warm upper ocean flow makes up a part of the Gulf Stream, and is in some respects indistinguishable from the basin-scale wind-driven, Sverdrup flow. At the northern boundary, some of this warm flow continues poleward into the Norwegian-Greenland Sea as the North Atlantic Current (or

Drift). This shallow, warm, poleward flow is balanced volumetrically by a deep, cold equatorward flow, also in western boundary currents. The resulting meridional flux of warm and cold water is a very important consequence of the global-scale, meridional overturning circulation. The overturning circulation is not driven directly by basin-scale winds, as are the upper ocean gyres of Fig. 2, and an overturning circulation does not arise in the present experiments.

4.2 Initial density and velocity

There are three sensible ways to initialize density stratification and velocity depending upon the scope and goals of the experiment.

First, imagine that the aim is to model all aspects of the circulation, including the existence and scale of the main thermocline. In that case it would be appropriate to start with a homogeneous ocean, and to apply surface fluxes of heat, fresh water and wind stress that might eventually yield a main thermocline. An ambitious and interesting problem, but not attempted here.

Second, suppose the goal is to make the best possible estimate of the circulation, using every available asset, including first order observations of density, SSH, etc. This is the reanalysis project, and is an appropriate way to model and estimate higher order properties of the circulation such as meridional heat transport and secular changes. Not the present goal.

Third, the middle ground occupied here is to take for granted that the main thermocline exists, but that it is flat, initially, throughout the basin, and that the velocity is zero,

$$h(x,y,t=0) = constant \;\; and \;\; \mathbf{V}(x,y) = 0 \;\; \text{for all} \;\; (x,y). \tag{34}$$

For a single layer model, $h = 500$ m, and the density difference $\delta\rho = 2$ kg m^{-3} are reasonable, but more on the stratification in Sec. 3.6. The aim of these experiments will be to see how and how fast this stratification and velocity will adjust to an imposed wind stress.

4.3 Wind stress and its curl

The energy source in these experiments is a wind stress, $\tau(x,y)$, a tangential force per unit area imposed on the sea surface (the subscript $_o$ needed in Sec. 1.3 has been dropped since only the surface value of wind stress will be relevant from here on). The wind stress field has to be specified from outside the model, and here it will be represented by an idealization of the time-mean wind stress that has been

computed from observed winds over the oceans, Figs. (8 and 3).[11] So far as the Sverdrup relation is concerned, the crucial property of the wind stress field is the curl, $\nabla \times \tau(x, y)$. The shallow water model requires the wind stress itself, and here, just to keep it simple, we will specify the zonal component τ^x only, and assume that τ^x is independent of x, thus

$$\tau^x(y) = \xi \sin(n\pi y/L), \tag{35}$$

where the amplitude ξ is a positive constant. For the standard case of Sec. 3, $n = 1$, and the wind stress is eastward over the northern half of the basin, which mimics westerly winds, and westward on the southern half of the basin, i.e., easterlies (Fig. 16). The amplitude is taken to be $\xi = 0.1$ Pa, or about what is estimated for the mean wind stress by the westerlies. In the experiment of Sec. 3, this wind stress field is assumed to be constant in time once it is switched on. (In Sec. 5.1, the amplitude, ξ, will be made to oscillate with an annual cycle, and in Sec. 5.3 the wind stress will be made meridional.)

A very important parameter of (35) is the meridional length scale of the wind field; for n = 1,

$$L_\tau = L/n\pi \approx 1200 \text{ km}.$$

This is comparable to though a little less than two other important horizontal scales in this problem, the basin scale

$$L = 3600 \text{ km},$$

and the planetary scale on which f varies,

$$R_f = R_E/2 \approx 3300 \text{ km},$$

where R_E is the radius of the Earth. All of these length scales are much greater than the natural horizontal length scale of the baroclinic ocean, the baroclinic radius of deformation at latitude = 30 deg,

$$R_d \approx 40 \text{ km}.$$

The wind stress is applied to the surface layer of the model ocean as if it was a body force absorbed evenly throughout the surface layer. Thus the acceleration due to wind stress alone is just

$$\frac{D\mathbf{v_1}}{Dt} = \frac{\tau}{\rho_o h_1}, \tag{36}$$

which is a valid approximation of the full momentum balance for very short times, $t \ll 1/f$, a few hours or less. In a shallow water model, $d_{Ek} = h_1$, and here we have chosen $h = 250$ m (three layer model), or

---

[11]There are now more than a dozen wind stress climatologies that are consistent at the semi-quantitative level needed here (see Townsend, T. L., H. E. Hurlburt and P. J. Hogan, 2000, 'Modeled Sverdrup flow in the North Atlantic from 11 different wind stress climatologies', *Dyn. Atmos. Oceans*, **32**, 373-417.) The differences in detail between the various wind stress climatologies make an easily detectable and in some ways important difference in the computed Sverdrup flow, as does the basin topography.

500 m (single layer reduced gravity model), in order to have a realistic baroclinic wave speed. In the real, stratified ocean, d_{Ek} is less than this, typically 25 - 100 m. The Ekman current in this model is thus considerably weaker than in the real ocean, but the Ekman transport and the Sverdrup transport are the same whether the wind stress is absorbed in a comparatively thin surface layer (as actually occurs) or over the entire upper ocean layer that is wind-driven in the Sverdrup sense, as happens in a shallow water model.

The curl of this wind stress is

$$\nabla \times \tau(x, y) \;=\; -\frac{\partial \tau^x}{\partial y} \;=\; -\frac{n \pi \xi}{L} \cos{(\pi y / L)}, \tag{37}$$

has an amplitude $\xi / L_\tau \simeq 0.8 \times 10^{-7}$ N m^{-3} ($n = 1$). This is comparable to typical values of stress curl seen in Fig. (3), but less than the maximum values, which are roughly 2×10^{-7} N m^{-3}. The sign of the wind stress curl defines three regions: a central subtropical region where the stress curl is negative (clockwise turning), and tropical and subpolar regions where the curl is positive (anti-clockwise), Fig. (16).

This idealized stress field is perhaps least realistic for the tropical region insofar as τ^x goes to zero on the equator where observations indicate a fairly weak but nonzero westward wind stess. This error in the tropical winds is left in place because the goal is not so much a realistic simulation of the observed ocean circulation — which would require much more than just a better wind field — but rather to investigate how the wind-driven circulation varies with latitude. The idealized stress field Eqn. (35) is appropriate to this goal since the wind stress curl magnitude of (35) is the same over the three regions (tropical, subtropical and subpolar). β is also the same, and hence so too is the Sverdrup transport. The actual transport of the subpolar and tropical gyres is, however, *not* the same as Sverdrup transport because of zonal boundary effects that extend many hundreds of kilometers into the tropical and subpolar gyres (Sec. 5.2.3).

4.4   An expedient parameterization of drag on ocean currents

With a wind stress included, and if the intention is to integrate up to a possible steady state, then there has to be some mechanism to dissipate the energy and potential vorticity that are supplied by the wind. The present model follows the classic treatment by Stommel (1948)[1] in choosing a linear drag that is proportional to and anti-parallel to the velocity,

$$drag \;=\; -rh_o \mathbf{V}, \tag{38}$$

sometimes called Stokes drag. This has the dimensions of a stress/density, and the resulting acceleration is $-rh_o \mathbf{V}/h$ (as in the single particle model of Part 1, Section 5, aside from varying layer thickness). The
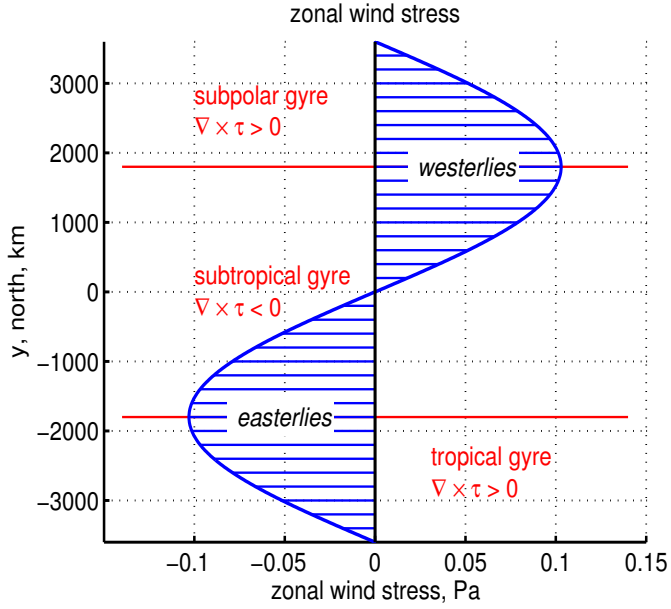
Figure 16: An idealized, zonal wind stress field that is applied to the shallow water model. The horizontal red lines appear in subsequent figures to show the axes of the easterly and westerly wind maxima, and thus the boundaries of the stress curl — negative (clockwise) in the large subtropical region between the westerly and easterly axes, and positive (anti-clockwise) over the smaller tropical and subpolar regions. These red lines correspond closely to the gyre boundaries.

coefficient r is taken to be $r = 1/(15 \text{ days})$, the smallest value of r that will allow the ocean circulation in this system (wind stress included) to reach a near steady state. Given a nominal layer thickness, $h \approx h_o$, the Ekman number at 30 ^{o}N is $E = r/f \approx 0.01$. This E seems quite small, but nevertheless, the model dynamics are almost certainly much more viscous overall than is the real ocean. Some later experiments will reveal find how this value of r is related to the natural width of the western boundary current, the radius of deformation.

In some contexts it might be argued that the Stokes drag represented by Eqn. (38) is a crude treatment of bottom drag. However, that is not plausible here since the active layer is not imagined to be in contact with a sea floor. It is probably better to think of the Stokes drag as nothing more than the simplest form of a drag or dissipation process that permits a steady state in this model.

4.5   Momentum and vorticity balances

With wind stress and drag included, the shallow water continuity (thickness balance) and momentum equations (derived in Part 2) are

$$\frac{Dh}{Dt} = \frac{\partial h}{\partial t} + \mathbf{V} \cdot \nabla h = -h \nabla \cdot \mathbf{V}, \tag{39}$$

$$\frac{D\mathbf{V}}{Dt} = \frac{\partial \mathbf{V}}{\partial t} + \mathbf{V} \cdot \nabla \mathbf{V} = -\nabla P / \rho_o - f \mathbf{k} \times \mathbf{V} + \frac{\tau}{\rho_o h} - \frac{rh_o}{h} \mathbf{V}. \tag{40}$$

The P is hydrostatic pressure anomaly defined in the next subsection. Notice that the thickness balance (39) is adiabatic in the sense that the thickness can change only by way of a divergent thickness flux, and

hence the net (basin integral) thickness is conserved.[12] This is not true for the momentum balance because of the wind stress source term and the Stokes drag dissipation term.

The shallow water potential vorticity is

$$q = \frac{\nabla \times \mathbf{V} + f}{h},$$

(41)

and the q-balance is

$$\frac{Dq}{Dt} = \frac{\partial q}{\partial t} + \mathbf{V} \cdot \nabla q = \frac{1}{\rho_o h}\nabla \times \frac{\tau}{h} - \frac{rh_o}{h}\nabla \times \frac{\mathbf{V}}{h}.$$

(42)

Part 3 studied free Rossby waves that could be described via the mechanisms of q conservation, $Dq/Dt = 0$. Rossby wave-like motions are possible also in (42) and are a crucial part of the time-dependent dynamics discussed in Sec. 3.3.

4.6   Models of stratification and pressure

The last task is to connect the hydrostatic pressure P with the mass field, i.e., the stratification. Two models are used here.

4.6.1   Single layer, reduced gravity model, 1l-rg

The stratification model used most extensively exactly the shallow water, single layer, reduced gravity model of Parts 2 and 3, *viz.*, a single active upper ocean layer above a quiescent (infinitely deep) abyssal layer. In that event, the hydrostatic pressure anomaly within the upper ocean layer is just

$$P = g\delta\rho(h - h_o)$$

(43)

which gives a high pressure (anomaly) where the layer thickness is large. The equivalent SSH, which is useful for comparison to the observed SSH (Figs. 1 and 2) is just

$$\eta_1 = \frac{\delta\rho}{\rho_0}(h - h_o).$$

(44)

---

[12]This adiabatic property is especially convenient for some diagnostics of the time-changing stratification. However, it is also a liability, insofar as the layer thickness given by (39) can vanish under some plausible forcing regimes, especially at high latitudes. Vanishing layer thickness means instant death for a numerical integration. A partial remedy is to start with a fairly thick initial layer, 500 m, as is done here. Better would be the inclusion of a vertical mixing process that kept the upper layer thickness finite at all times, but which is not attempted here.
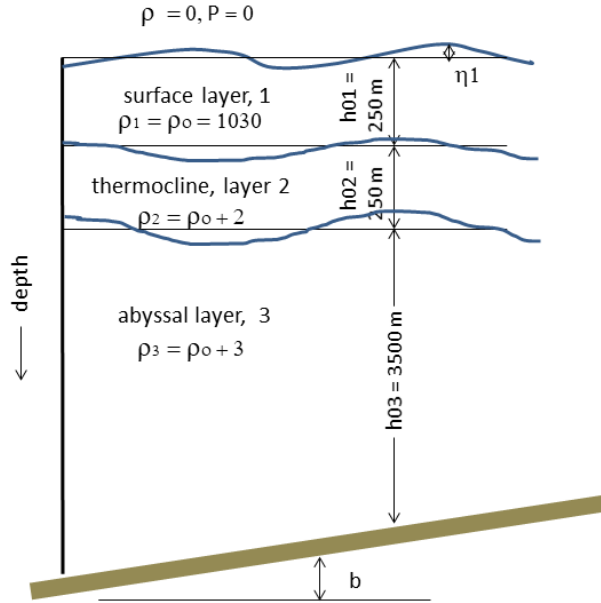
Figure 17: A three layer representation of the density stratification of the open ocean. The density and the thickness of each layer is noted. These thickness and density values are most apropos the subtropical ocean, but are presumed to hold throughout the basin. In this study the bottom depth b is presumed constant, i.e., a flat bottom.

The initial thickness is chosen to be fairly large, $h_o = 500$ m, and the density difference fairly small, $\delta\rho = 2$ kg m^{-3}. The nominal gravity wave speed is thus $= \sqrt{g\delta\rho h_o/\rho} = 3$ m sec^{-1}, which is a realistic baroclinic gravity wave speed for the subtropics, but a little high for the tropics and subpolar regions of the ocean. The radius of deformation at 30° is $R_d = 42$ km, and the equatorial radius of deformation is $R_{deq} = \sqrt{C/\beta} = 400$ km.

4.6.2 Three layer, free surface model, 3l-fs

In this somewhat more realistic model, the stratification is represented by two upper ocean layers, and a comparatively thick abyssal layer (Fig. 17). This is still quite a truncated representation of the ocean's stratification, but it is sufficient to make a few important points (Sec. 8). The surface layer, h_1, is presumed to absorb all of the wind stress. Layer 2 is the thermocline, which follows the same momentum balance as does layer 1, though with zero wind stress, and layer 3 is the thick abyssal layer, same comment. In general, the thickness of the abyssal layer should include a significant term due to the spatially variable sea floor depth, which for now is taken to be uniform, $b = 0$. This three layer model is a straightforward generalization of the shallow water (layered) model of Parts 2 and 3, sometimes referred to as a stacked shallow water model. The initial thickness and the constant density difference, $\delta\rho$, across the top of these layers is taken to be

h_{0i}, m	$\rho_i, \text{kg m}^{-3}$	$\delta\rho_i, \text{kg m}^{-3}$
250	1030	1030
250	1032	2
3500	1033	1

The density and pressure of the overlying atmosphere are presumed to vanish and hence the density contrast across the sea surface, the top of layer 1, is $\delta\rho_1 = \rho_o = 1030 \text{ kg m}^{-3}$, the nominal density of sea water. The density contrast across the top of layers 2 and 3 is very much less, $\delta\rho_2 = 2 \text{ kg m}^{-3}$ and $\delta\rho_3 = 1 \text{ kg m}^{-3}$. In that sense, the ocean is very weakly stratified internally. Nevertheless, this internal stratification is of first importance for many oceanic phenomenon. The surface layer thickness is taken to be 250 m to delay the occurrence of $h \to 0$, and so is too large by a factor of about five. Hence the wind-driven surface layer currents in this model are weak compared to observations.

Layer thickness is a conserved quantity, barring vertical mixing (which undoubtedly occurs), meaning that the thickness of a given layer can change only if there is a divergence of volume flux within that layer, i.e.,

$$\frac{\partial h_1}{\partial t} = -\left(\frac{\partial (h_1 u_1)}{\partial x} + \frac{\partial (h_1 v_1)}{\partial y} \right), \tag{45a}$$

$$\frac{\partial h_2}{\partial t} = -\left(\frac{\partial (h_2 u_2)}{\partial x} + \frac{\partial (h_2 v_2)}{\partial y} \right), \tag{45b}$$

$$\frac{\partial h_3}{\partial t} = -\left(\frac{\partial (h_3 u_3)}{\partial x} + \frac{\partial (h_3 v_3)}{\partial y} \right). \tag{45c}$$

The horizontally-varying pressure anomaly is due to the displacement of the density surfaces away from their nominal, resting, flat state. From the bottom up, the interface displacements are

$$\eta_3 = h_3 - h_{o3} - b, \tag{46a}$$

$$\eta_2 = \eta_3 + h_2 - h_{o2}, \tag{46b}$$

$$\eta_1 = \eta_3 + \eta_2 + h_1 - h_{o1}. \tag{46c}$$

The motions of interest have very gentle accelerations compared to g, and so the pressure anomaly that accompanies the displaced density field may be assumed hydrostatic, i.e., due to the weight of the overlying water column. The hydrostatic pressure anomaly within each layer is then, from the surface layer down,

$$P_1 = g\rho_o \eta_1, \tag{47a}$$

$$P_2 = P_1 + g\delta\rho_2 \eta_2, \tag{47b}$$

$$P_3 = P_2 + g\delta\rho_3 \eta_3. \tag{47c}$$

The height of a given density interface thus depends upon the thickness of the fluid layers below, while the pressure depends upon the displaced density surfaces above. This bottom-up density/thickness relationship and top-down pressure/density relationship is what you would expect physically from hydrostatic pressure.

4.7   Appendix to Sec. 3: Normal modes of the 3l-fs model; one fast, two slow

The description of the motions that develop in the 3l-fs system may be aided by reference to the normal modes of the system. In fact, the normal modes show up fairly distinctly in the solutions that follow. A method for computing the normal modes was discussed in Part 2, Sec. 4.2 (and implemented via the Matlab script twolayer_eig.m available online, Sec 7.1) and so we will go straight to the results, the eigenvectors of velocity and thickness, and the eigenvalues that are the gravity wave (non-rotating) phase speeds of the modes,

Barotropic mode
gravity wave phase speed $C \approx \sqrt{g(h_1 + h_2 + h_3)} = 200$ m sec^{-1}
radius of deformation at 30° N, $R_d = C/f = 2800$ km
long Rossby wave speed at 30° N, $\beta R_d^2 = 142$ m sec^{-1} = 1230 km day^{-1}.

$$\begin{pmatrix} u & h \\ 1 & 0.07 \\ 1 & 0.07 \\ 1 & 1 \end{pmatrix}$$

Baroclinic mode 1
phase speed $\approx \sqrt{g(\delta\rho_2 + \delta\rho_3)(h_1 + h_2)/\rho_o} = 2.9$ m sec^{-1}
radius of deformation, 42 km
long Rossby wave speed, 0.033 m sec^{-1} = 2.9 km day^{-1}.

$$\begin{pmatrix} u & h \\ 1 & -0.7 \\ 0.41 & -0.3 \\ -0.1 & 1 \end{pmatrix}$$

Baroclinic mode 2
phase speed $\approx \sqrt{g\,\delta\rho_3\, h_1/\rho_o} = 1.5$ m sec^{-1}
radius of deformation, 22 km
long Rossby wave speed, 0.009 m sec^{-1} = 0.8 km day^{-1}.

$$\begin{pmatrix} u & h \\ 1 & 1 \\ -1 & -1 \\ 0 & 0 \end{pmatrix}$$

The eigenvectors of velocity are normalized so that the surface layer has an amplitude of 1; the thickness eigenvectors are normalized so that the largest amplitude in any layer is 1, Fig. (18).

Compared with the reduced gravity model, the crucial new property of this system is that it supports a barotropic gravity wave having a very, very fast phase speed, 200 m sec^{-1} ≈ 1700 km day^{-1}. Thus, a barotropic gravity wave can traverse an entire ocean basin in a few days, vs many months for a baroclinic wave. The corresponding long Rossby wave is almost as fast, ≈ 1200 km day^{-1}. The interface displacements of a barotropic mode are in phase with depth, but are largest at the sea surface and decrease linearly to zero at the bottom (not apparent in this figure). The pressure gradient is thus determined almost entirely by the displacement of the sea surface, and the associated barotropic velocity is essentially uniform with depth. When we say 'barotropic', this is what is intended. Such a barotropic motion is the only thing possible in a model having no internal stratification whatever. In this case there is internal stratification, and so there are also two baroclinic normal modes that, are, by comparison, quite sluggish, having phase speeds approx. 3 m sec^{-1} and 1.5 m sec^{-1}. The velocity in these baroclinic normal modes is depth-dependent, and has vanishing transport when integrated over the full water column. This is the
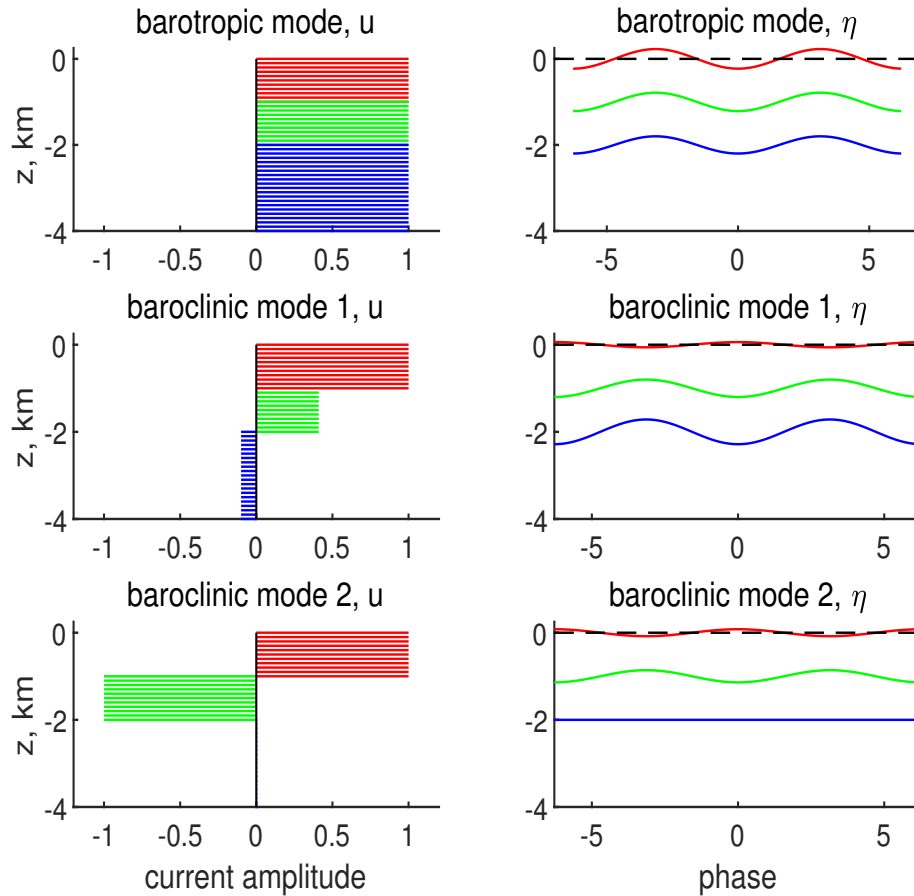
Figure 18: **(left)** Eigenvectors of the velocity from the three layer model. The layer-to-layer relative amplitudes of the velocity eigenvectors are meaningful, but their apparent thickness and thus depth is not to scale in this figure (the upper layer thicknesses have been quadrupled for the purpose of illustration). **(right)** Interface displacement computed from the eigenvectors of thickness by integrating from the bottom up, as in Eqn. (46). The amplitude of the interface displacements is schematic only but the phases are meaningful. For example, in the first baroclinic mode, the surface layer and the thermocline move up and down in phase in a 'sinuous' mode. Baroclinic mode 2 is confined almost entirely to the thermocline and surface layers, and is a 'varicose' mode in which the thickness changes in these layers are of almost equal magnitude and are out of phase.

usual meaning of 'baroclinic'. Baroclinic and barotropic waves can co-exist, or be present in isolation.

These normal modes are orthogonal and span the space, in the sense that any free motions (e.g., any wave) that can occur in the three layer model can be formed as the linear sum of these modes. Since all of the eigenvectors are required to make a complete set, there is no one that is more important than the others. However, the first baroclinic mode does have the most prominent role in the basin-scale adjustment process to an imposed wind, *viz.* the changeover from a (largely) barotropic state that forms very quickly after the wind starts, to a baroclinic, surface intensified state (Sec. 3.3) at much longer times. This is implicit in the choice of parameters of the single layer, reduced gravity model that was intended to mimic the first baroclinic mode of this more complete multi-layered model or of the real ocean.

5 The baroclinic circulation of the 1l-rg solution develops in four stages

Now, finally, we are ready to integrate and find some solutions (!). First up will be the single layer, reduced gravity model (secs. 5, 6 and 7), and then the more complex three layer model (Sec. 8).[13] The wind stress is switched on to full amplitude at time = 0 and held constant for 30 years. This long time is necessary to allow the solution to reach a (nearly) basin-wide steady state.[14] The circulation develops in four more or less distinct, temporal (but noncontiguous) stages that are characterized by the onset of specific phenomenon.

5.1 Stage 1: Short time, local response to the wind

5.1.1 Time scales: fast, slow, and steady

During the first few hours, the current is accelerated down wind at a rate $du/dt = \tau/(\rho_o h)$ (Eqn. 36). The Coriolis force turns the current to the right (northern hemisphere) after a time $1/f$, and hence a scale

---

[13]It would be more efficient of space on paper to if jump straight to the more complex model. But for the purposes of an introduction to this material, it seems (to this author) that it is preferable to start slowly and as simply as possible, and then add complexity. Be assured that everything that you may learn about the 1l-rg solution will be valuable in understanding the more complete results that will follow in Sec. 8.

[14]The wind has been blowing over the real oceans for a very long time. While the resulting circulation is seldom completely steady, nevertheless it isn't time-dependent because of an adjustment to a switched on wind, as occurs in these model experiments. The aim in integrating the model for so long is to be sure to get past the start up transient.
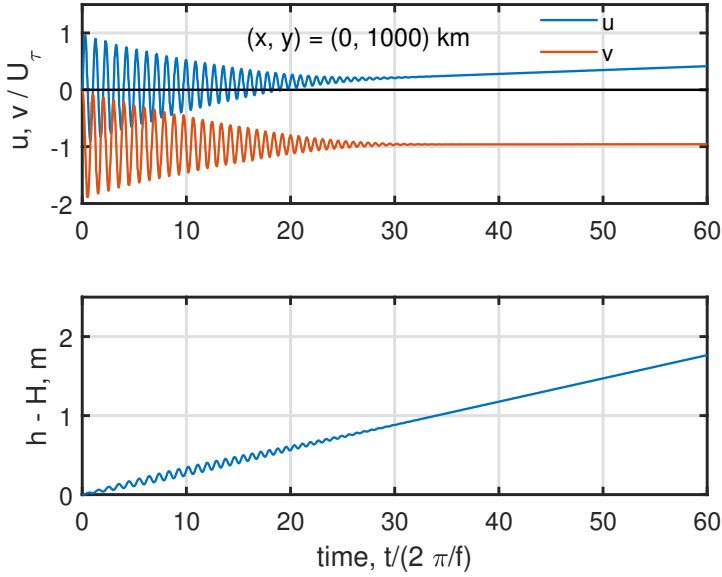
Figure 19: The short time evolution of currents. These data were sampled at 20 min. intervals on the northern side of the subtropical gyre, $(x, y) = (0, 1000)$ km. This site was chosen since there is an appreciable wind stress, $\tau^x = 0.08$ N m^{-2}, which is eastward, and also a significant divergence of the Ekman transport. **(upper)** A time series of east and north current components, u and v. These are shown in units of the wind-driven velocity scale, U_τ. The high frequency oscillations are near-inertial motion; the time-mean (steady) v is southward Ekman flow which in these units has the value -1. **(lower)** Layer thickness anomaly, $h - h_o$, which shows a steady increase at about 15 m year^{-1}. This increase in layer thickness is caused by the convergence of Ekman transport, and the slow increase of the east current seen above is the associated zonal geostrophic flow (discussed in Sec 4.2). Notice the very small but dynamically significant oscillations of thickness in the first several weeks. These are evidence that the high frequency oscillations seen here are best described as near-inertial (very long wavelength) gravity wave motions.

estimate of the wind driven current amplitude that accounts for rotation is just

$$U_\tau = \frac{\tau}{\rho_o \, h f}. \tag{48}$$

The current components and the thickness sampled at a site on the northern side of the subtropical gyre (Fig. 19) display show three distinct time scales. There are fast time scale near-inertial motions having a period $1/f$, which is about a day at mid-latitudes. There is a very slow increase of the zonal current and of the layer thickness that here looks like a linear trend. Over a much longer time (shown below), this will emerge as a low frequency Rossby wave-like motion, and/or a part of the developing basin-scale circulation that is of primary interest. There is also a steady current in the meridional component, Ekman flow, that is the key intermediary between the wind and the basin-scale circulation.

Given the main interest is the large scale, low frequency circulation, then it is reasonable to ask whether it is desirable or necessary to also compute the high frequency phenomenon, the inertial motion. The shallow water system naturally includes both kinds of motions, but the high frequencies can be

47

suppressed easily enough by ramping up the wind stress over a few weeks (vs. the nominal, impulsive start). The resulting low frequency and steady circulation is the same either way the integration is started.[15] Thus, while inertial motion is ubiquitous in the oceans and is very important in some contexts, nevertheless it is not important here, and further discussion has been moved to an Appendix at the end of this section.

5.1.2 Ekman currents and transport.

The wind-driven current has a time-mean (Eqn. 60) that is consistent with Ekman balance modified very slightly by friction,

$$\begin{pmatrix} u \\ v \end{pmatrix} / U_\tau \approx -\left(\frac{1}{1+E^2} \right) \begin{pmatrix} E \\ -1 \end{pmatrix}. \tag{49}$$

This approximate solution for Ekman flow is indistinguishable from the solution computed by the shallow water model. The Ekman currents are present within hours of the start-up, and persist for the duration of the experiment since the wind stress is held steady. The amplitude of the Ekman current is $\propto U_\tau$, and is unrealistically small in the 1l-rg model because the layer thickness, $h_o \approx 500$ m, is much greater than a plausible Ekman layer thickness, more like 50 m. The direction of the Ekman current is approximately perpendicular and to the right of the wind stress, and so is southward at the site shown in Fig. (46) where the wind stress is eastward.

The Ekman transport is

$$M_{Ek}^y = hV_{S1} = -\frac{\tau^x}{\rho_o f} = -\frac{\xi}{\rho_o f} \sin(\pi y/L), \tag{50}$$

and is independent of the layer thickness. At the site shown in Fig. (46), which is equivalent to about 41 N, the Ekman transport is $M_{Ek}^y \approx -1.3$ m^2 sec^{-1}, which is a significant magnitude. To find the consequent *volume* transport, $[l^3 \ t^{-1}]$, this M has to integrated over a horizontal distance, say the width of the North Atlantic basin, to find a volume transport (symbol N) at this y (latitude) of about $N_{Ek} = M_{Ek}2L = -10 \times 10^6$ m^{3}sec^{-1}, or 10 Sv, southward. This is a significant fraction of the total meridional transport at this latitude. Moreover, Ekman transport will be made up from the shallowest and generally the warmest water in the water column, and so makes a very important contribution to the heat flux carried by the ocean circulation. While Ekman transport is significant in its own right, it has an even more important indirect role in generating the changes in layer thickness that lead to geostrophic and Sverdrup transports, discussed in Sec. 5.2 and forward.

---

[15]This important result (no memory of the startup scenario) is consistent with the fundamental notion of the quasi-geostrophic system that the important low frequency motions are not far from geostrophic balance. The quasi-geostrophic system makes approximations (constant layer thickness, and a constant, background f, though with β) that are not consistent with some aspects of the shallow water solutions found here. Most GFD texts[2] include a discussion of quasi-geostrophic theory, and a superb online source aimed mainly at meteorologists is http://www.meteor.iastate.edu/classes/mt411/powerpoint/METR4424qgtheory.pdf

5.1.3 Latitudinal dependence; trouble on the equator?

It is notable that the amplitude of Ekman transport goes as $1/f$, and so for a given wind stress, the Ekman transport is considerably larger in the tropics than in the subpolar region. The same applies for a given pressure gradient and the amplitude of geostrophic currents.

The (near) equatorial region is noteworthy with respect to this latitudinal dependence insofar as $1/f$ is singular, and hence geostrophy and the Ekman relation imply a blowup of equatorial currents. However, the Coriolis force is not a dominant process on or very near the equator, as the Ekman and geostrophic relations presume, and happily, no such a blowup occurs in the numerical model solution. A somewhat trivial and parochial reason is that the wind stress given by Eqn. (35) has been assumed to vanish on the equator. But even with a significant equatorial stress included, which is more realistic of the real ocean, near-equatorial wind-forced currents are effectively limited by a rapid baroclinic response manifested in (or by) equatorial Kelvin wave propagation (Part 3, Sec. 4), which sets up a basin-wide pressure gradient that opposes the wind stress within only a couple of weeks. In other words, something else happens, a Kelvin wave and more, that was not anticipated by the rotational scaling Eqn. (48). In the experiments that discussed here, the circulation very near the equator is a consequence mainly of the larger scale circulation in the tropical gyre, which is the main interest, and so there is not occasion to discuss the (very interesting) equatorial phenomena.

5.2 Stage 2: Locally wind-forced, zonal geostrophic currents

5.2.1 Divergent Ekman transport changes the mass field

While Ekman transport is significant in its own right, it has an even more important indirect role by generating changes in layer thickness (mass field) and thus the pressure field. This indirect effect of the wind is apparent within only a few weeks as a slowly growing change in layer thickness (Fig. 46, lower) that continues for a few hundred or a few thousand days, depending upon location. The sense and the magnitude of the change is predicted well by the thickness tendency due to the divergence of Ekman transport alone (no geostrophic flows, yet) (Eqn. 12),

$$\frac{\partial h_{Ek}}{\partial t} = -\nabla \cdot (h\mathbf{V_{Ek}}) = -\frac{1}{\rho_o}\nabla \times (\frac{\tau}{f}),$$

and in the special case considered here that τ is $\tau^x(y)$ only, then

$$\frac{\partial h_{Ek}}{\partial t} = \frac{1}{\rho_o}\frac{\partial}{\partial y}\left(\frac{\tau^x}{f}\right) = \frac{1}{\rho_o f}\left(\frac{\partial \tau^x}{\partial y} - \frac{\beta}{f}\tau^x\right), \tag{51}$$
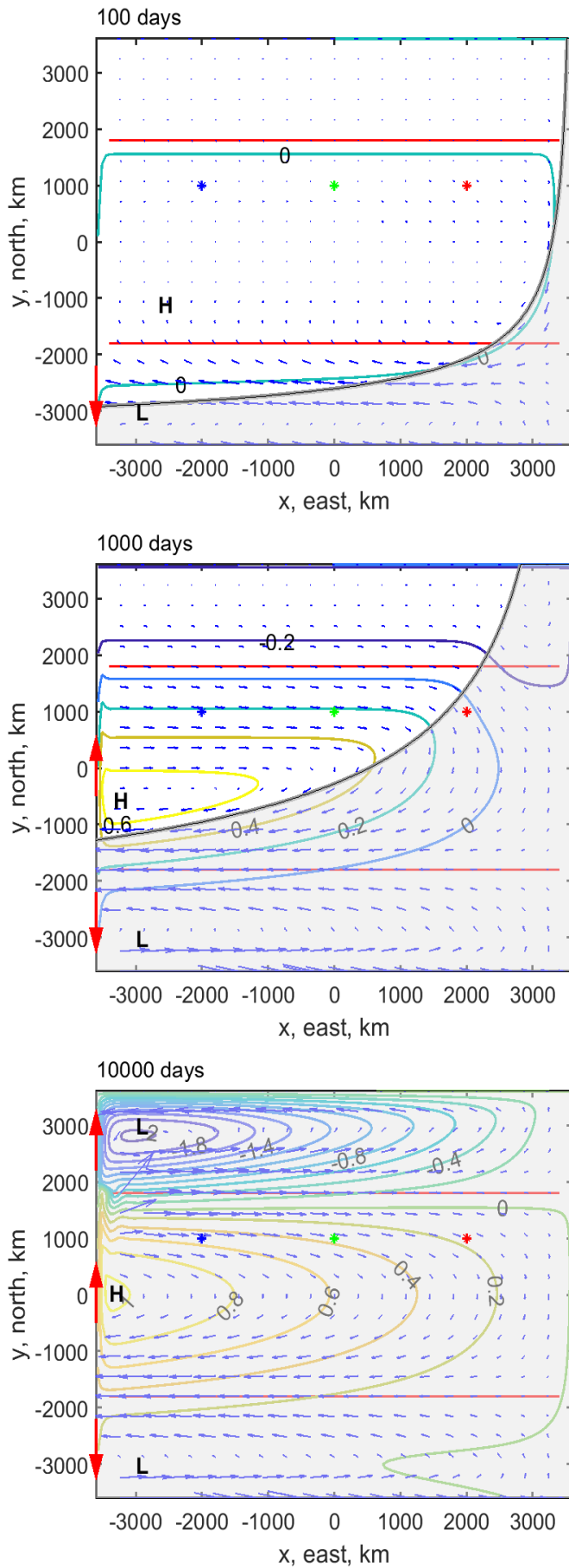
Figure 20: Three snapshots from the basic case, wind-driven experiment computed by the 1l-rg model and sampled at, from top to bottom, 100, 1000 and 10,000 days after the wind stress was switched on. The last time appears to be in a quasi-steady state throughout the interior of the basin. The thin red horizontal lines are the axis of the westerly and easterly wind stress (Fig. 16). The contours are of the inferred SSH anomaly in units of the Sverdrup geostrophic slope (Fig. 22) at basin center times the basin width, $2L$, about 0.4 m in this case. The field of small blue arrows are the current, though with the comparatively very large currents within the wbc omitted (shown in Sec. 3.3.2). The largest currents shown here are approx. 0.3 m sec^{-1}. The sense of the wbc is indicated by the red arrows on the west edge of the model domain. The blue, green and red dots along $y = 1000$ km mark the positions sampled in Fig. (23). The gray shading extends westward from the eastern boundary at the y-dependent speed of a long, baroclinic Rossby wave, $-\beta R_d^2$, and was sketched on top of the solution. Notice that the unshaded region to the north and west of the wave front (in the top two panels) shows mostly zonal currents, said to be the Stage 2 response. The shaded region to the south and east of the wave front is in Stage 3, Sverdrup flow. An animation of these data is threegyres.mp4 included in aCt-videos.zip[??]
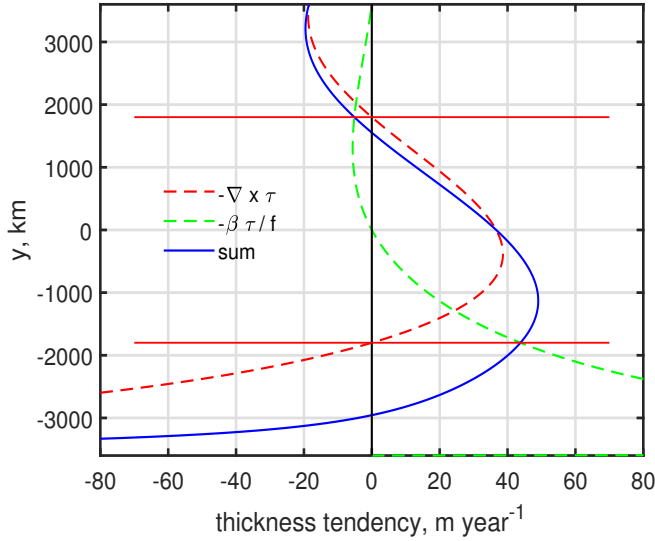
Figure 21: The divergence of the Ekman transport, Eqn. (51) (blue line), given the wind stress field Eqn. (35). Divergence of Ekman transport causes thickness tendency, which is a very significant aspect of the wind forcing on the ocean. At higher latitudes the divergence is due mainly to the curl of the wind stress $(\partial \tau^x / \partial y)/(\rho_o f)$ (dashed red line). At lower latitudes, the beta-induced divergence of the meridional Ekman transport $-\beta \tau^x / (\rho_o f^2)$ (dashed green line) is appreciable.

which varies with y only. This has terms proportional to the wind stress curl and to β times the meridional component of the Ekman transport. Both terms are important, with the beta term being especially important at lower latitudes on account of the factor $1/f^2$. (Fig. 21).

At the site sampled in Fig. (19), $y = 1000$ km on the north side of the subtropical gyre, the Ekman transport is convergent, and the rate of change in layer thickness is positive, and about 12 m year^{-1}. At the same distance from the gyre center but to the south side where the wind stress curl is the same but f considerably smaller, the thickness tendency is 45 m year^{-1}. The interface is pushed downwards by the converging Ekman transport, often called 'Ekman pumping'. When converted to SSH perturbation via the reduced gravity approximation, the equivalent SSH change is about 0.1 m per 500 days, Fig. (22), at the gyre center. This raised SSH indicates a growing high pressure that characterizes the subtropical gyre. Over the tropical and subpolar regions, the sense of the Ekman divergence is reversed and hence the layer thickness is decreased, and the interface is raised, 'Ekman suction'. The resulting SSH and surface pressure anomaly is then a low, that will characterize the steady subpolar and tropical gyres.

Because the wind stress field is assumed here to vary with y only, the Ekman pumping (or suction) also varies with y only (is independent of x) Fig. (22). Because the wind stress is constant once the wind stress is switched on, the Ekman pumping-induced thickness tendency given by Eqn. (51), is constant in time. The period during which the actual thickness rate of change is constant is said to be the Stage 2 of the transient response. Judging from Fig. (22), the duration of Stage 2 depends very much upon location: at $(x, y) = (0, 0)$ the thickness rate of change is constant for about 1000 days, and then becomes very small as Stage 3 Sverdrup flow begins to develop at that site (more on this in the next section). At the same y but closer to the eastern boundary, say $x = 2000$ km, the Stage 2 steady Ekman pumping goes on for only about 500 days.
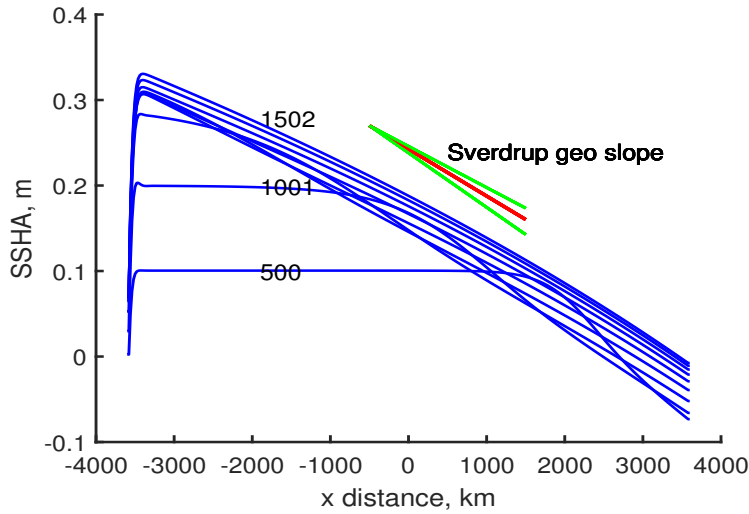
51

Figure 22: A sequence of sea surface height sections, $\eta(x)$, sampled at 500 day intervals up to 5000 days along $y = 0$, the center of the subtropical gyre. These were computed from the layer thickness via the reduced gravity approximation, Eqn. (44). The Stage 2 response is a steady rise of the sea surface, approx. 0.1 m per 500 days at this y, with no zonal tilt ($\eta(x)$ looks to be flat in this section during Stage 2). Stage 3 begins when the sea surface slopes down to the east and becomes quasi-steady; at $x = 2000$ km (eastern side of the basin) this starts at about 500 days, and at $x = -2000$ km (western side of the basin) the same thing starts much later, at about 1400 days. At this latitude, $\tau^x = 0$, and the meridional Ekman transport vanishes. Thus the quasi-steady meridional current over the interior region, $x \geq -3400$ km, is geostrophic and may be characterized by the zonal slope of the sea surface. The geostrophic slope expected from the Sverdrup relation Eqn. (1) for this y and given an average layer thickness, $h = 580$ m, is the red line that tilts down to the east. The flanking green lines are the sea surface slope for $h = 500$ and $h = 660$ m, which are found at the eastern and western ends of the section where the slope is slightly less and slightly greater than the average. This is a small but noticeable finite amplitude effect.

In this experiment — conducted in a closed basin and with a wind stress field that is independent of x — it is very compelling that the duration of Stage 2 is greater with greater distance from the eastern boundary. However, this need not be the case if the important zonal length scale comes from the wind field rather than the distance to the eastern boundary (an experiment discussed in Sec. 7.3).

5.2.2 Zonal geostrophic currents accompany the changing mass field

The change in layer thickness causes a pressure anomaly in the surface layer that develops very slowly compared to f, and so is accompanied by slowly growing, nearly geostrophic zonal currents,

$$\frac{\partial u_{S2}}{\partial t} = -\frac{g'}{\rho_o f}\frac{\partial^2}{\partial y^2}\left(\frac{\tau^x}{f}\right), \tag{52}$$
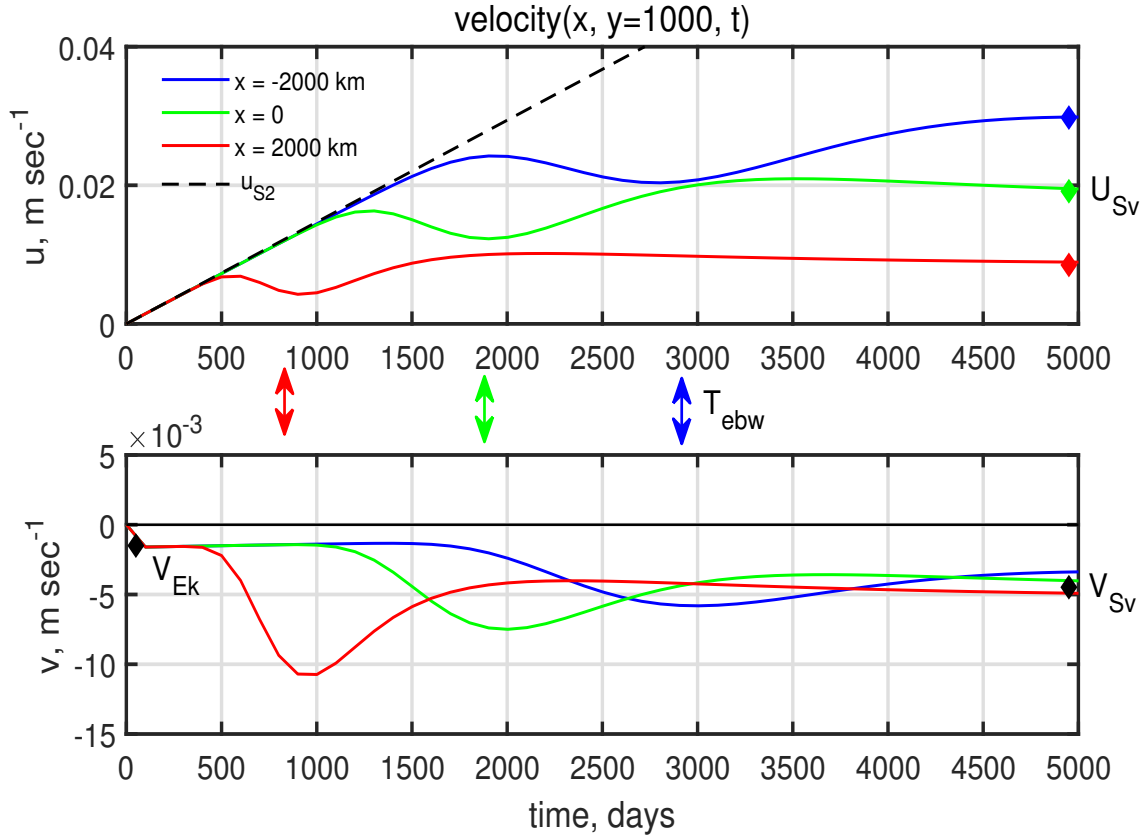
52

Figure 23: Zonal and meridional current components sampled in time along the northern side of the subtropical gyre, $y = 1000$ km, at three sites: $x = 2000$ km (red line), $x = 0$ (green line), and $x = -2000$ (blue line), which are nearest to farthest from the eastern boundary. The sampling time interval in this figure, 100 days, misses the inertial motions generated at start up (Sec. 4.1). (**upper**). Zonal or east current component. The dashed black line is the estimate by Eqn. (53) of the zonal geostrophic current produced by Ekman pumping at this y and is the same at all x. The actual current follows this very closely for a few hundred or a few thousand days, depending upon distance from the eastern boundary. The red, green and blue double arrows denote the time, T_{ebw}, when a long Rossby wave starting on the eastern boundary at $t = 0$ is expected to arrive at the corresponding x. At around $t = T_{ebw}$, the zonal current shows a low frequency oscillation and then settles into a quasi-steady state consistent with the expected Sverdrup flow, marked by the colored diamonds on the right margin. Notice that the steady state zonal current increases approximately linearly with distance from the eastern boundary. (**lower**) Meridional or north current component. For short times, $t \leq T_{ebw}$, the meridional current is Ekman flow, Eq. (10), which is the same at these sites and noted by the black diamond near the left margin. The transition from Ekman flow to Sverdrup flow occurs around the time T_{ebw}. The expected Sverdrup flow at this y and for a nominal h is noted by the black diamond at right.
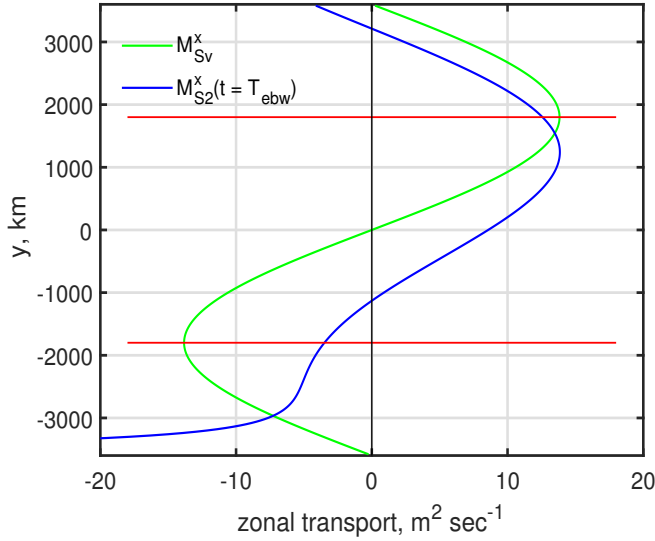
Figure 24: The zonal transport (per unit width) that accompanies the Sverdrup relation (green line that we will come to in Sec. 3.3) and the Stage 2 zonal current evaluated at $t = T_{ebw}$ (blue line) discussed in Sec. 4.1.3. At higher latitudes these currents are somewhat similar, but they are quite different at lower latitudes. The initial zonal currents in the interior closely match the Stage 2 profile (blue line) while the steady state zonal currents follow the Sverdrup profile (green line).

where the subscript $S2$ denotes that this is relevant to Stage 2 only. Because the stress is constant once switched on,

$$u_{S2}(y,t) = -\frac{g'}{\rho_o f}\frac{\partial^2}{\partial y^2}\left(\frac{\tau^x}{f}\right)t, \qquad (53)$$

where t is the time elapsed since the start. In this experiment, the Stage 2 geostrophic current is purely zonal, since the Ekman pumping varies with y only, and it is independent of x, as is the wind stress. This is bound to fail on or very near the equator, where the Ekman balance is not appropriate, and also near a meridional (north-south) boundary, which has far reaching effects discussed below. It is also entirely baroclinic, there being no free surface and no barotropic pressure anomaly possible in the 1l-rg model.

The Stage 2 geostrophic zonal current (53) evaluated at $y = 1000$ km is sketched onto Fig. (23, upper) as a dashed black line. This gives a very good account of the actual zonal currents in the interior of the basin for a period of time — within the central subtropical gyre, (Fig. 23, the green line was sampled at $x = 0$) Eqn. (53) is valid for about 1000 days, just as noted before in the discussion of the Stage 2 layer thickness. The duration of Stage 2 depends upon both the latitude, being greater at higher latitudes, and greater also with increasing distance from the eastern boundary (the red, green and blue lines of Fig. (23) are at the same y, but increasing distance from the eastern boundary). An explicit estimate of the duration of Stage 2 will follow from considering the onset of the Stage 3 (Sverdrup) response in the next section.

The Stage 2 zonal geostrophic current given by (53) is proportional to $1/f^2$, and, all else equal, is considerably larger at lower latitudes than at higher latitudes (Fig. 24). Most of this essay emphasizes the meridional Sverdrup flow and western boundary currents, since these transport sea water properties equatorward and poleward (subtropical gyre) and so are generally of greater significance for Earth's climate. However, this locally wind-forced, zonal current is a robust signal in the transient response of this model, and is also prominent in the response of the tropical ocean to an annually-varying wind (O3 of Sec. 1.1.3 and Sec. 6.1).

54

5.3   Stage 3: Blocking at the boundaries and the onset of meridional Sverdrup flow

Because the present experiment is set within a finite basin having meridional boundaries, the *x*-independence of the Stage 2 zonal geostrophic currents can not go on forever. The zonal flow that approaches a meridional boundary is blocked, and must turn either north or south. Meridional boundaries thus have the effect of breaking the zonal symmetry that characterizes the Stage 2 response. As this 'blocking effect' of meridional boundaries becomes important, the overall pattern of the layer thickness anomaly and geostrophic currents begins to resemble a closed, gyre-like circulation, e.g., within the eastern part of the subtropical gyre, $x > 2000$ km, this is evident by about 500 days (Fig. 49).[16]

The blocking effect of the eastern meridional boundary — a zonal tilt of SSH and thus a change from purely zonal to at least partly meridional flow — spreads westwards into the interior of the basin. At $y = 0$, equivalent to 30° N, this spreading is at a slow but steady rate of about 3 km per day (Fig. 49), which is roughly the westward propagation speed of mesoscale eddies at that latitude (Part 3). There are two fairly persuasive reasons to identify this westward 'spreading' of eastern boundary blocking as the westward propagation of a long, divergent Rossby wave reviewed in Sec 1.4. First, the balance of potential vorticity is consistent with long Rossby wave motions. The (low frequency) β-effect begins immediately with the meridional component of the current. Because the horizontal scale of the currents is the scale of the wind stress and very much larger than the radius of deformation, the β-effect produces mainly a change in layer thickness rather than a change of relative vorticity (Part 3, Section 2.4). In fact, the relative vorticity remains very, very small, i.e., $\nabla \times \mathbf{u} \ll f$ (this is not true near the *western* boundary, however). Thus the potential vorticity balance in the vicinity of the spreading eastern boundary blocking is linear and divergent, Eqn. (2), in common with long (baroclinic) Rossby waves. The motion evolves very slowly and is very nearly geostrophic, and so the first order wave/advection equation (18) is expected to be valid and predicts westward propagation at the baroclinic long Rossby wave speed (Eqn. 17). To test this, (Eqn. 17) has been used to define a gray-shaded mask that extends westward from the eastern boundary by

$$X \; = \; C_{longRo} \, t \; = \; -\beta \frac{C^2}{f^2} \, t, \tag{54}$$

Fig. (49).[17] The baroclinic long Rossby wave speed varies strongly with latitude; the gravity wave speed C is somewhat reduced at higher latitudes due to reduced stratification, but much more important at this early stage is the $1/f^2$ dependence, which indicates much larger C_{longRo} at lower latitudes. Notice that

---

[16]Imagine that the meridional boundaries are removed, and that the no-flow boundary condition on those boundaries is replaced by a symmetric or reentrant condition that $u(x = -L) = u(x = L)$, and the same for other variables. The domain would then be an east-west oriented channel, as more or less actually occurs in the Antarctic Circumpolar region. In a channel domain, the zonally-oriented thickness anomalies and geostrophic currents of the Stage 2 response would grow until the currents either became unstable and began to spread vertically and horizontally, or, drag on the current reached an equilibrium with the wind stress.

[17]The equatorial limit $f \to 0$ is handled by assuming that the westward wave speed can be no faster than the fastest, westward propagating equatorial Rossby wave, $-2C/3 \approx -2$ m sec^{-1}. See Part 3, Sec. 3 for a little more on equatorial wave dynamics.

the disruption of the Stage 2, zonal geostrophic flow is indeed closely coincident with the expectations of (54) at all latitudes (though with the near-equator aside, Fig. 49). Given this line of evidence, the westward spreading of the boundary blocking effect will be referred to as an 'eastern boundary Rossby wave', or 'ebw', despite that the profile $h(x,t)$ looks nothing like an elementary wave (Fig. 22).

The end of the Stage 2 local response to Ekman pumping and the start of the Stage 3 non-local or basin scale response may then be estimated by

$$Stage\ 2\ \rightarrow\ Stage\ 3: \quad t\ =\ T_{ebw}, \tag{55}$$

where

$$T_{ebw}\ =\ -\frac{(L-x)}{C_{longRo}} \tag{56}$$

with $(L-x)$ the distance from the eastern boundary. Thus T_{ebw} is $T_{ebw}(x,y)$ since C_{longRo} varies with y. Subsequent to T_{ebw}, the volume transport has a significant meridional component that approximates Sverdrup balance, Eqn. (1), Figs. (22) and (23), lower.

Judging from Fig. (23), the flow does not switch instantaneously from purely zonal to Sverdrupian at $t = T_{ebw}$. Rather, the eastern boundary wave has a very gradual leading edge, Fig. (22), and a close Sverdrup balance requires as much as $2*T_{ebw}$, which can be another few hundred or even a thousand days, depending upon latitude and distance from the eastern boundary. The key point is that the time required for the eastern boundary (blocking) effect to reach a given point in the interior is proportional to T_{ebw}, and thus is strongly dependent upon latitude and distance from the eastern boundary. In this important respect, the meridional flow of low latitude oceans exhibits a comparatively fast response to changing wind stress. The latitudinal-dependence of the baroclinic long Rossby wave speed Eqn. (17) is thus a very prominent, qualitative feature of the developing gyre circulation in this experiment, and often in the real ocean (Part 3, Sec. 2.6). (see Sec. 10.2, 5)[18]

5.4 Stage 4: Inter-gyre exchange, and basin-wide steady state

The three gyres come into steady state at quite different times, as described above, and clearly the laggard is the subpolar gyre. Even after 10 years, most of the subpolar region is still in Stage 2 and continuing to lose volume from the upper ocean since $\nabla \times \tau > 0$ (Ekman suction). The decrease of layer thickness within the subpolar gyre is quite pronounced, with h eventually reaching a minimum of about 100 m just

---

[18]Given that we are for now working with a single layer, baroclinic only model, there is only one long Rossby wave speed given by Eqn. (54). In the more complex model three layer model of Sec. 8 there will be other Rossby wave speeds, a very fast barotropic wave, and a slower, second mode, baroclinic wave that is associated with a sinuous motion of the thermocline (see Appendix to Sec. 3). The present baroclinic wave corresponds to the first baroclinic mode, and in-phase motion across the thermocline. If a model can represent only one wave mode, then this is the one to mimic.
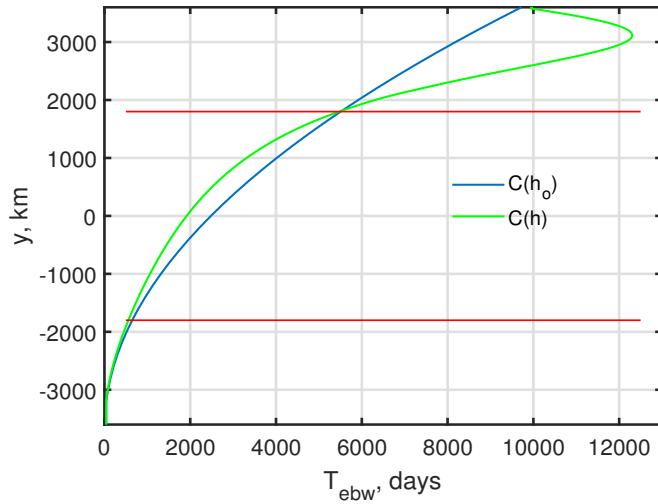
Figure 25: Transit time from the eastern boundary to the western boundary at the baroclinic, first mode, long Rossby wave speed. The blue line assumes the nominal layer thickness $ho = 500$ m for evaluating the baroclinic gravity wave speed, while the green line uses the actual, steady, zonal average thickness, which is somewhat different, especially in the western part of the subpolar gyre where $h \approx 100$ m. The expected transit times for the gyre centers are: tropical gyre, 350 days; subtropical gyre, 2500 (2000) days; subpolar gyre, 7500 (12000) days.

offshore of the western boundary current (Fig. 49, bottom). The basin-wide volume of the single layer of this model is conserved (there being no mechanism to convert abyssal water to upper ocean water, for example) and so the fluid that is expelled from the subpolar gyre is absorbed into the subtropics and tropics where the layers continue to slowly thicken more or less uniformly over the basin, long after the current in these gyres has reached a near steady state. A literal steady state of the subtropics, i.e., constant h and constant **v**, here dubbed Stage 4, requires that the entire basin, subpolar region included, must be swept by an eastern boundary Rossby wave. Thus a basin-wide steady state requires an elapsed time

$$Stage\ 4: \quad t = max(T_{ebw}) = \frac{2L(f_o + \beta L)^2}{\beta C^2},$$

where *max* is evaluated over the basin as a whole. Given a nominal value of the gravity wave speed, $C = 3$ m sec^{-1}, then $max(T_{ebw}) \approx 9200$ days. In fact, the numerical solution indicates a somewhat longer time, closer to 12,000 days, mainly because the gravity wave speed is significantly reduced within the subpolar gyre (Fig. 25) due to the greatly reduced layer thickness in especially the western part of the gyre (Fig. 49, lower panel). (see Sec. 10.2, 4) This is one of several finite amplitude effects associated with large thickness changes away from the (arbitrary) initial condition of uniform upper ocean thickness.

Time out for a pop quiz. Suppose you were asked — How long does it take to establish steady Sverdrup flow in a mid-latitude basin? If all that you knew was the solution above, then you might reply,

Oh, several thousand days ... the eastern boundary wave is so slow ... yada, yada, yada.

Well, yes, but be warned that this response is incomplete, unless you make clear that it recognizes the *baroclinic* response only, while omitting the possible barotropic response. In practice, baroclinic is often implicit, since the baroclinic response is observable in historical (and modern) field data, and is most important for transport processes, e.g., meridional heat transport. But as will be seen in Sec. 8, a *barotropic* response, including Sverdrup flow, occurs much, much faster than seen here, and is then very

57

slowly supplanted by the baroclinic response described above. So, if the question is posed exactly as above, then a better (because more complete) response is

Just a couple of weeks ..... the barotropic waves are so fast, you know .....

5.5   Western boundary currents

At the same time that the interior of the basin is developing very slow and broadly distributed zonal and meridional (Sverdrup) currents, something quite different transpires near the western boundary. In the subtropical gyre, the flow near the western boundary is northward and very fast, up to 1 m sec^{-1}, within a narrow O(100 km) western boundary current (wbc). This western boundary current is a crucial part of the basin-scale flow, accounting for volume, energy and vorticity balance for the basin overall.

The Stage 2 response includes zonal currents that impinge on the western boundary just as much as occurs on the eastern boundary. The result is necessarily meridional currents along the western boundary that are subject to a low frequency beta effect. Propagation of this western boundary blocking into the interior by wave propagation requires an *eastward* group velocity. You may recall from Part 3, Sec. 2.3, that short baroclinic Rossby waves have an eastward group velocity, but the maximum eastward group velocity of these waves is very, very slow, only a few hundred meters per day, which is just a few percent of the western group velocity of long waves, C_{longRo}. Moreover, eastward group velocity obtains only for short waves, $kR_d \leq -1$ and $k \leq 0$. Such short waves are just barely resolved in the present numerical solution, and so it is not surprising there is no evidence of eastward spreading or propagation. Instead, the meridional currents along the western boundary appear to be effectively trapped onto the boundary on a width of 50 - 100 km (Fig. 30), which is roughly the local radius of deformation (discussed below in the Appendix).

The volume transport of a wbc is estimated by

$$N_{wb} = \int_{-L}^{-L+L_{wb}} v \, h dx,$$

where L_{wb} = 150 km, by inspection (or several times R_d). The steady state wbc of the subtropical gyre has a volume transport of about 28 Sv, and northward, which is opposite the Sverdrup volume transport of the interior. The western boundary currents of the tropical and subpolar gyres are southward, and opposite the Sverdrup transport in those regions.

The immediate cause of a western boundary current is zonal inflow: in the subtropical gyre, there is an inflow to the wbc at latitudes $0 > y > -L/4$, and an outflow at latitudes $L/4 > y > 0$. During the first one thousand days of the experiment, the zonal current near the wbc is mainly the Stage 2 geostrophic flow discussed in the previous subsection. As time runs, the inflow is better described as the
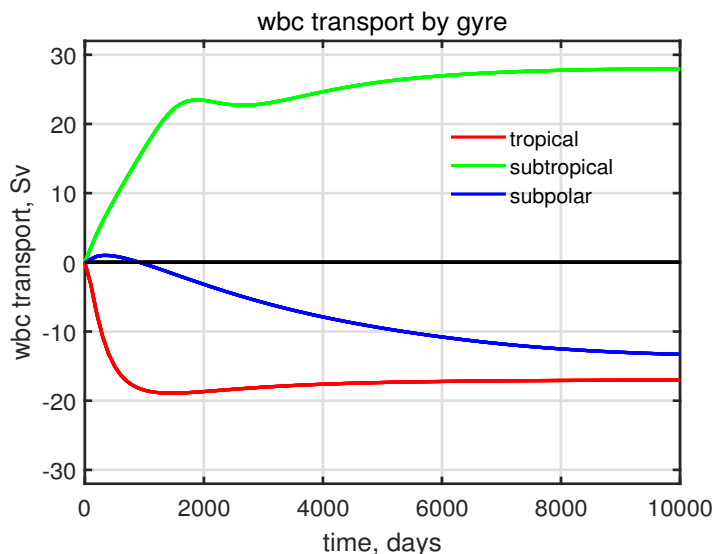
Figure 26: Meridional volume transport N_{wb} within the western boundary currents of the three gyres. These were sampled at the north-south center of the gyres. Notice that the wbc of the tropical gyre reaches a steady state within about 700 days after the start of the experiment, while the wbc of the subpolar gyre requires much longer, roughly 12,000 days.

Sverdrup zonal flow. From this we can infer that the time scale for development of a wbc is proportional to the time scale of U_{S2} and thus proportional to $1/f^2$, i.e., much faster at lower latitudes (Fig. 30, cf upper and lower panels). The subtropical wbc begins to appear within a few hundred days after the start of the experiment, and reaches its full, steady state amplitude in about 2000 days. This is roughly the same time scale on which the subtropical gyre interior reaches steady state Sverdrup flow, and comparable to the transit time of the eastern boundary Rossby wave. Two things to note: the arrival of the eastern boundary Rossby wave on the western boundary is *not* the dramatic event that seems to be implied, and, the coincidence in time does not imply that the eastern boundary Rossby wave is the cause of the western boundary current except in a very indirect way. The arrival of the eastern boundary wave implies that the interior region to the east and equatorward (subtropical gyre) is close to being in steady state with regards to meridional transport and the Sverdrup relation, and that is what really counts. The same attends the volume transports of the wbc in the other gyres: — wbc steady state requires about 1000 days in the tropical gyre, and about 10,000 - 12,000 days in the subpolar gyre (Fig. 26), a factor of roughly ten.

There is a very strong hint in the discussion above that a wbc is just a mirror of (compensates for) the Sverdrup flow of the interior. To test this in detail, we can evaluate the mass balance over a control volume that is the entire southern half of the basin, the light green shading of Fig. (27) having an area A. The areally integrated continuity equation appropriate to this control volume is

$$A\frac{dh_{avg}}{dt} = \oint h\mathbf{V}\cdot\mathbf{n}ds$$

since our shallow water model has no source term, i.e., no mechanism to convert upper layer water to abyssal water, for example. Thus the areal-average thickness of the layer within the control volume can change only if there is a net volume flux across the horizontal sides of the control volume. The line integral may be divided into pieces that represent the flow across specific sides of the control volume,
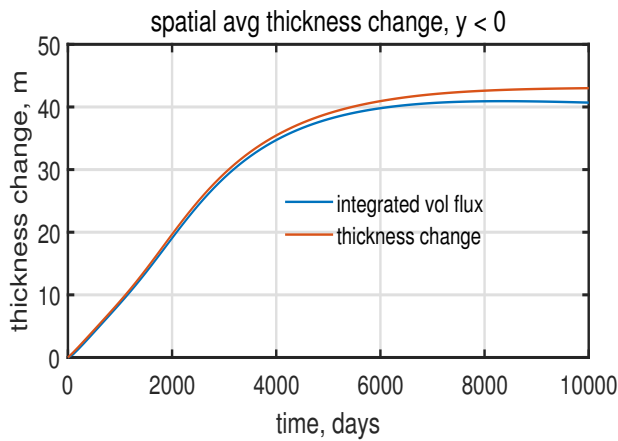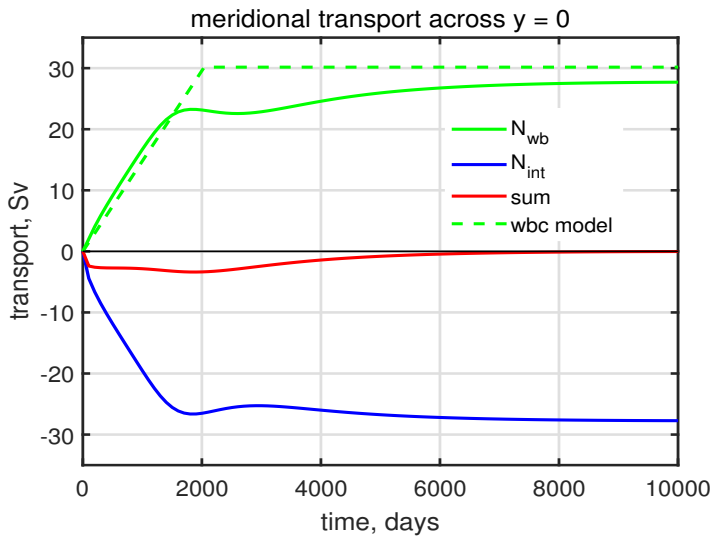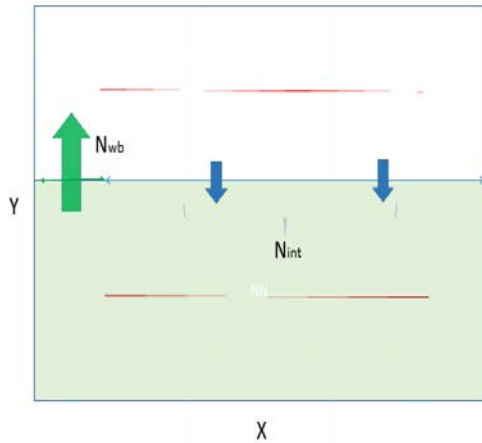
Figure 27: **(upper)** A control volume (light green area A) defined over the southern half of the basin. The volume transport through $y = 0$ is evaluated over a western boundary region, N_{wb}, and the interior, N_{Sv}. **(middle)** The volume transports through $y = 0$ (green and blue lines) and their sum (red line). The dashed green line is a model of wbc transport, Eqns. (62) and (63) discussed in the Appendix to this section. **(lower)** The time-integrated net volume flux into the control volume (blue line) and the observed thickness change over the control volume (red line), about 40 m. Given the adiabatic continuity equation (39), these should be exactly equal aside from numerical errors.

e.g., in this case

$$N_{int} = \int_{-L+L_{wb}}^{L} vh\,dx,$$

is the volume transport across $y = 0$ in the interior of the basin (no need to identify this as Sverdrup flow), and the volume flux of the comparatively very narrow and intense northward flowing western boundary current (Fig. 30) is N_{wb}, already noted. The integrated mass balance (continuity equation) then reads

$$A\frac{dh_{avg}}{dt} = N_{int} + N_{wb}.$$

Either of the volume flux terms is considerably larger than the storage term, but they do not sum to zero: during the first several thousand days of the experiment there is a small but significant net meridional transport across $y = 0$, $N_{Sv} + N_{wb}$, (the red line of Fig. 27, middle). The subtropical gyre is a region of increased layer thickness, about 40 m on areal average, and thus elevated SSH and higher pressure. Indeed, the subtropical gyre is characterized by this high pressure, as noted above. The volume of fluid required to thicken the layer in the region south of $y = 0$ is provided by (must be provided by) the basin-wide meridional volume flux across $y = 0$ (Fig. 27, lower). As the region to the south of $y = 0$ reaches a steady state and $\partial h/\partial t = 0$, which requires a little more than 5000 days, the net volume flux across $y = 0$ also vanishes. This is somewhat longer than the time required to reach a steady state within the subtropical gyre interior at this latitude.

Remarks on the real Gulf Stream. This picture of a simple, direct compensation between interior and wbc transport is valid in a wind-driven circulation experiment set within an enclosed basin. However, the real Gulf Stream has a considerably more complex relationship with the interior. There is no doubt a significant wind-driven component to the Gulf Stream transport of this sort, but there is more. The global overturning circulation noted several times in this essay includes about 15 Sv of upper ocean flow to the north and occurring within the wbc, and a comparable return flow of very cold water to the south within dense bottom currents. Thus the real, baroclinic Gulf Stream (above about 1500 m, say) has a magnitude about half again greater than the Sverdrup transport of the subtropical gyre. A second process, eddy generation via instability of the Gulf Stream, produces fairly narrow, recirculating flows on either side of the Gulf Stream (near Cape Hatteras) that are mainly barotropic. The amplitude of the associated currents is not large compared to the surface flow, but because this flow is depth-independent, carries a very large transport. If only the northeastward flow is considered (and the compensating southwestward flow on the flanks omitted), then the estimated Gulf Stream transport can be very large, exceeding 100 Sv. These barotropic recirculating flows may not contribute to meridional heat flux, say, but they surely do make fraught the estimation of the wind-driven component of the real Gulf Stream.
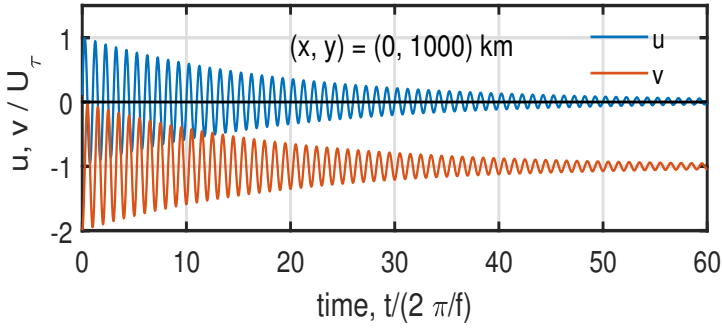
Figure 28: The solution for local, damped wind-driven motion, Eqn. (60) that may be compared to the full model solution, Fig. (19). There is no layer thickness shown here since in this local model there is no velocity divergence, and hence $h = h_o$ and constant. For that reason there is also no linear trend in the zonal component.

5.6 Appendix to Sec. 4

5.6.1 A local model of wind-driven inertial and Ekman motions

The dominant motions in the first several weeks after the wind is switched on are inertial motions and Ekman currents (Fig. 19). These are essentially local phenomenon that may be modelled by the linearized subset of Eqn. (40) in which all the terms involving horizontal spatial derivatives are omitted,

$$\frac{\partial h}{\partial t} = 0, \tag{57}$$

$$\frac{\partial u}{\partial t} = fv - ru + \frac{\tau^x}{\rho_o h}, \tag{58}$$

$$\frac{\partial v}{\partial t} = -fu - rv.$$

You may notice that these equations are exactly the form used to model the motion of a dense parcel released onto a slope (Part 1, Sec. 5), though here the external force is a wind stress rather than a buoyancy force. These equations are local in the sense that they apply to what amounts to a single parcel, or since the equations are linear, a single position, and that does not interact in any way with its surroundings, i.e., no pressure gradient and no advection.

Given an initial condition that is a state of rest,

$$u(t = 0) = 0 \text{ and } v(t = 0) = 0,$$

the solution for the so-called Stage 1 velocity is, in dimensional form,

$$\begin{pmatrix} u \\ v \end{pmatrix} = \frac{\tau^x}{\rho_o f h} \left(\frac{1}{1 + (r/f)^2} \right) \begin{pmatrix} r/f + \exp(-rt)(\sin(ft) + (r/f)\cos(ft)) \\ -1 - \exp(-rt)(\cos(ft) - (r/f)\sin(ft)) \end{pmatrix}, \tag{59}$$

In non-dimensional form the same solution is

$$\begin{pmatrix} u \\ v \end{pmatrix} / U_\tau = \left(\frac{1}{1 + E^2} \right) \begin{pmatrix} E + \exp(-E\gamma)(\sin(\gamma) + E\cos(\gamma)) \\ -1 - \exp(-E\gamma)(\cos(\gamma) - E\sin(\gamma)) \end{pmatrix}, \tag{60}$$

62

where

$$\gamma = tf$$

is time scaled by the rotation time, $1/f$,

$$E = r/f \qquad (61)$$

is the Ekman number, and the velocity scale

$$U_\tau = \tau^x/(\rho_o fh)$$

repeats Eqn. (48). The velocity of the local model (60) is the sum of a time-dependent inertial oscillation and a time-independent Ekman flow (Fig. 28).

Inertial oscillations are a clockwise rotation of the velocity at a rate f; at 30 N, the frequency is the Earth's rotation rate, 7.292 $\times 10^{-5}$ sec^{-1}, and the period is approximately one day.[19] At the site sampled in Figs. (46) and (28) $(x, y) = (0, 1000)$ km, equivalent to about 41 ^{o}N, the inertial period is about 17 hours and the wind stress is about $\tau^x = 0.008$ N m $^{-2}$. The amplitude of the inertial oscillation at this site is thus $U_\tau \approx 0.002$ m sec^{-1}, which is unrealistically small because of the excessively thick wind-driven layer, $h = 500$ m. If the amplitude of inertial oscillations played an important part in the low frequency response (they do not), then this would be a serious shortcoming of a single layer shallow water model that was configured to have a reasonable baroclinic wave speed. The inertial oscillation of (60) decay with time as $\exp(-Eft)$, e-folding in 15 days due to Stokes drag.

The inertial oscillations computed by the full shallow water model Fig. (19) differ from the solution of the local model (60) in that the frequency of rotation is a few percent greater than f (very hard to see this in the present figures) and the amplitude decay is somewhat faster than is given by the frictional e-folding alone. These two features plus the very small but nevertheless significant oscillation of the layer thickness (Fig. 19, lower) indicate that what look like inertial oscillations in the numerical model solution are better described as very long wavelength, near-inertial gravity waves. The longer term (several weeks) evolution of the inertia-gravity waves is significantly influenced by the variable f of this shallow water model, which leads to propagation towards the equator.

One of the subthemes of this essay is the latitudinal dependence of the ocean response and circulation. With respect to the steady circulation, the natural demarcation of latitude is by gyre, i.e., supolar gyre, subtropical gyre. At this very early stage there are no gyres, and so to investigate how the response varies with latitude it is sufficient to pick two sites, the easterly and westerly wind maxima, roughly 15 N and 45 N, and consider the zonal, u velocity component only (Fig. 29). The data are shown in two formats; in dimensional form (Fig. 29, left column) and in nondimensional form (right column) in which the speed is normalized with $U_\tau = \tau/(\rho_o fh)$ and time with the local inertial period, IP $= 2\pi/f$. The dimensional format doesn't require any explanation (which is a good thing) but neither does it give

---

[19]The inertial period is less than a day by the fraction $\approx 1/365$. Can you recall from Part 1 why the inertial period at 30 N is less than a day, and why that value?
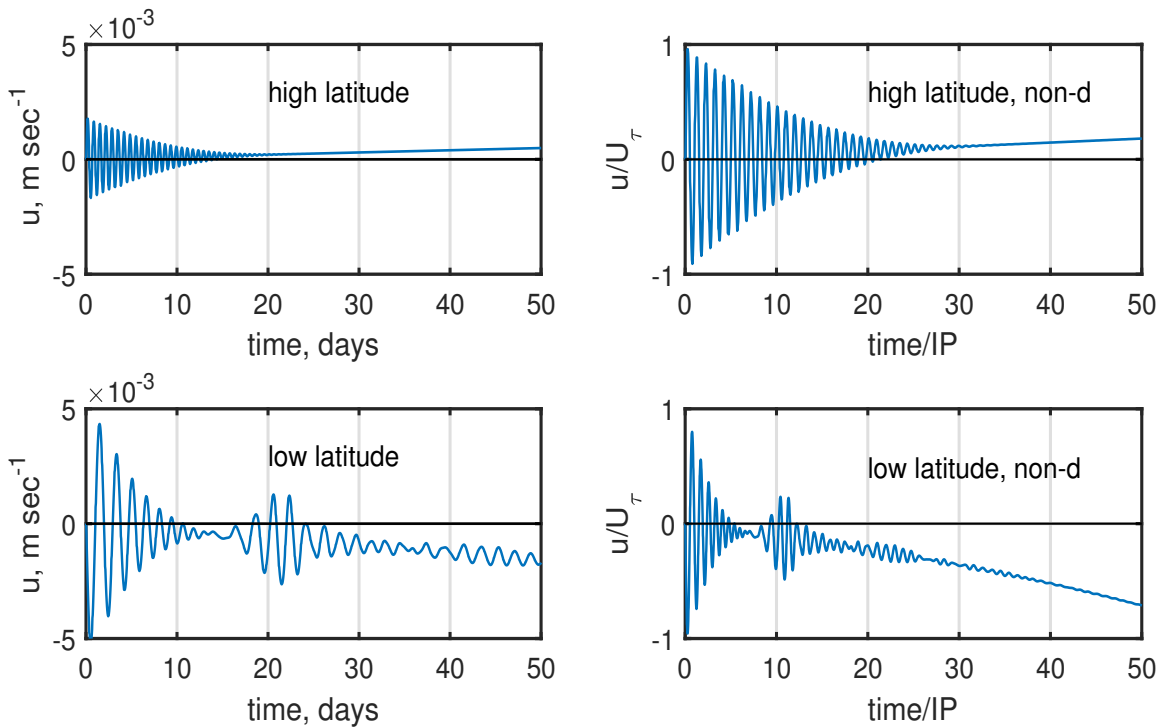
Figure 29: The zonal or *u* component of velocity sampled at two sites, a comparatively high latitude site on the axis of the westerly winds, **(upper row)** and a low latitude site, the axis of the easterly winds **(lower row)** . The data are plotted in dimensional format **(left column)** and in a non-dimensional format **(right column)**. The former emphasizes the significant differences in the response due to the differing latitude, while the latter makes clear that the sites have two things in common; the amplitude of near-inertial motion goes as U_τ and the period of the oscillation is approximately the local inertial period.

anything more than a qualitative hint at parameter dependence, i.e., it is clear that the amplitude of inertial motion and the period of the inertial motion is greater at lower latitude.

Given the non-dimensional format, it is evident that the amplitude is ≈ 1 at both sites, evidence that the amplitude does indeed vary with f and τ as U_τ implies it should. Moreover, the period of the oscillation is very close to 1 IP at both sites and thus the period of the high frequency oscillation is $\propto 1/f$. Neither of these results is the least bit surprising given the solution Eqn. (60), but could have made these inferences even without an explicit solution given the appropriate nondimensional scaling. The latter may be found by dimensional analysis and then verified with numerical experiments, a procedure that is generally far more accessible than is an explicit solution. If the main goal of a modeling study is to explore and expose parameter dependence rather than simulation of an observed case, then the non-dimensional format will often have real merit. That is certainly a part of the goal here, and so a nondimensional format (units) will be used when it adds value.

5.6.2 Simple models of a western boundary current

Transport in a transient wbc.   A very simple estimate of the time-dependent western boundary transport can be constructed on the basis that the wbc transport will be opposite and equal to the meridional Sverdrup transport to the east of the eastern boundary Rossby wave, i.e., as if

$$N_{int} + N_{wb} = 0.$$

and now $N_{int} = N_{Sv}$. While the eastern boundary wave is in transit across the basin,

$$0 < t < T_{ebw}(x = -L, y); \quad N_{wb} = -\frac{\nabla \times \tau}{\rho_o \beta} C_{longRo} \, t = -N_{Sv} \tag{62}$$

The wind stress curl and the long Rossby wave speed are evaluated at the y of the wbc observation, in Fig. (26), the center of the subtropical gyre, $y = 0$. After the wave arrives on the western boundary, the western boundary transport is assumed to exactly compensate the steady state Sverdrup transport across the basin interior and so for longer times,

$$t > T_{ebw}; \quad N_{wb} = constant = -\frac{\nabla \times \tau}{\rho_o \beta} 2L. \tag{63}$$

This estimate (62) and (63) is shown as the green dotted line of Fig. (27) middle, and is a plausible first description of the actual (numerical) boundary current transport, though far from perfect. There are two ways that this model and this estimate are inconsistent in detail with the numerical solution: the transition from Stage 2 purely zonal, local flow to Stage 3 Sverdrup flow is not instantaneous as Eqn. (62) assumes, and, the northward wbc transport does not return all of the southward Sverdrup transport during the first several thousand days of the experiment when some fluid is stored at the rate of several Sv within the thickening layer south of $y = 0$. These fairly significant details aside, what is most striking and robust is that a wbc develops much faster in the tropical gyre, within very roughly 1000 days, than it does in the subpolar gyre, where the time scale is closer to 10,000 days (Fig. 26). This very large difference in the rise time of the wbc in these gyres is a consequence of the $1/f^2$ dependence of the Stage 2, locally wind-forced geostrophic current, Eqn. (53), and of the long Rossby wave transit time, Eqn. (56).

Western boundary current width.   The water that makes up the western boundary current of the subtropcial gyre flows into the boundary current from the eastern side. This inflow begins with the start of the Stage 2 zonal current, and continues into the steady state. Assuming that the inflowing water conserves potential vorticity and that the across stream momentum balance is geostrophic, leads to an estimate of the boundary current profile and width. (See Stommel (1966) [1], Ch. 8, who has an interesting discussion of this applied to the actual Gulf Stream.) The relative vorticity is approximated well by the x variation of the north component of the current, and hence the potential vorticity inside and just outside of the western boundary current are

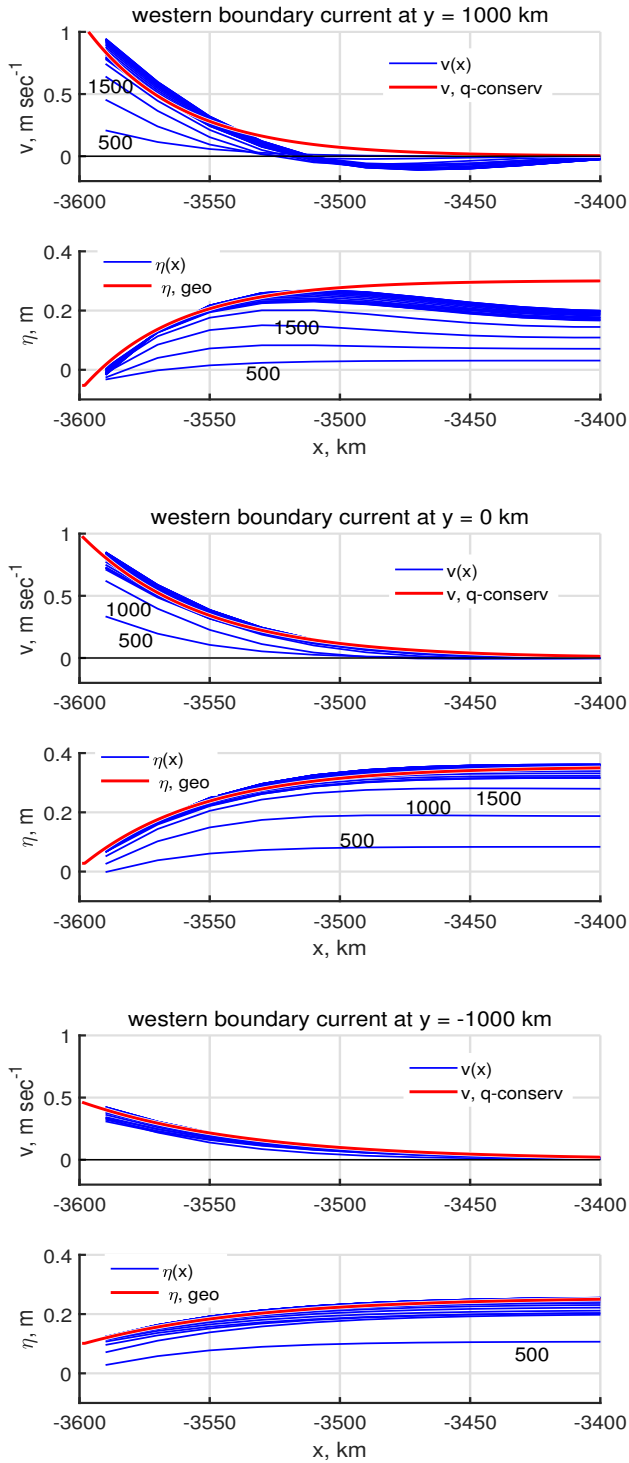$$\frac{f + \frac{\partial v}{\partial x}}{h} = \frac{f}{h_0}, \tag{64}$$

Figure 30: Zonal profiles of the north velocity and the SSH anomaly within 200 km of the western boundary at three sites within the developing subtropical gyre: **(upper)** $y = 1000$ km, on the north side of the subtropical gyre, **(middle)**, $y = 0$, the center of the subtropical gyre, and **(lower)** $y = -1000$ km, the south side of the subtropical gyre. Profiles are shown as the blue lines at 500 day intervals. The north velocity expected for a q-conserving inflow is shown as the red line, an exponential with the x scale being the radius of deformation, at $y = 1000$ km, $R_d = 36$ km; at $y = 0$, $R_d = 45$ km, and at $y = -1000$ km, $R_d = 64$ km (discussed in Sec. 3.2). The corresponding SSH anomaly profiles are computed from the respective q-conserving velocity using geostrophy (also plotted as a red line). Notice that currents and stratification at the more southerly site (lower panels) reach steady state in about 500 days, while the higher latitude site (upper panels) requires about 2000 days.

where h_0 is the thickness just outside the boundary current. If we evaluate this at $y = 0$, $h_0 \approx 600$ m. The momentum balance is very nearly geostrophic,

$$fv = g' \frac{\partial h}{\partial x},$$

which may be combined with (64) to form a single equation for the boundary current velocity,

$$\frac{\partial^2 v}{\partial x^2} = \frac{f^2}{g' h_0} v. \tag{65}$$

This has exponential solutions

$$v(x) = V_0 \exp(\pm((x+L)/R_d), \tag{66}$$

where $R_d = \sqrt{g'h}/f$ is the familiar radius of deformation. Suitable boundary conditions are that $v \to 0$ as $x + L$ becomes large, which selects the minus sign in the exponential. For the central latitude of the subtropical gyre, $y = 0$ of Fig. (27), $V_0 = 1.0$ m sec^{-1}. The solution for $v(x)$ is then complete, and the corresponding geostrophic thickness, represented here by the SSH anomaly η, may then be easily computed as well (Fig. 27, red lines). These make quite good representations of the actual velocity and thickness (or η), which suggests that the width of the western boundary current is approximated well by the radius of deformation, the natural length scale of the shallow water model. That is a neat and satisfying result that will be cited repeatedly in the description of the circulation. However, closer inspection and thought suggests that there may be more to this than the simple, local inflow model takes account of. First, this simple model doesn't work as well along the northern side of the subtropical gyre, $y = 1000$ km (upper panel of Fig. 30) where the boundary layer current appears to have a reversal offshore that is not captured by the monotonic profile (66). In one respect that is not all bad, since that region is characterized by *outlfow* from the wbc into the interior, not an inflow. So, there is evidently more to the wbc dynamics than just (65). Second, the water that makes up the wbc at $y = 0$, say, came mostly from lower latitudes, not from a local inflow. If the wbc current was q conserving along stream, then the q at that latitude should be lower than the local q. Later it will be clear that frictional effects should be significant in the western boundary current, and friction acts to increase q along the path of the current. Friction implies a length scale that, for the r used here, is the same order as R_d (Sec. 4.2.2). It appears that while Eqn. (65) works very well in a numerical sense, local inflow and q conservation are not a complete explanation.

6   The (almost) steady circulation

The currents and stratification in the interior of the basin eventually reach an instantaneous steady state, $\partial(\ )/\partial t = 0$. However, there is one region where the flow never becomes even approximately steady, the confluence of the western boundary currents of the subtropical and subpolar gyres at around $y = 1800$ km. There the colliding western boundary currents meander and produce intense, mesoscale eddies of both

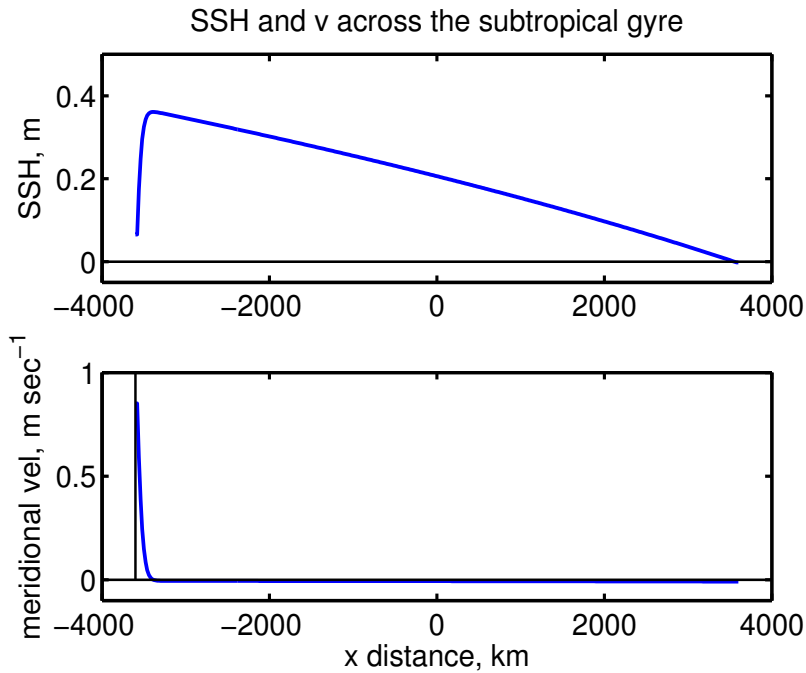SSH and v across the subtropical gyre

Figure 31: **(upper)** A zonal section of SSH across the center of the subtropical gyre, $y = 0$, computed from layer thickness anomaly via the reduced gravity approximation. The basin-scale variation of SSH is much like that seen in the North Atlantic (Fig. 1); a very narrow western boundary current and a broad interior with almost uniform slope down to the east. Notice, though, that the amplitude of the SSH high in this model solution is considerably less than is observed in the real North Atlantic subpolar gyre (about which more in Sec. 7). **(lower)** The meridional velocity along the section above. The velocity is very nearly geostrophic and is northward and very fast in a thin western boundary current, up to about 1 m sec^{-1}. The interior, meridional velocity is southward and very slow, a little less than 0.01 m sec^{-1}.

signs. The eddies remain close to the western boundary, and do not appear to affect the interior region. The confluence region does become steady in the statistical sense that the eddy amplitude, size and frequency are no longer changing after about 10,000 days. 'Steady' in reference to the basin-wide circulation, is really a shorthand for steady excepting the wbc confluence region.

One straightforward way to characterize the basin-wide, steady circulation is to simply make a cut of SSH anomaly and northward velocity through the center of the subtropical gyre Fig. (31), which may be compared to Fig. (1). There is a comparatively very narrow western boundary region, e-folding on the radius of deformation and so the full width is O(100 km), within which SSH slopes up to the east and the current is northward and fast, up to 1 m sec^{-1}. Over the much broader interior region — the rest of the basin — there is a quasi-linear decrease of SSH all the way to the eastern boundary (Fig. 31). Given the zonally uniform wind stress curl of the model winds, this nearly constant slope of SSH would be expected for a linear Sverdrup interior for which $\delta h \ll H_o$. This is the shallow water model-equivalent of the east-west asymmetry of the observed wind-driven ocean circulation noted as O2 in Sec. 1.1.

6.1 A streamfunction depiction of the circulation

A second and very useful way to characterize the basin-wide steady circulation is to construct a map of the streamfunction. When the solution is in steady state, $\partial h/\partial t = 0$, the volume transport, $\mathbf{M} = H\mathbf{V}$, is nondivergent, $\nabla \cdot \mathbf{M} = 0$. In that case the vector field $\mathbf{M}(x,y)$ may be represented by a scalar field, the streamfunction, $\Psi(x,y)$, without loss of information. The streamfunction is related to the east and north components of $\mathbf{M}$ by

$$\frac{\partial \Psi}{\partial y} = HU \quad \text{and} \quad \frac{\partial \Psi}{\partial x} = -HV, \tag{67}$$

or in a vector form,

$$\mathbf{M} = -\mathbf{k} \times \nabla \Psi$$

where the upper case H and U, V are the steady state thickness and velocity components. The sign convention of (67) is arbitrary, and is reversed in some applications. The streamfunction may be computed from the vector field by integrating either of (67). Here we integrate the HV term westward, starting from the eastern boundary,

$$\Psi(x,y) = \Psi(L,y) - \int_L^x H(x,y)V(x,y)dx. \tag{68}$$

The dimensions (units) of this streamfunction is volume transport, $\text{m}^3 \text{ sec}^{-1}$. The volume transport of major ocean currents is in the range 1 - 150 $\times 10^6 \text{ m}^3 \text{ sec}^{-1}$ and often reported in a non-SI but widely used and accepted unit, 'Sverdrups', with 1 Sv = $10^6 \text{ m}^3 \text{ sec}^{-1}$. The normal component of the velocity vanishes on all of the side walls, and hence $\Psi(L,y) = constant$, that may as well be taken to be zero. It would be equally valid to perform an integration of HU in the y direction. The resulting streamfunction lines (Fig. 32, left) are everywhere parallel to $\mathbf{M}$, and hence the streamfunction makes an intuitive presentation of the direction of the underlying vector field. With this choice of sign, lower values of Ψ are to the right of the vectors (which is opposite the geostrophic relationship for SSH). The density of streamfunction lines is proportional to the magnitude of $\mathbf{M}$ and notice that $\partial \Psi/\partial x$ is very large in thin western boundary regions where the wbc current is correspondingly very large compared to the currents in the interior of the basin.

Sverdrup transport may also be represented by a streamfunction (Fig. 32, right), here computed from Eqns. (1) and (68) and integrating westward from the eastern boundary,

$$\Psi_{Sv}(x,y) = \Psi_{Sv}(L,y) + \frac{1}{\rho_o \beta} \int_L^x \nabla \times \tau(x,y)dx. \tag{69}$$

The starting value is taken to be $\Psi_{Sv}(L,y) = 0$ for all y, which ensures that there is no normal flow through the eastern boundary. Since only one integration is needed to compute Ψ_{Sv}, no additional boundary data may be applied and so the Sverdrup streamfunction can not satisfy a no normal flow condition through any of the other boundaries. In this case the stress curl $\nabla \times \tau(x,y) = -\partial \tau^x/\partial y$ and independent of x and hence the streamfunction is

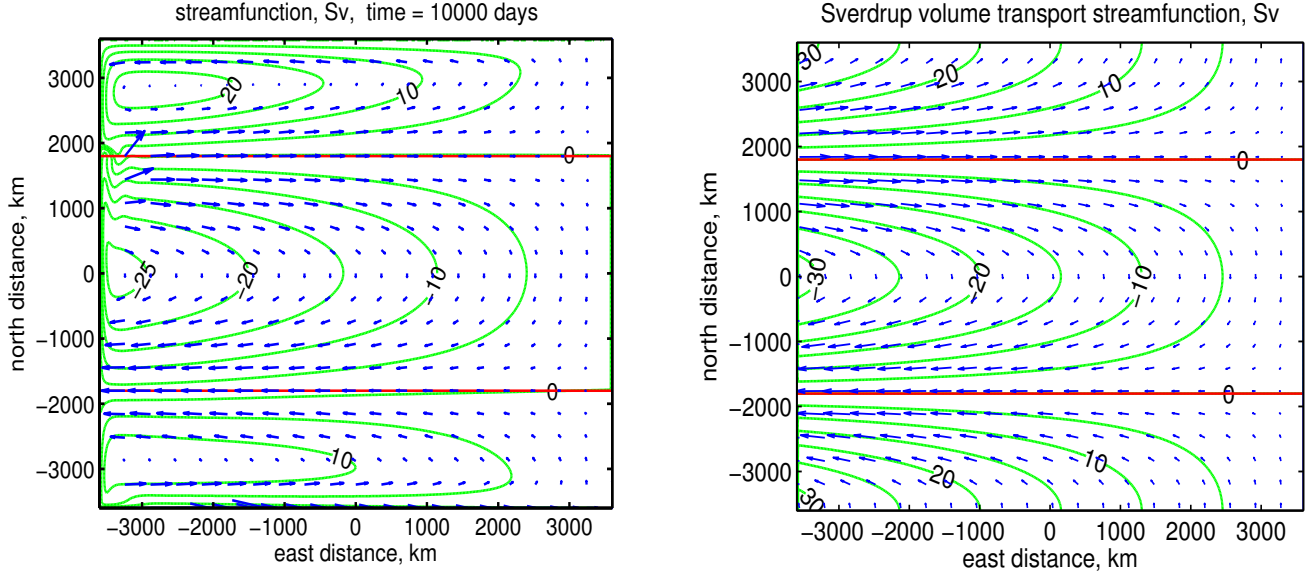$$\Psi_{Sv}(x,y) = -\frac{(L-x)}{\rho_o \beta}\frac{\partial \tau^x}{\partial y}. \tag{70}$$

69

Figure 32: **(left)** The volume transport streamfunction (green lines) computed from the steady state numerical solution by integrating Eqn. (68) starting from the eastern boundary. Labeled in Sverdrups, 10^6 m^3 sec^{-1}. The blue vectors are the volume transport per unit width, **M**, and are parallel to lines of constant streamfunction. The very large **M** vectors in the western boundary regions are omitted here but shown in a later Fig. 14. The red horizontal lines are the axes of the westerly and easterly winds, and also approximate gyre boundaries. **(right)** The Sverdrup volume transport streamfunction (green lines) computed from the wind stress of the numerical experiment (Fig. 16) and Eqn. (69) and starting from the eastern boundary. In the numerical model-computed streamfunction field at left, $\Psi = 0$ is found on all of the boundaries, indicating no normal flow through the boundaries, as should hold exactly. The Sverdrup streamfunction at right can not satisfy a zero normal flow condition on more than one boundary, here chosen to be the eastern boundary.

The zonal component of mass transport is then

$$HU = \frac{\partial}{\partial y}\Psi_{Sv}(x,y) = -\frac{(L-x)}{\rho_o \beta}\frac{\partial^2 \tau^x}{\partial y^2}, \tag{71}$$

and the meridional component is Sverdrup transport,

$$HV = -\frac{\partial}{\partial x}\Psi_{Sv}(x,y) = -\frac{1}{\rho_o \beta}\frac{\partial \tau^x}{\partial y}, \tag{72}$$

as expected.

A comparison of the two streamfunction fields (Fig. 32) is one way to see where Sverdrup balance is valid in the numerical solution. The steady circulation in this experiment consist of three gyres within which the meridional flow has the sign of the wind stress curl, e.g., equatorward in the subtropical gyre where $\nabla \times \tau < 0$, and so qualitatively consistent with the Sverdrup relation Eqn. (1). Each of these gyres is very strongly compressed onto the western side of the basin in the sense that the largest SSH and thus
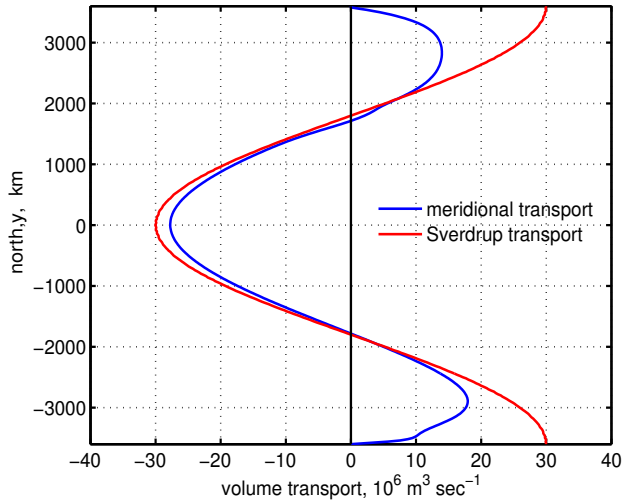
70

Figure 33: The north-south variation of the zonally-integrated meridional transport computed from the steady model solution (blue line) and computed via the ideal Sverdrup transport relation, Eqn. (1) (red line). The integration extends from the eastern boundary to just outside of the western boundary current. Notice that the actual (numerical) meridional transport vanishes on the zonal boundaries at $y = \pm 3600$ km due to a no normal flow boundary condition. This is something that the Sverdrup relation (red line) can take no account of. The north-south extent of the affected zonal boundary region is 500 - 1000 km, which is a significant part of the tropical and subpolar gyres.

the largest pressure anomaly is found about a hundred kilometers offshore of the western boundary. (see Sec. 10.2, #6)

Another and more quantitative way is to evaluate the interior meridional transport for all y, Fig (33). The Sverdrup relation gives a fairly accurate account of the meridional transport over the interior of most of the subtropical gyre, and to a much lesser degree, the subpolar and tropical gyres. The Sverdrup relation is clearly not valid within a western boundary region, nor is it valid within roughly 500 - 1000 km of the northern and southern zonal boundary regions. In these zonal boundary regions the Sverdrup relation indicates significant meridional flow which does not happen in the numerical model solution. What is perhaps surprising is how broad the affected zonal boundary regions are (more on this in Sec. 6.2.3). One consequence of such broad zonal boundary regions is that the transport of the western boundary currents of the tropical and the subpolar gyres is somewhat less than is the transport of the subtropical gyre, which (in this model) is not similarly affected by a zonal boundary (Fig. 26).

6.2 Dynamics of the steady circulation: the balance of potential vorticity

The dynamics of the circulation may be described most fruitfully in terms of the balance of potential vorticity, Eqn. (42), here expanded and multiplied by H,

$$\beta V H = \frac{1}{\rho_o}\nabla\times\tau - rho_o\nabla\times\mathbf{V} + HOT, \qquad (73)$$

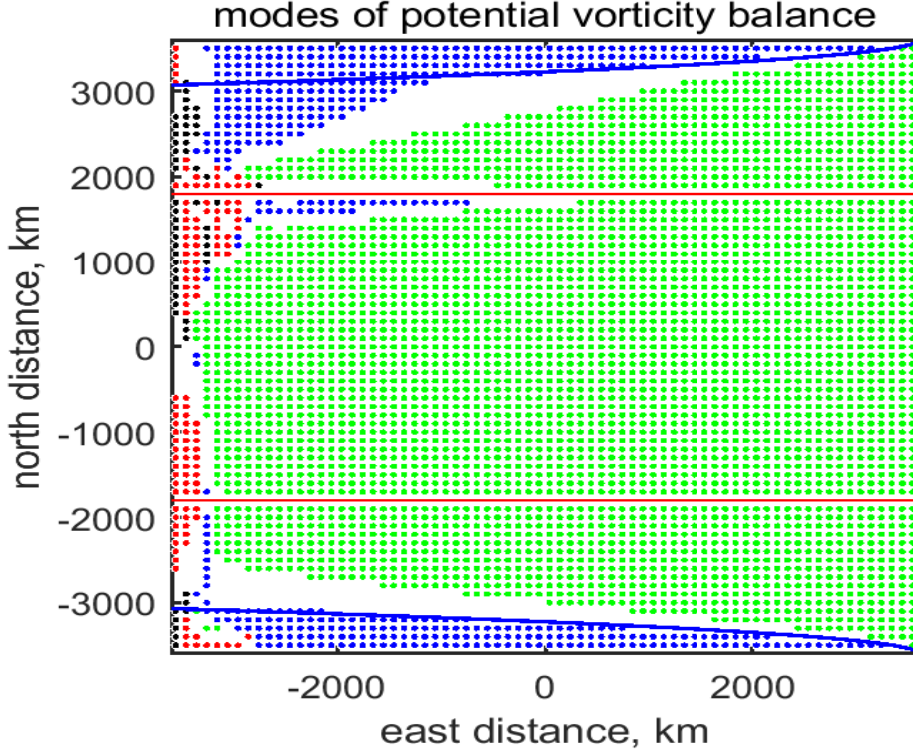$$beta = curl\ tau + curl\ drag + higher\ order\ terms.$$

71

Figure 34: The steady potential vorticity balance characterized by the distribution of the modes (approximate two term balances) of Eqn. (73). Horizontal red lines are the gyre (wind stress curl) boundaries as before. A **green dot** indicates that the Sverdrup mode, $beta = curltau$, accounts for more than 90% of the variance of the steady potential vorticity balance at that point. This (approximate) Sverdrup balance holds over about 75% of the basin. A **black dot**, shows where $beta = drag$ is the dominant mode, mainly near the western boundary. A **blue dot** indicates the mode $0 = curltau + drag$ found near the northern and southern zonal boundaries . A **red dot** indicates that the HOT, the collection of nonlinear terms, was larger than two of the linear terms. If there is **no colored dot**, then there is no dominant mode, and the balance of potential vorticity is shared among at least three of the terms of Eqn. (73). The blue lines near the northern and southern zonal boundaries are a simple, linear estimate of zonal boundary region width that is discussed in Sec. 5.2.3.

The higher order terms are the collected nonlinear terms involving the advection of potential vorticity and the gradient of layer thickness;

$$HOT = -H\mathbf{V}\cdot\nabla\xi \; + \; h_oHQ\mathbf{V}\cdot\nabla H \; - \; \frac{1}{\rho_o h}\tau\times\nabla H \; + \; \frac{rh_o}{H}\mathbf{V}\times\nabla H.$$

In general, the steady potential vorticity balance includes a contribution from all of these terms, including the HOT. However, in this solution the nonlinear HOT terms are important only in special places (marked with red dots in Fig. 34) where large currents are combined with large horizontal gradients, e.g., the confluence of the subtropical and subpolar western boundary currents near $(x,y) = (-L, L/2) = (-3600, 1800)$ km.

6.2.1 Sverdrup interior

Aside from these important but spatially limited regions, the steady potential vorticity balance can be characterized by the regional distribution of two term balances or modes among the linear terms of Eqn. (73), Fig. (34). One of these, the Sverdrup mode,

$$\beta V H \quad = \quad \frac{\nabla \times \tau}{\rho_o},\tag{74}$$
$$beta \quad = \quad curltau,$$

accounts for at least 90% of the variance of the potential vorticity balance over most of the interior region of the basin (the green dots of Fig. 34), especially within the subtropical gyre, and which is often and appropriately called the Sverdrup interior.

Eqn. (42) describes the potential vorticity balance at a fixed point. Consider a site in the subtropical gyre interior where the wind stress curl is negative, which by itself would cause Q to decrease with time. A steady state will occur if the meridional flow advects higher Q water from the north at the same rate (opposite sign) of the stress curl tendency. Since the potential vorticity in the interior is approximated well by the planetary vorticity, $Q \approx f/h_o$ (with h_o a constant), then this occurs by the advection of planetary vorticity, $V \partial f / \partial y$, as if f was a fluid property. For this steady, Sverdrup balance to exist throughout the interior of the basin, there must be some mechanism that serves to recharge the higher latitudes (within the subtropical gyre) with high Q water, or specifically, with water having $Q \approx f/h_o$. What is the source of this high Q water? The western boundary current, described next. (see Sec. 10.2, 7)

6.2.2 Western boundary currents

The Sverdrup balance certainly does not hold within the western boundary currents (Figs. 31 and 32), where the meridional current is counter to the Sverdrup flow. The beta effect on a fast-flowing wbc current is in any case far larger than can be balanced by the curl of the wind stress (as occurs in the Sverdrup interior), and so in this model the steady vorticity balance within a wbc is mainly between the beta effect and the curl of the friction, 'drag',

$$\beta V H \quad \approx \quad - \quad rho_o \nabla \times \mathbf{V},\tag{75}$$
$$beta \qquad \qquad drag.$$

For example, the western boundary current of the subtropical gyre has very large negative relative vorticity (Fig. 30) , and a correspondingly large, positive, curl of the friction, or 'drag'. This drag largely balances the negative vorticity tendency of the beta effect, allowing a steady state within the subtropical wbc. Regions where this frictional balance holds in the sense described above are denoted by the black dots in Fig. (34), and are very near the western boundary in all three gyres.

An Ekman number equivalent for the vorticity balance,

$$E_Q = \frac{drag}{beta} = \frac{r\nabla \times \mathbf{V}}{\beta V},$$

(76)

ignoring signs and taking $H = h_o$. The usual Ekman number is the ratio of frictional force to Coriolis force, but in this case it is the curl of the friction divided by (compared to) the beta effect (see Sec. 10.2, #11). To evaluate E_Q it is helpful to use a streamfunction representation of the velocity and its curl,

$$V \approx \frac{\Psi}{L_{wb}},$$

where L_{wb} is the east-west width of the wbc, which for now we will treat as an unknown. Within the narrow western boundary current, the horizontal scale in the x direction (normal to the boundary) is much less than the scale in the y direction and hence the curl of the velocity (the Laplacian of the streamfunction) is approximately

$$\nabla \times \mathbf{V} = \nabla^2 \Psi \approx \frac{\partial^2 \Psi}{\partial x^2} \approx \frac{\Psi}{L_{wb}^2}.$$

Using these estimates in (76) gives

$$E_Q = \frac{r}{\beta L_{wb}}.$$

(77)

If the balance is indeed Eqn. (75), then it should also be the case that $E_Q \approx 1$ and readily solve for the purely frictional wbc width, $L_{wb} = L_{fric}$ to find

$$L_{fric} = \frac{r}{\beta}.$$

(78)

Notice that this L_{fric} does not depend upon f, and so should be the same along the entire western boundary. Neither does it depend upon stratification and so should obtain even for a fully barotropic wbc. There will be an opportunity to check that with a three-layer model in Sec. 8.

For the present values of r and β this $L_{fric} \approx 50$ km, which is numerically about the same as the (subtropical) first mode, baroclinic radius of deformation (Sec. 4.7). Said a little differently, for the present r, the Q balance of a wbc having a width equal to the radius of deformation is significantly frictional. Recall that in this experiment, the value $r = 1/15$ days, was chosen in an *ad hoc* manner, the minimum r (least viscous) that permitted a near steady state solution. This is a partial rationalization of this choice. However, there is no independent means for identifying an appropriate value of r (that I know of), and no reason to assert that the physical process of dissipation by or in a wbc is well-represented by linear drag. Given all of this, we have to be very chary about interpreting this solution as if it were a realistic model of an actual wbc.

The shallow water model solution is worth understanding on its own, however, and at a minimum it is essential to know what happens when r is changed; say that r is doubled to 1/7.5 days. This makes the

solution somewhat more viscous. The pattern of the Sverdrup interior is nearly unchanged, and the amplitude of the Sverdrup transport is reduced only very slightly, a few percent. The Sverdrup interior is thus not much affected by the choice of r. The wbc becomes somewhat thicker, as (78) indicates it should. Since the wbc transport is reduced and the wbc width increased, the wbc speed is reduced considerably, by about 30%. In that event the flow is steady throughout the model domain. More interesting is the solution when r is reduced to half the present value, to $r = 1/30$ days. The volume transport in the interior is then a few percent greater and so is a slightly better match to the ideal Sverdrup transport. But again the overall pattern of the interior circulation is indistinguishable from the nominal experiment. The width of the subtropical wbc is slightly narrower, though not nearly as much as the purely frictional boundary layer width (78) suggests, and so it appears that $L_{wb} = R_d$ is a lower limit that obtains for smallish friction. The wbc current speed is slightly greater, by about 10%, and so the inertia of the wbc is also greater. The nonlinear terms of the q balance are enhanced, and the colliding western boundary currents at the subpolar/subtropical gyre confluence (on the western boundary at about $y = 1800$ km; the largest red dot region of Fig. 34) are considerably more vigorous than in the nominal experiment (Fig. 49, lower). This kind of unstable, eddying flow is an important and very interesting characteristic of nearly all strong ocean currents that are not constrained by topography. However, this aspect of boundary current dynamics is sensitively dependent upon details of the ocean bottom topography and the vertical structure of currents, among others, and so is outside the scope of this essay (see Sec. 10.2, Problems 9 and 11).

6.2.3   Zonal boundary regions

There are extensive regions adjacent to the zonal boundaries (northern and southern boundaries) where the ideal Sverdrup balance does not hold, as evident in the qualitative mismatch of Sverdrup transport with the actual transport within about 500 to 1000 km of the zonal boundaries (Figs. 32 and 33). As noted at the outset, the Sverdrup balance *per se* is unable to satisfy the boundary condition that the meridional current must vanish on the zonal boundaries, and so if there is wind stress curl on these boundaries (as there is here, Fig. 16) then the Sverdrup balance will necessarily fail; something else must happen. Very near the zonal boundaries there is no meridional velocity and thus no β effect. The steady, linear potential vorticity balance in this model must reduce to the steady, linear, forced, damped mode,

$$
\begin{aligned}
0 \quad &= \quad \frac{1}{\rho_o}\nabla \times \tau \quad - \quad rh_o\nabla \times \mathbf{V} \qquad\qquad (79)\\
&= \quad curltau \quad + \quad drag,
\end{aligned}
$$

indicated by blue dots in Fig. (34).

Like the wbc, this boundary region is also highly anisotropic (typical of all boundary layers), but in this case the meridional, north-south scale is much less than the zonal, east-west scale and hence

$\nabla^2 \Psi \approx \frac{\partial^2 \Psi}{\partial y^2}$. The balance (79) may then be written via the streamfunction as

$$0 \approx \frac{1}{\rho_o} \nabla \times \tau + r \frac{\partial^2 \Psi}{\partial y^2}.$$

The curl of the drag has to be large enough to balance the wind stress curl in the zonal boundary region, and the question is what zonal boundary layer width, L_{zb}, is required to achieve this? Estimating $\partial(\ )/\partial y \approx 1/L_{zb}$ and $\partial^2(\ )/\partial y^2 \approx 1/L_{zb}^2$, then

$$0 = \frac{1}{\rho_o} \nabla \times \tau - \frac{r}{L_{zb}^2} \Psi.$$

It is not obvious what Ψ should be, but as a first guess, let's try the Sverdrup streamfunction, Eqn. (69), even though the Sverdrup Ψ can not be correct right on the boundary. Given a tentative estimate $\Psi = (L - x) \nabla \times \tau / \rho_o \beta$, where $L - x$ is the distance from the eastern boundary (positive), the boundary layer width is easily found to be

$$L_{zb} = \sqrt{\frac{r(L - x)}{\beta}}. \tag{80}$$

This is sketched onto Fig. (34 as blue lines near the southern and northern zonal boundaries. At the midpoint of a zonal boundary, $x = 0$, $L_{zb} \approx 400$ km, which is a reasonable estimate of the half-width of the zonal boundary region evident in Figs. (34) and (33). Notice that the region significantly affected by the zonal boundary dynamics (the width of which is defined by the no dot transition region between the blue and green regions) is about twice this width.

The width of this boundary layer estimate decreases toward the east, which is qualitatively consistent with the distribution of modal balances, i.e., a narrower blue region toward the east. An eastward decrease of L_{zb} arises because, while the vorticity needed to achieve the balance $0 = curltau + drag$ on the zonal boundary is uniform along the boundary (recall that $curltau$ is here taken to be uniform in x, which is generally not true over the real oceans, Fig. 3) and hence the zonal current, which is qualitatively the zonal component implicit in the Sverdrup relation, decreases eastward. As a consequence, the north-south horizontal scale over which the current varies must also decrease eastward in order to have the necessary relative vorticity and thus curl of the frictional drag sufficient to balance the curl of the wind stress.

Like the western boundary layer, the width of the zonal boundary regions is expected to be independent of f and thus should be the same along the southern and northern zonal boundaries since the imposed wind stress is the same on those boundaries (Sec. 3.2). However, judging from the east-west distribution of q-balance modes found in the numerical model solution (Fig. 34), the zonal boundary layer is in fact markedly wider in the western-most third of the sub-polar zonal boundary region. The reason for this discrepancy is mainly that the subpolar gyre of this numerical experiment has a significantly reduced layer thickness compared to the initial thickness, h is as little as 100 m in the western subpolar gyre, and hence there is considerably greater drag than is accounted for by the linear equation (79) that presumed $H = h_o = 500$ m. A straightforward experimental test of this hypothesis

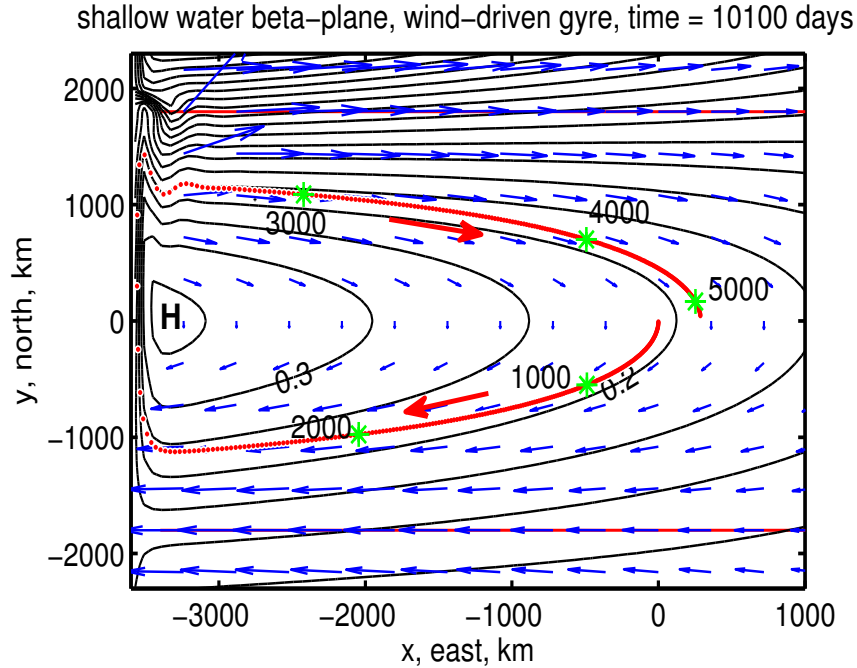shallow water beta–plane, wind–driven gyre, time = 10100 days

Figure 35: The (almost) steady subtropical gyre, shown by contours of SSH anomaly and a field of velocity vectors. A parcel trajectory that was started at $(x, y) = (0, 0)$ and followed for 5,500 days is the red line. The green asterisks along the trajectory are at 1000 day intervals. The parcel entered the western boundary current at about 2,600 days after starting, and it exited the western boundary current about 200 days later. The parcel returned close to its starting position. Notice that the trajectory is almost parallel to isolines of SSH, but not exactly so.

follows from setting the imposed wind stress small enough — $\tau_o = 0.01$ N m^{-2} suffices — that the dynamics are linear in the respect that $H \approx h_o$ throughout the model domain. In that case the comparison between the numerical and the estimated boundary layer width (80) is quite good at all longitudes outside of the wbc. Thus the linear estimate of zonal boundary layer width (80) is valid for a linear problem, and it is straightforward to understand the sense and the approximate magnitude of the finite amplitude effects that occur when there are large spatial variations in layer thickness, as do occur in this numerical solution.

6.3   Appendix to Sec. 6: A (Lagrangian) trip around the subtropical gyre

In the previous section, the analysis considered the currents, vorticity, etc., as observed at fixed locations, a point of view often dubbed 'Eulerian'. This is the natural starting point, since the shallow water equations and their numerical implementation are Eulerian. However, our intuition for classical mechanics has roots in a parcel-following, or 'Lagrangian' description, since the m and the a of $F = ma$ are the mass and acceleration of a specific chunk of material, and not the fluid properties observed at a point in space (the Eulerian view). This section will take this kind of parcel-following view on a complete trip around the gyre. Besides connecting a little better with our intuition for mechanics, this
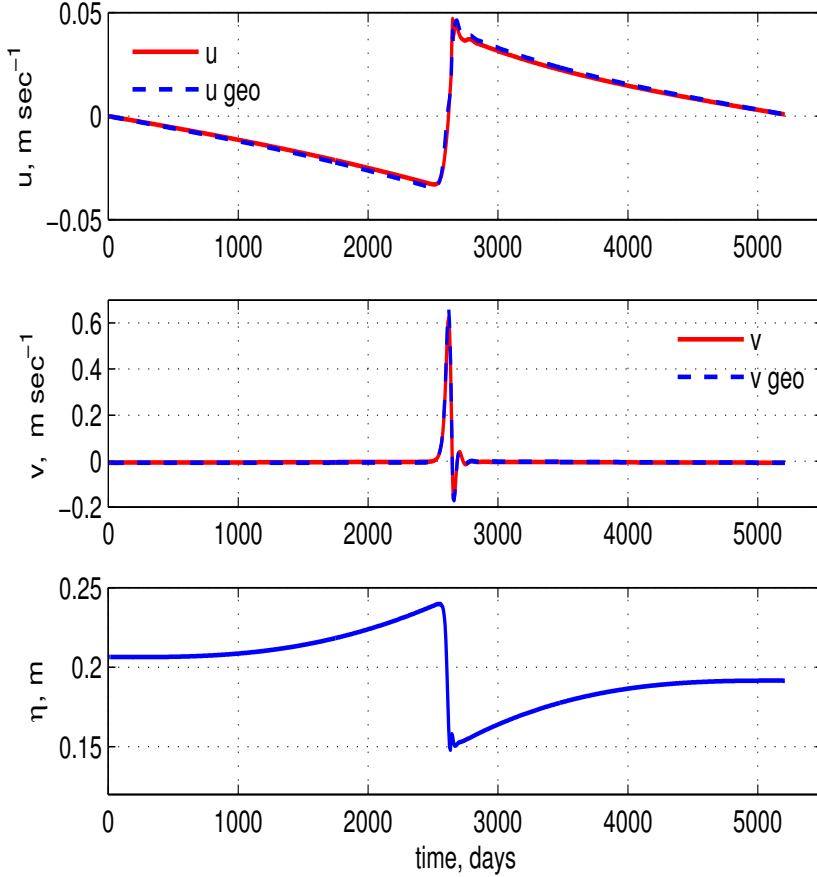
77

Figure 36: Velocity components along the trajectory of Fig. (35). **(upper)** East velocity (red line) and the geostrophic velocity estimated from the layer thickness (dashed blue line). **(middle)** North component of velocity. Note the very large change in the scale compared to the east component above. The actual velocity and the geostrophic velocity are close enough that the lines are difficult to distinguish. **(lower)** The SSH anomaly along the trajectory. While within the interior region, the parcel slowly climbs the SSH high of the subtropical gyre. While in the wbc, it descends comparatively very rapidly.

also gives a holistic view of the circulation in that it helps to show that the western boundary current is an essential component of a steady circulation.

A Lagrangian description starts with the solution for parcel trajectories, $X(t;(X_o,Y_o)), Y(t;(X_o,Y_o))$ by integrating the velocity along the path of a specific parcel,

$$X(t) = \int_0^t U(x,y)dt + X_o, \quad \text{and,} \quad Y(t) = \int_0^t V(x,y)dt + Y_o, \quad (81)$$

where (X_o, Y_o) is the initial position and the $t = 0$ here is the time this integration starts (not the starting time of the numerical integration as in Sec. 3). The key thing is that the (x,y) dependence of the velocity field is continually updated as the integration proceeds, i.e., the (x, y) in the integrand is set $= (X, Y)$ at each time step. Since the velocity field is available only at the 20 km resolution of the numerical model, the evaluation of velocity at an arbitrary parcel position requires an interpolation of the discrete model data, which is bound to incur some error, much like the finite difference evaluation of a derivative.

The initial position may be chosen anywhere in the model domain; the trajectory shown in red in Fig. (35) was started in the center, $(X_o, Y_o) = (0, 0)$. The initial position is, in effect, the tag on the parcel

78

that happened to be there at the time t_o. Not surprisingly, different initial positions result in different trajectories. In this circulation, small initial position differences yield only rather small trajectory differences (some examples to follow). A flow having this property may be described as 'laminar'.[20]

A complete trip around the subtropical gyre from this starting position $(X_o, Y_o) = (0, 0)$ requires a little more than 5000 days and extends over about 11,000 km. If the circulation was exactly steady (it isn't quite), and if the integration method used to construct the trajectory was without error (it can not be), then the parcel would return to its starting point. However, this parcel didn't quite make it (Fig. 35). Nevertheless, the interesting changes in parcel properties along the track are considerably larger than the starting point/ending point mismatch, and so the semi-quantitative inferences from this trajectory are valid.

Assuming that the fluid is not at rest, then there is no Lagrangian steady state comparable to the steady state of an Eulerian frame. Rather, fluid parcels continuously change position and generally all other properties with time. To find the potential vorticity of the parcel, we can either evaluate the (presumably known) $q(x,y)$ field at the parcel position, or, integrate the q conservation equation along the trajectory.

6.3.1 Momentum balance and energy exchanges

The relationship of parcel motion to the local slope of the SSH anomaly (the pressure or geopotential anomaly) is closely analogous to the motion of a dense parcel on a slope studied in Part 1. Differences in detail include that the slope changes quite a lot along the trajectory, especially near the western boundary, and, there is an additional external force, the wind stress, which is essential for compensating the slow but inexorable effects of friction.

During the first several hundred days, the parcel moved very slowly toward the south, which is consistent with the meridional Sverdrup flow at the starting latitude. Eventually, the parcel turned toward the southwest (Fig. 36) and began to pick up some speed. The trajectory was roughly parallel to the SSH lines with higher SSH to the right. Thus the parcel motion was, to a first approximation, geostrophic.

An important but small departure from strict geostrophy is that the parcel had a rather small, systematic component of motion across the SSH lines. While the parcel was in the interior, it slowly climbed up the SSH high of the subtropical gyre. The damping effect of friction alone would cause the parcel to descend the local SSH slope, though at a very small angle consistent with the small Ekman number, E is O(0.01). The small component of motion toward higher SSH is a consequence of the wind

---

[20]If instead the sensitivity to initial position was large, then the flow would be characterized as chaotic or turbulent. Most large scale fluid flows, and including the real ocean circulation, are turbulent in this sense.
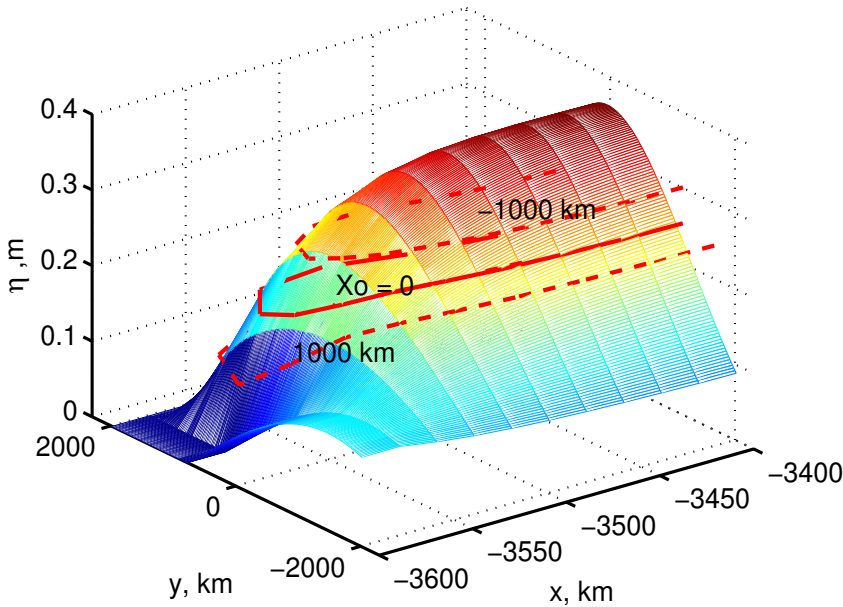
Figure 37: Three trajectories superimposed on the SSH anomaly, η, of the western side of the subtropical gyre. The trajectories differ in their starting points, X_o, that is noted. The solid red trajectory has $X_o = 0$ and is shown also in Fig. (35). Notice that the x scale is greatly expanded compared to the y scale so that the very large zonal slope of SSH within the wbc and its relationship to these trajectories is apparent.

stress. From an energy perspective, the positive wind work experienced by the parcel when it was in the interior was stored as gravitational potential energy.

After several thousand days, the parcel began to approach the western boundary, where the SSH topography was by comparison, very steep, about two orders of magnitude greater than in the interior. As the parcel neared the western boundary it accelerated to the north, reaching speeds of O(1 m sec^{-1}), or about two orders of magnitude greater than the speeds that characterize the slow, Sverdrup flow of the interior. The parcel motion never showed any significant inertial motion, and the momentum balance remained almost geostrophic (Fig. 36, middle). This implies that the acceleration associated with the steep wbc topography was slowly-varying compared to the rotation time, $1/f$. The kinetic energy associated with this rapid northward flow came from the potential energy that was released as the parcel descended about 0.1 m while within the western boundary current (Fig. 36, lower). There was also some energy loss to friction. After about 200 days, the parcel left the western boundary current and entered the slow eastward flow along the north side of the subtropical gyre. While moving eastward, it slowly climbed back up the high SSH of the subtropical gyre and returned fairly close to its starting value of SSH anomaly.

6.3.2 Potential vorticity balance along a trajectory

Potential vorticity conservation provides another way to think of the Sverdrup relation. Given that the field of q is presumed to be steady at fixed locations, $\partial q / \partial t = 0$, then the q of the moving parcel is just

the q at its present position (this sounds both profound and trivial at the same, but be sure to understand this before going on). Moreover, the spatial variation of potential vorticity is due mainly to the spatial variation of f, at least in the subtropical gyre interior, where the circulation is very slow. The parcel was subject to the overlying wind stress, whose curl was negative, and thus would tend to reduce the q of the parcel (Fig. 38, upper). Since the q of the parcel had to be consistent with the q of the presumed steady field, the parcel must move southward toward lower q, given that the q field is dominated by the meridional variation of f. Said a little differently, the southward motion of the parcel must be just sufficient to keep the q of the parcel consistent with the steady field of potential vorticity, $(\nabla \times v + f)/h$. In the subtropical gyre, the spatial variation of q is due mainly to the latitudinal variation of f, and hence the Sverdrup relation. This is a rigorous argument for the Sverdrup relation, given the assumptions of a steady, linear q balance. However, it feels awfully thin as an explanation for existence of the circulation in the first place. And, you might add, so does the usual (Eulerian) Sverdrup relation.

It is a fair surmise that a parcel can not be subject solely to a negative wind stress curl, or else the basin-wide average of q would surely decrease with time, which is not consistent with the steady state of the Eulerian circulation. It must be the case that parcels occasionally experience a process that increases q — a (relatively) quick pass through the western boundary current where there is a very strong, positive curl of the drag. This positive drag curl resets the parcel's q to a value that is consistent with the interior q (Fig. 38) where it reenters the Sverdrup interior. Thus the western boundary current is a crucial part of the gyre-scale circulation with respect to potential vorticity.

7   Experiments with other wind fields and basin configurations

The idealized wind field and square basin considered up to now are an appropriate model configuration for this introduction to wind-driven circulation, but these choices make the solution specific (special) in ways that may not be obvious. This section will consider briefly three other, equally idealized wind fields and/or basin configurations that will help reveal several important aspects of the wind-driven circulation.

7.1   Annually-varying winds and the baroclinic circulation

The experiment described in Secs. 5 and 6 assumed that the wind field was steady, once switched on, and had an amplitude modeled loosely on the long-term, observed mean. On the other hand, almost everyone with experience living in a coastal region will attest that the wind over the ocean is very seldom steady for more than a few hours or at most a few days. Wind varies on a wide range of time scales, including with the changing seasons, and in some regions it varies quite a lot; the annual variation of the westerlies over the northern North Atlantic is roughly $\pm 50\%$ of the annual mean, with the highest winds and wind
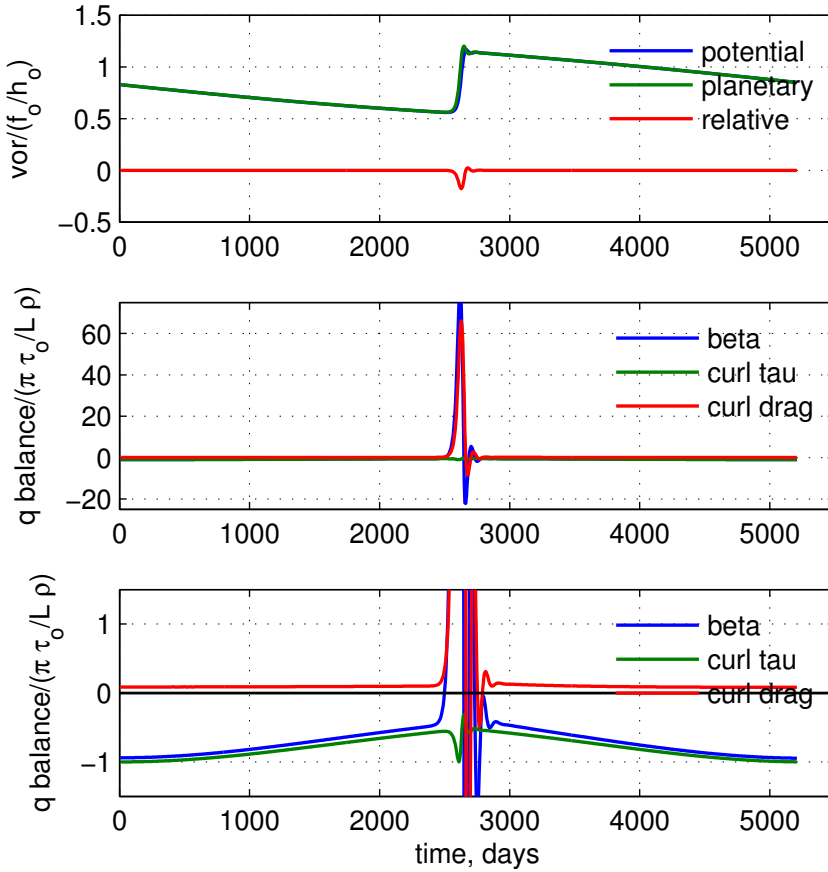
Figure 38: Potential vorticity along the trajectory of Fig. (35). (**upper**) The full potential vorticity (blue line), the planetary vorticity (green line) and the relative vorticity (red line). These are normalized by f_o/h_o. Notice that the relative vorticity is very small except when the parcel is within the western boundary current where it has a maximum magnitude of -1/4 (normalized). (**middle**) Leading terms in the potential vorticity balance, Eqn. (73). These data are normalized by a nominal wind stress curl, 8×10^{-8} m sec^{-2}. When plotted at this scale, about all that can be told is that the beta term is approximately balanced by the drag curl term while the parcel is within the western boundary current. (**lower**) Same data as above, but with a clipped ordinate that reveals the interior balance between the beta term and wind stress curl.

stress curl during winter, Figs. (8) and (9). The annual variation of easterly wind magnitude is somewhat less, though the annual migration of the Inter-Tropical Convergence Zone (furthest north in summer) produces a large annual variation in the local wind stress curl over the tropical North Atlantic.[5] Meridional winds show an especially marked annual variation that also contributes significantly to the annual variation of stress curl. Given this large amplitude annual variation of the wind, not to mention the day-to-day variation with the weather, one might argue that the time-mean wind scarcely exists, outside of climatologies.

Given that the rise time of the basin-wide circulation in the subtropics is O(1000 days), it is a reasonable guess that the annual cycle of the ocean circulation will be small but let's find out by calculating the solution for an idealized, annually-varying wind stress,

$$\tau^x(x,y,t) = (0.1 + 0.05\sin(2\pi t/365))\sin(\pi y/L),$$

where t is the time in days. Note that this wind stress amplitude varies quite a lot, between 0.05 and 0.15 Pa. This annually-varying wind was applied from the start of an integration that was continued past 10,000 days. The solution never comes to a steady state, but the annual cycle in the ocean circulation

seasonal wind–driven gyre, 10530 days, $\tau_o = 0.05$ Pa

seasonal wind–driven gyre, 10707 days, $\tau_o = 0.15$ Pa
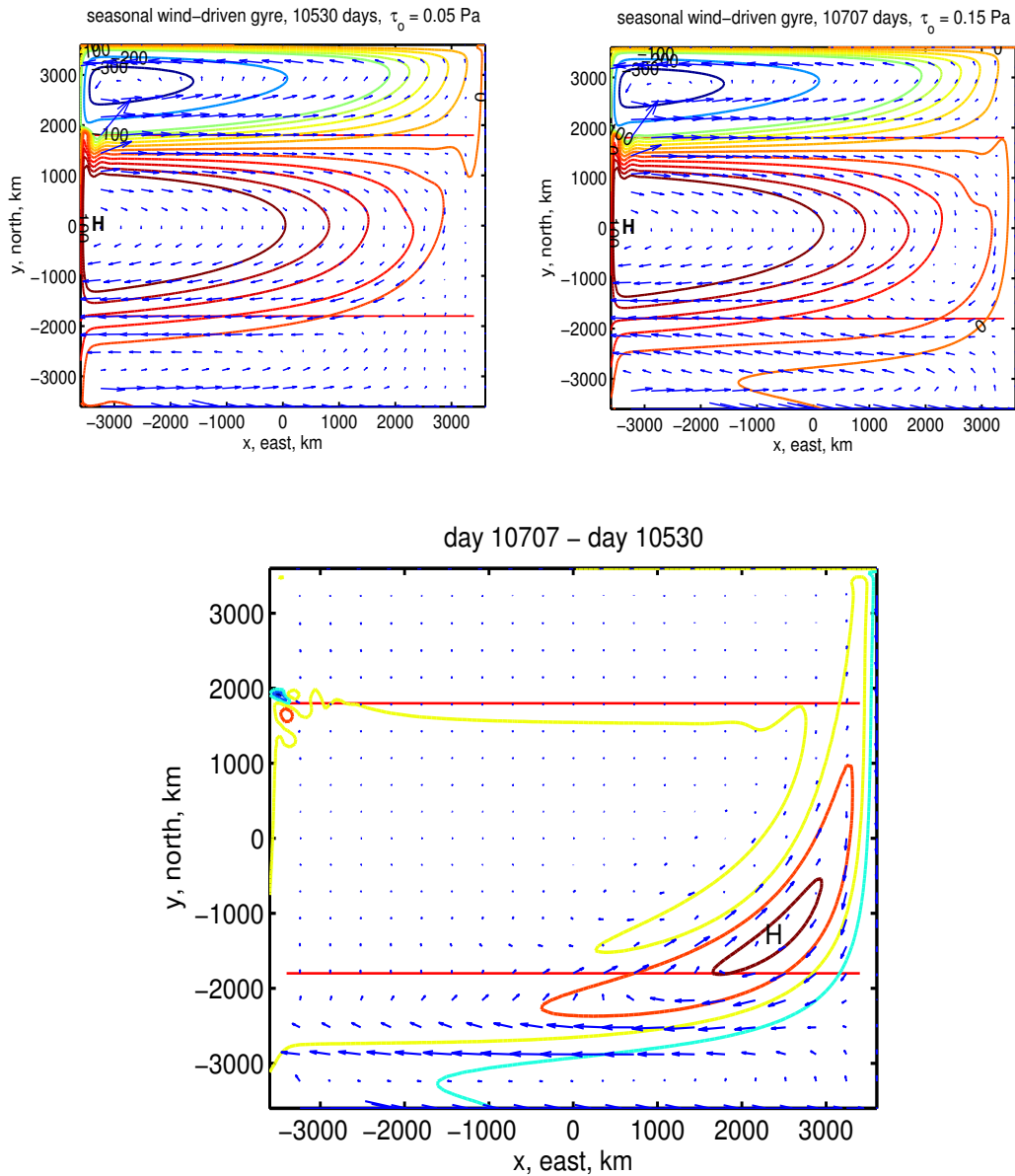
day 10707 – day 10530

Figure 39: **(upper)** Two snapshots of the circulation taken 180 days apart and near a minimum (left) and maximum (right) of the tropical circulation. The latter occurs about one month after the maximum of the annually-varying wind stress amplitude. An animation of these data is available from https://www2.whoi.edu/staff/jprice/seasonal-gyres **(lower)** The difference of the two snapshots, showing the pattern of the annual cycle. Notice the small, intense eddies near the western boundary at about $y = 1800$ km, the confluence of the subpolar and subtropical western boundary currents. This kind of time-dependent eddy variability arises from an instability of the ocean currents, and so is present even with a steady wind stress.
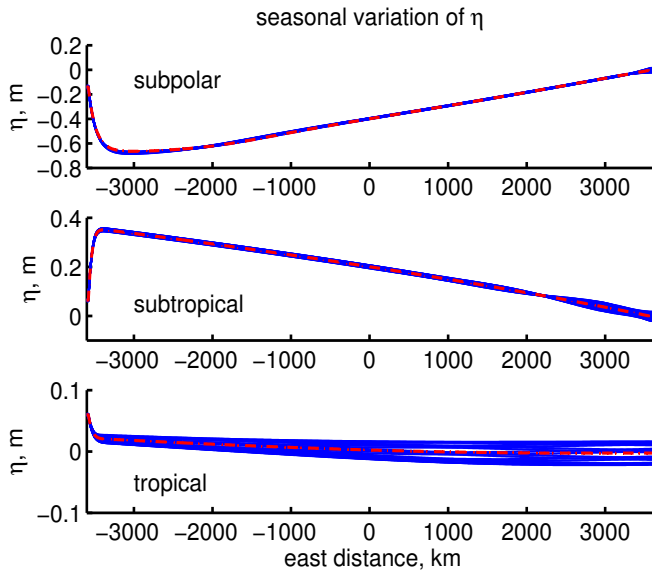
Figure 40: Zonal profiles of SSH, $\eta(x)$, from the annually-varying winds experiment. These profiles were taken through the centers of the three gyres noted. The blue lines were taken at 40 day intervals after time = 10,000 days when the solution appeared to be in a statistically steady state. The single red dashed line is a slice through the base case solution having steady winds, and notice that it goes through the center of the envelope of blue lines. Notice too that the η scale differs considerably between the three panels, consistent with the considerably larger η in the subpolar gyre.

becomes stationary in the sense that it repeats from one year to the next and so the startup transient has been minimized by 10,000 days.

Snapshots of the resulting circulation at times that are near the minimum and maximum response in the tropical gyre are in Fig. (39), and a series of slices through the center of the gyres shows the (inferred) η (Fig. 40). The $\eta(x)$ from the steady wind experiment (red dashed line) runs through the center of the envelope of the time-varying $\eta(x,t)$, indicating that the dynamics are effectively linear, i.e., the time-mean of the solution computed with an oscillating wind stress is very nearly the same as the solution computed with the time-mean of the wind stress. The first result of this experiment is that if the steady or long time-mean of the ocean circulation was the only thing of interest, then we would not have to be concerned with resolving explicitly the annual variation of the wind; the long term (yearly or more) time-mean of the wind stress would evidently suffice, at least for this model.

A second important result of this experiment is that the amplitude of the annual variation in the ocean varies greatly with latitude. Specifically, the tropical gyre responds much more vigorously to the annually-changing wind than does either the subtropical or especially the subpolar gyre. This is consistent with the basic start up experiment, which showed a much faster rise of the tropical gyre vs. the subpolar gyre. The amplitude of the annual variation in the ocean depends very much upon the variable of interest. For example, the zonal current sampled on the north side of the middle of the tropical gyre (Fig. 41, solid red line) varies by $\pm 50\%$ in this experiment, or the same as the wind stress. The explanation for this vigorous low-latitude response appears to be as simple and direct as the $\propto 1/f^2$ dependence of the local, wind-induced (Stage 2) geostrophic current, Eqn. (53). The observed annual variation of zonal currents in the tropics is likely of this sort.[5] There is also an annual period eastern boundary wave that has an appreciable amplitude in the lower subtropics. This wave penetrates only about one wavelength into the interior.

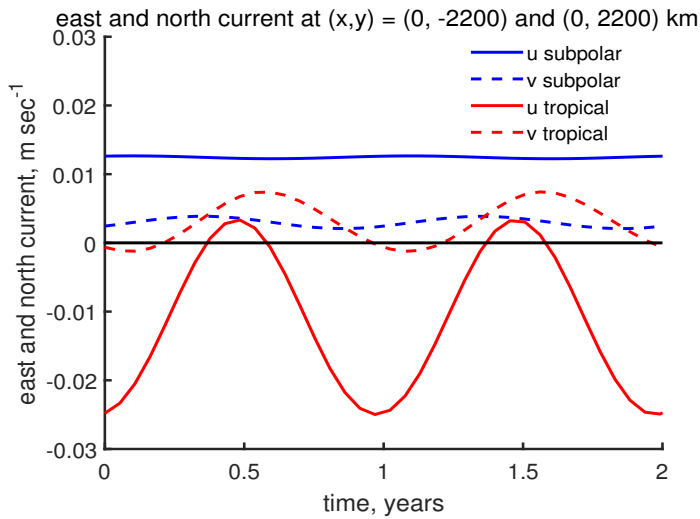east and north current at (x,y) = (0, -2200) and (0, 2200) km

Figure 41: East and north component of the current from the annually-varying wind experiment. The current was sampled at two sites, on the south side of the subpolar gyre $(x, y) = (0, 2200)$ km (solid and dashed blue lines), and on the north side of the tropical gyre at $(x, y) = (0, -2200)$ km (solid and dashed red lines). The current at the subpolar site is almost constant in time despite a significant annual variation of the wind stress. The current at the tropical site oscillates by about $\pm 50\%$ around a mean, which is very close to the steady state current found in the steady wind stress experiment of Sec. 3.

wbc transports by gyre
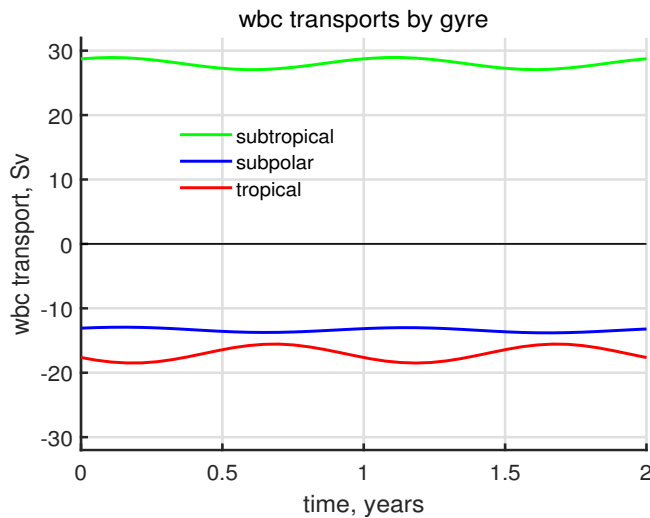
Figure 42: Transports of the western boundary current in each of the gyres from the annually-varying wind experiment. Colors are as in Fig. (26). Notice that the annual variation of the wbc transport in the tropical gyre (red line) is modest when compared to the very large annual variation of especially the zonal current in the interior of that gyre, cf. the red, solid line of Fig. (41).

Wbc transport is one measure of the gyre circulation: in the subpolar gyre, the wbc transport varies by about ± 0.3 Sv, in the subtropical gyre by about ± 0.7 Sv, and in the tropical gyre, by about ± 1.2 Sv or only about $\pm 8\%$ (Fig. 42). The latter is much less than the response of zonal currents in the tropics, just noted. The western boundary current transport is a bulk property of a gyre, and responds on the time scale of the basin-wide meridional (Sverdrup) flow, $2L/C_{longRo}$, Eqn. (56). The long Rossby wave speed is $\propto 1/f^2$ and much faster within the tropical gyre, but nevertheless, the rise time of the wbc transport of the tropical gyre is many hundreds of days (Fig. 26) and fairly long compared to the time scale of the annually-varying wind, a few months. The response time of the subtropical and subpolar gyres is much longer still, a thousand to many thousands of days, and hence the wbc transport of higher latitude gyres varies even less in response to annually-varying wind.

7.2 A wind stress field with no curl

The discussion of wind stress has emphasized importance of the curl of the wind stress curl, rather than the stress itself. And yet, the Ekman transport depends only upon the stress, and the Stage 2 response includes a term proportional to the β-induced divergence of the Ekman transport, and thus the stress itself. This raises the question, can there be a steady circulation driven by wind stress alone, that is, by a stress field with no curl?

This suggests an experiment in which a spatially uniform stress is imposed over the ocean basin. To avoid troublesome instances of vanishing layer thickness near boundaries, the stress is made very small, 0.01 N m^{-2}. The amplitude of the resulting currents and layer thickness are also very small, but not too troublesome if the goal is to find the structure of the response, rather than its amplitude.

If the spatially uniform stress is eastward, say, then the Ekman transport is southward throughout the basin, and divergent, Eqn. (51). For short times, $t \leq 1000$ days, this produces a thinning of the active layer (low pressure) that is most pronounced at lower latitudes, while also causing a pileup of water near the equatorial boundary where there is a growing high pressure. The resulting zonal current near the equatorial boundary is thus eastward, and there is a weaker, more distributed westward flow at higher latitudes, evident at $y > $ -2000 km in Fig. (43) (upper and middle).

These zonal currents are necessarily turned into the meridional direction along the eastern boundary, and the result is to initiate a long Rossby wave-like front that propagates westward across the basin. This eastern boundary Rossby wave signals the adjustment toward a steady state, and not too long after the Rossby wave passage the stratification (layer thickness) and flow are indeed quasi-steady. The steady state sea surface (inferred from the layer thickness) slopes up toward the east so that a zonal pressure gradient opposes the wind stress. Most notably, the current in the adjusted steady state vanishes. The bottom line is that absent a curl of the wind stress, there is a vanishing meridional flow in the interior. This is, of course, consistent with expectations of the Sverdrup relation. Given a closed basin, neither can there be a steady zonal flow. (see Sec. 10.2, #12)

7.3 Meridional winds over a basin without sidewalls (a channel)

One last experiment: consider a basin with dimensions as before, but now replace the no normal flow boundary condition on the eastern and western boundaries with a reentrant boundary condition, i.e., for the zonal velocity,

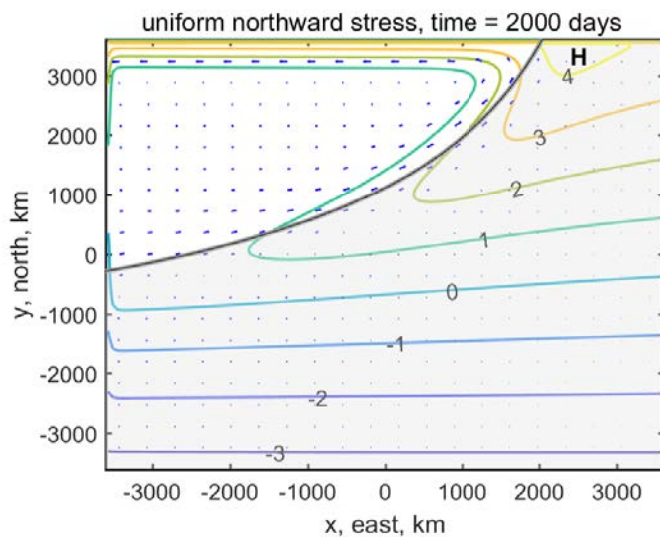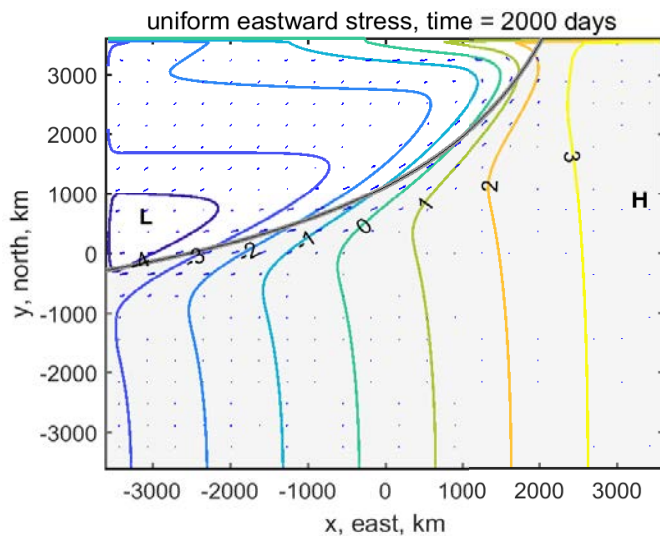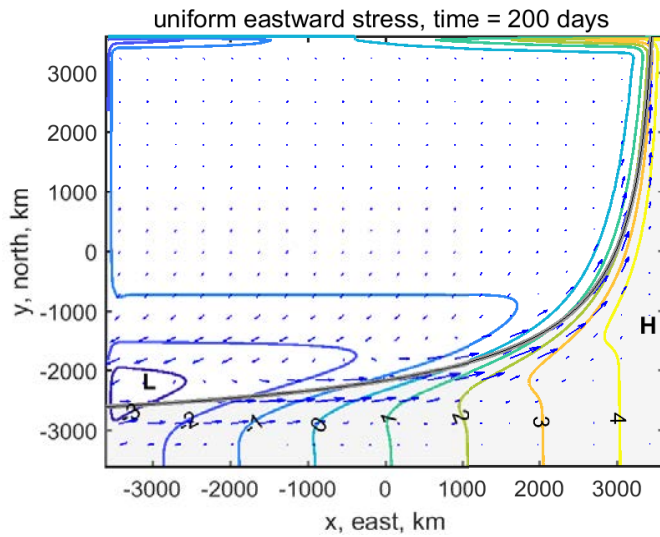$$u(x = -L) \; = \; u(x = L),$$

86

Figure 43: **(upper)** and **(middle)** Two snapshots from a wind-driven experiment in which the wind stress was spatially uniform and eastward at a very small value, 0.01 N m^{-2}. The times were 200 and 2000 days after the stress was switched on. The contours are of the anomaly of layer thickness, in meters. The blue arrows are the current, though with the comparatively very large currents within boundary currents omitted. The gray shading extends westward from the eastern boundary at the y-dependent speed of a long Rossby wave. **(lower)** A snapshot at 2000 days from an experiment in which the wind stress was spatially uniform and northward.

wind stress, τ^y, and north current
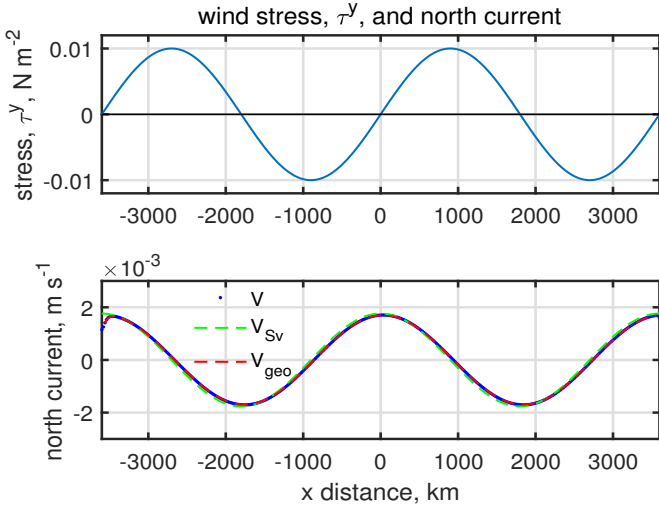
Figure 44: **(upper)** The x profile of the northward wind stress field applied in the channel experiment. The stress was independent of y. **(lower)** The north component of current across $y = 0$ at time = 10,000 days (blue dotted line) along with the expected Sverdrup current (green dashed line) and the meridional, geostrophic current estimated from the thickness field (red dashed line). These are almost identical, and hence the steady meridional flow in this experiment is both geostrophic and Sverdrup, there being no meridional Ekman flow.

as if the basin was a channel that wrapped all the way around a cylinder. Similar boundary conditions are applied to h and v. The wind stress is presumed to be in the *meridional* direction. To be consistent with the channel configuration and the reentrant boundary conditions,

$$\tau^y(x) = \tau_0 \sin(2\pi x/L), \tag{82}$$

(Fig. 44, upper) so that $\tau^y(-L) = \tau^y(L)$ and independent of y. The stress amplitude is made very small, $\tau_o = 0.01$ N m^{-2}, to avoid vanishing layer thickness in boundary currents. Meridional winds certainly do occur over the oceans, especially near boundaries (Fig. 5), but a basin-wide, meridional wind stress field of this sort is found in approximate form only in the Arabian Sea (Part 5). This idealized wind stress field helps to make an important point regarding the role of an eastern boundary vis-á-vis the Sverdrup relation. Given the boundary condition (82) the zonal length scale of the stress field will be written

$$L_\tau^x = L/2\pi,$$

to distinguish from the distance to the eastern boundary that plays such a prominent role in the closed basin cases considered to now.

The Ekman transport that accompanies this meridional wind stress is zonal, and is divergent. The resulting Stage 2 thickness anomaly grows linearly with time as

$$h_{S2} = \frac{\tau_o}{\rho_o f L_\tau^x} \cos(2\pi x/L) \, t,$$

and forms alternate highs and lows, Fig. (45). The Stage 2 meridional geostrophic current is

$$v_{S2} = \frac{\tau_o g'}{\rho_o f^2 L_\tau^{x2}} \sin(2\pi x/L) \, t \tag{83}$$

88

where f is $f(y)$, and so v_{S2} is much bigger at lower latitudes (smaller y) as we have seen before. Like the Stage 2 response of the closed basin cases, this steadily accelerating current persists for only a finite time, hundreds or thousands of days depending upon y, after which it is supplanted by a nearly steady Sverdrup balance,

$$v_{Sv} = \frac{\tau_o}{\rho_o L_\tau^x \beta H} \cos{(2\pi x/L)}.$$

In this experiment, where there is no eastern boundary, the near-steady Sverdrup balance develops first at low latitude, and then spreads northward. At a given y, the adjustment occurs in the time required for a long Rossby wave to propagate westward over the distance L_τ^x, the length scale of the wind stress. The northward extent of the adjusted region is then estimated by

$$L_\tau^x = \frac{\beta C^2}{f^2} t, \tag{84}$$

where f is $f(y)$. Using the beta-plane representation of $f(y)$ and solving for the northward extent of the adjusted region, Y, gives

$$Y = \sqrt{\frac{C^2}{\beta L_\tau^x}} \, t^{1/2}, \tag{85}$$

which is used to define the gray shading of Fig. (45). This makes a plausible estimate of the y that separates the Stage 2 response to the north from the quasi-steady Sverdrup regime to the south. Since L_τ^x is proportional to the basin scale, and so this one case is not completely convincing. The test is that when the east-west scale of the wind stress is made smaller, say $L_\tau^x = L/4\pi$ and thus $\tau^y(x) \propto \sin{(4\pi x/L)}$, while holding the basin width L constant, the adjustment to Sverdrup balance at a given y occurs in half the time seen in this case.

This experiment shows that the relevant east-west scale for adjustment to Sverdrup balance is the smaller of the zonal scales that is imposed on the meridional flow. In the case of a closed basin with zonal winds that are independent of x, that scale is the distance to the eastern boundary. In the present experiment, this zonal scale comes from the wind field itself. This is an important result used in Part 5 to rationalize the very rapid response of the Arabian Sea to monsoon winds.

8 Barotropic and baroclinic circulation of the three layer, free surface model, 3l-fs

In this section we will take a look at the same experiment — same winds and basin — but solved with the more capable three layer model described in Sec. 4.6.2 and dubbed 3l-fs. Compared with the single layer, reduced gravity model, this new model has a somewhat thinner surface layer that absorbs the wind stress,
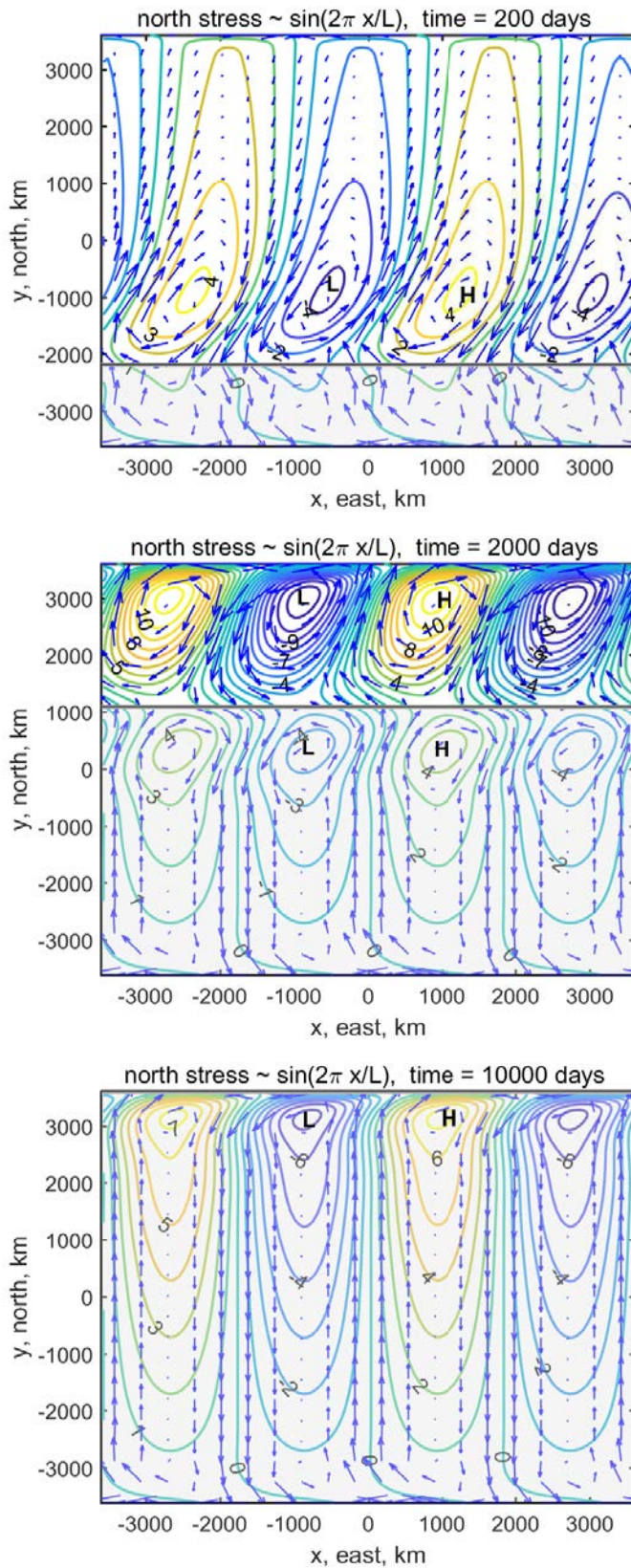
Figure 45: Snapshots from a wind-driven experiment in which the basin is a channel, and the wind stress was northward and x-dependent (Fig. 44, upper). The stress was set to a very small value, 0.01 N m^{-2}. Times were 200, 1000 and 10000 days (upper, middle, lower) after the stress was switched on. The contours are the anomaly of layer thickness in meters and the blue arrows are the current, though with boundary currents omitted. The gray shading extends northward from the southern boundary to a distance Y determined by the time, the y-dependent long Rossby wave speed and the zonal scale of the wind, L_τ, via Eqn. (85). Poleward of Y the flow is in Stage 2. Notice that there is clear evidence of westward propagation in especially the southern part of this region. Equatorward of Y the flow is adjusted to a near steady state Sverdrup balance (Fig. 44, lower). At a given y, the progression from Stage 2 to Sverdrup flow occurs at the same time across the entire channel (independent of x).

90

a thermocline layer, and a thick, active abyssal layer. It solves for a free sea surface and so the pressure anomaly is computed from the mass field in a completely straightforward way (Sec. 4) with no appeal to the reduced gravity approximation.

The baroclinic phenomena of the reduced gravity model are contained within the three layer model, let $h_2 \to 0$, and $h_3 \to \infty$, though with somewhat different amplitudes. The important point is that everything that was learned from the reduced gravity model makes a useful contribution towards understanding the more comprehensive (and also more interesting) results described next. The solution of the 3l-fs model contains additional phenomenon, and especially barotropic phenomena, that are different in amplitude and time scale from the purely baroclinic phenomenon of 1l-rg, but are not truly different in kind.

The new solution is certainly more voluminous in the sense that $u = u(x, y, z, t)$ in place of $u = u(x, y, t)$. Though the z dimensionality is still strongly truncated, it is nevertheless challenging to display the full solution in a manuscript. To start, the emphasize will be one 'latitude', $y = -1000$ km, which is on the south side of the subtropical gyre. At this latitude there is both an appreciable wind stress, $\tau^x = -0.075$ Pa toward the west, and a significant stress curl, $\nabla \times \tau = -5.8 \times 10^{-8}$ Pa m^{-1}, which implies clockwise turning. The data from this latitude are shown in three forms. 1) At the basin center 'longitude', $(x, y) = (0, -1000)$ km, the current east and north components for each layer are shown for the first 30 days in Fig. (46). 2) The meridional component of the transport at the same site but for short, medium and long times is in Fig. (47). 3) The meridional volume transport across the interior of the basin is in Fig. (48).

8.1   Inertial motion and Ekman transport in the surface layer

For short times, a few tens of days, the surface layer current and transport is familiar from the reduced gravity model, or for that matter, a purely local model, viz., near-inertial currents in both components, and Ekman transport in the meridional component, (the surface layer is represented by the red lines of Figs. (46) - (48). At the site sampled in these figures, $y = -1000$ km, the wind stress is westward, hence the Ekman transport is positive (northward) and has the magnitude expected for the wind stress at this site. This Ekman transport occurs throughout the model domain, though of course with varying amplitude and sign depending upon the local wind stress (just as in Sec. 4.1).
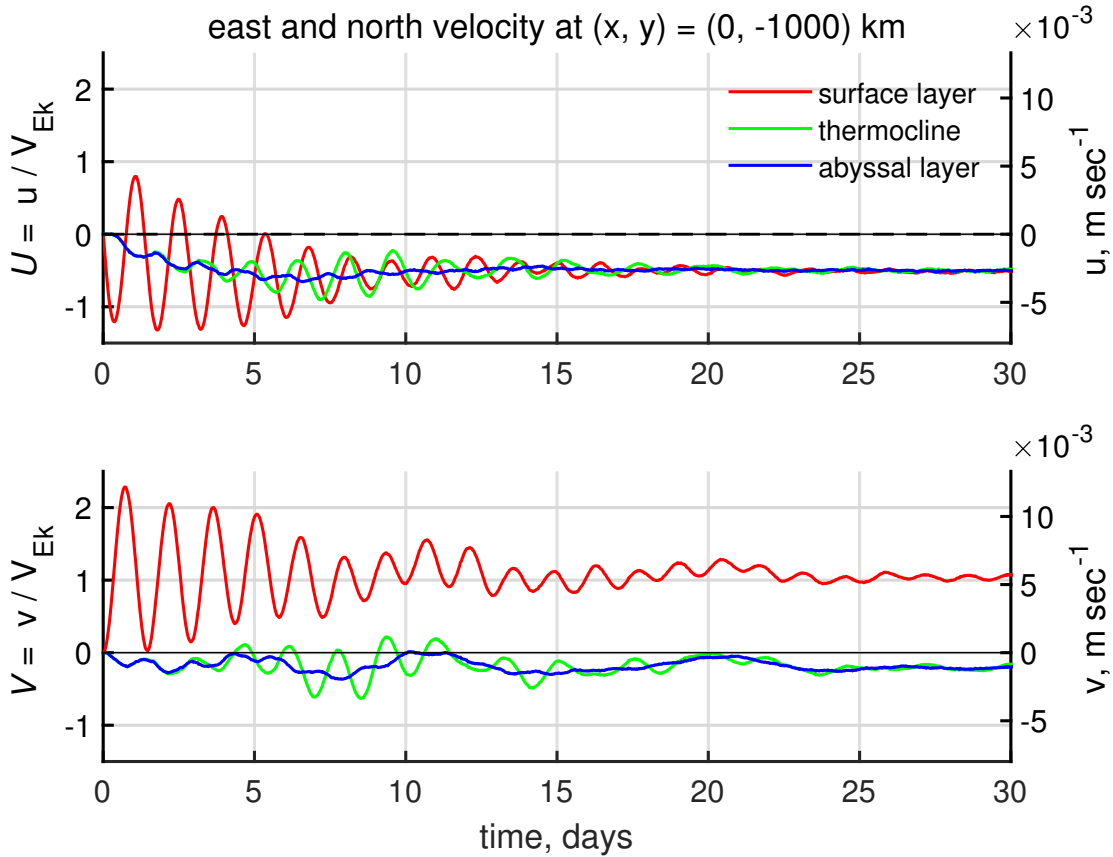
Figure 46: The short time evolution of the east and north components of the current computed by the three-layer model and sampled on the southern side of the subtropical gyre, $(x, y) = (0, -1000)$ km. Currents are normalized by the Ekman velocity scale, Eqn. (48), evaluated at this location, $V_{Ek} = 5 \times 10^{-3}$ m sec^{-1}. **(upper)** East currents in each of the the three layers; surface layer currents are in red, etc. The high frequency oscillations seen here are near-inertial motion. The time-mean of u is associated with barotropic Sverdrup flow discussed in the main text. **(lower)** North currents. The time mean dimensional current is about 5×10^{-3} m sec^{-1} and the non-dimensional value is about 1. This is as expected if the surface layer current is mainly Ekman flow. Layers 2 and 3 are unaffected by the direct wind stress, but nevertheless evidence a small, southerly barotropic Sverdrup flow that is modulated by barotropic Rossby waves having a period of about five days. The barotropic (depth independent) motions are much more prominent in the transport, bext figure.
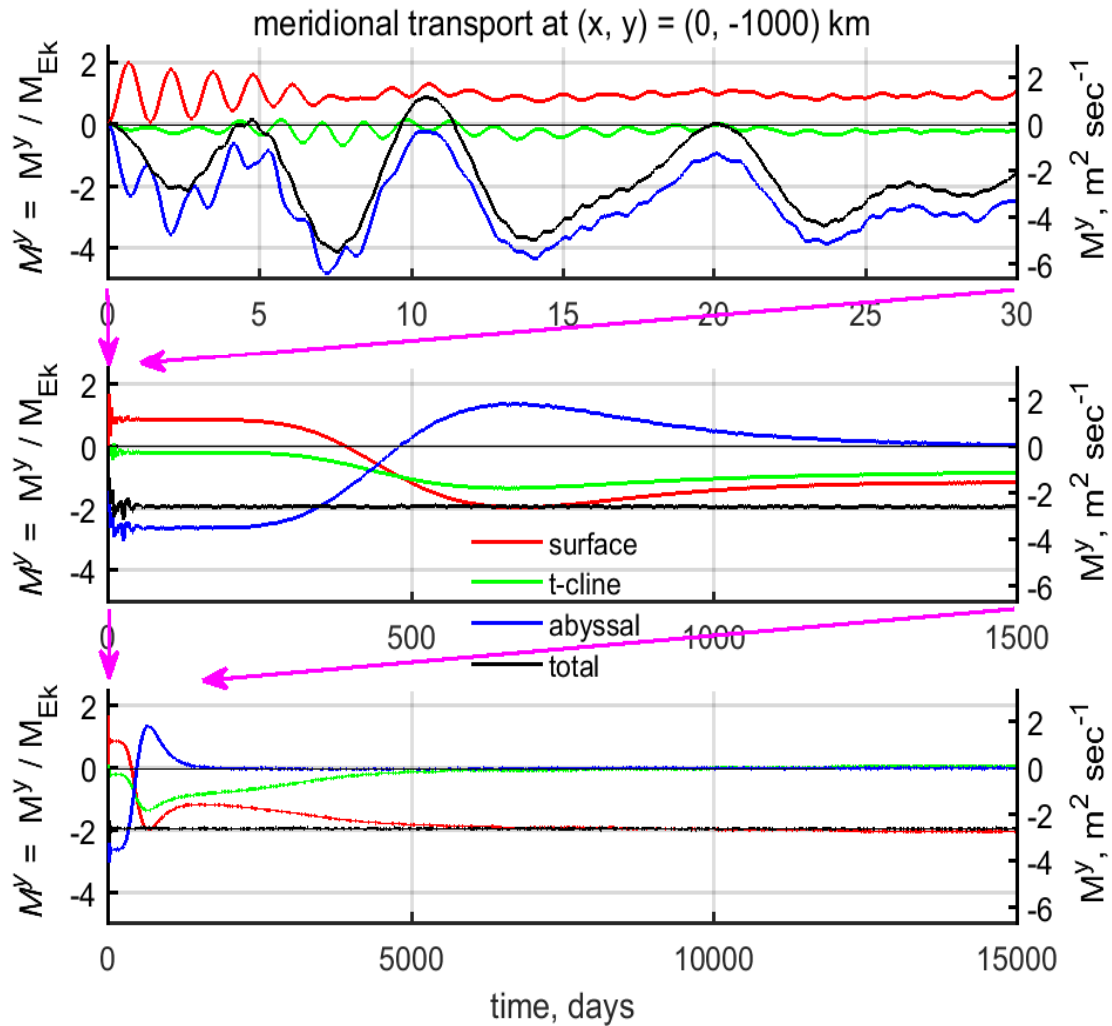
Figure 47: The meridional component of the transport at $(x, y) = (0, -1000)$ km. The data are shown on three time scales, **(upper)** 0 - 30 days, **(middle)** 0 - 1500 days, and **(lower)** 0 - 15000 days. Dimensional scale is shown at right, and nondimensional scale is at left. In this figure the transport is normalized with the expected Ekman transport magnitude at this y, $M_{Ek} \approx 1$ m^2 sec^{-1}. The surface layer transport (red line) is mainly Ekman transport and is northward. The total transport (all three layers) is the black line, which notice, has a very large contribution from the abyssal layer at short times, and is southward.
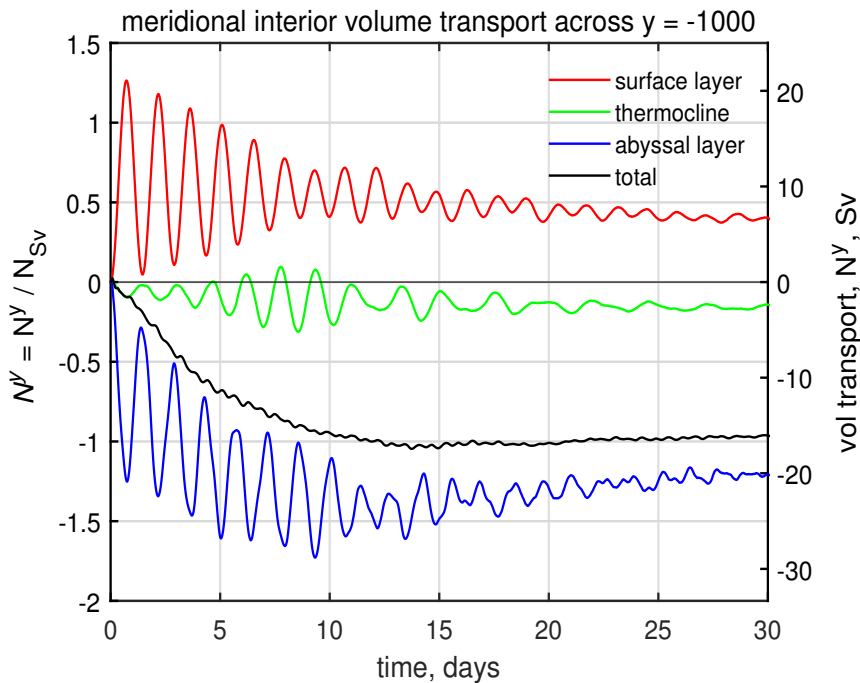
Figure 48: Meridional volume transport in the basin interior across y = -1000 km. The transport has been integrated from the eastern boundary to within 200 km of the western boundary. The volume transport within the surface layer (red line) is mainly Ekman transport and is northward as in the previous figure. The volume transport in the thermocline and abyssal layers is shown by green and blue lines; the sum over the three layers (the full water column) is the total volume transport shown as the black line. The dimensional scale is at right, and a nondimensional scale based upon the expected Sverdrup transport magnitude at this y, $N_{Sv} = 17$ Sv, is at left. Notice that the total transport appears to be quasi-steady from day 10 onward, and is -1 in these nondimensional units. Hence, the total transport is consistent with Sverdrup transport at this y.

8.2 Transient, barotropic flows

Over the region of negative stress curl that becomes the subtropical gyre, the Ekman transport is convergent. If that was all that was relevant, this Ekman convergence would thicken the surface layer at a rate of about 3 cm per day. In the context of a reduced gravity model, this produces a slowly growing baroclinic pressure gradient, and consequently a slowly increasing baroclinic, geostrophic current. By slowly is meant that it takes hundreds of days for this purely baroclinic process to produce an appreciable pressure gradient. The presence of an active (or free) sea surface and an active abyssal layer in the present model gives a much quicker barotropic response. A thickening of the surface layer by a few centimeters will tend to cause a positive displacement of the sea surface by a few centimeters/2. A displacement of the Layer 2 interface by this amount is hardly noticeable, but a displacement of the sea surface by a few centimeters is quite significant insofar as it produces a significant pressure gradient and thus flow within the thick abyssal layer. The resulting abyssal and thermocline layer currents are small amplitude, but the associated transport (current times thickness) is large since the abyssal layer is very thick, (Fig. 47). For short times, a few weeks or even just a few days (Fig. (48, upper) the meridional transport at the observation site $(x, y) = (0, -1000)$ km shows a time mean to the south, and a pronounced oscillation having a period of about five days. These oscillations are associated with short, barotropic Rossby waves, which like higher frequency inertial oscillations, are an unintended byproduct

94

of the impulsive start of the wind stress.

8.3 Basin scale circulation; barotropic Sverdrup flow

The convergence of Ekman transport in the middle of the model domain leads to a small positive SSH anomaly and thus a high pressure, Figs. (49) and (50). On day 1, SSH was a fairly symmetric mound with an amplitude of about 1 cm, centered in the model domain, and accompanied by geostrophic currents that flowed clockwise around the high pressure. These currents were subject to the beta-effect, divergence where the flow was southerly and convergent where it was northerly. The result is that the growing SSH anomaly had a tendency for a beta-induced westward translation, just as we have seen in mesoscale eddies, for example. A key difference is the rate, $O(1000 \text{ km day}^{-1})$, which is much, much faster than westward translation of baroclinic mesoscale eddies and baroclinic Rossby waves. This speed is in the range of long, barotropic Rossby waves. By day 3, the positive η_1 hump was compressed up against the western boundary, and by day 10 the slope over the interior of the subtropics was an almost uniform tilt down from west to east. The plan view of the SSH shows cyclonic gyres in the tropics and subpolar regions and an anti-cyclonic gyre that fills the subtropics. Thus within the first ten days of the experiment, the ocean circulation develops as three gyres that in many respects — save for their depth-independence and small amplitude — are a foretelling of the baroclinic circulation that will follow in the next several years of this integration, and that characterized the purely baroclinic circulation of the 1l-rg model.

If the barotropic flow in the interior is consistent with the Sverdrup relation, then the barotropic meridional velocity is

$$V_{Sv-btr} = \frac{1}{\rho_o H \beta} \nabla \times \tau.$$

Along $y = 0$, the center of the subtropical gyre, the expected Sverdrup flow has a dimensional amplitude $V_{Sv-btr} = 1.0 \times 10^{-3} \text{ m sec}^{-1}$. In the gyre center $y = 0$, the wind stress and Ekman flow vanish, and so this V_{Sv-btr} is nearly geostrophic. The sea surface slope is thus expected to be

$$\frac{\partial \eta_{Sv-btr}}{\partial x} = \frac{f}{g} V_{Sv-btr} = \frac{f}{\rho_o g H \beta} \nabla \times \tau. \tag{86}$$

If this holds across the entire basin, then the SSH amplitude across the basin is just

$$\eta_{Sv-btr} = 2L \frac{\partial \eta_{Sv-btr}}{\partial x} = \frac{2fL}{\rho_o g H \beta} \nabla \times \tau. \tag{87}$$

For the present experiment at $y = 0$, $\eta_{Sv-btr} \approx 0.06$ m. These estimates are very close to the slope and SSH amplitude found in the numerical experiment, Fig. (50), but are much, much less than the amplitude found in the western subtropical North Atlantic, which is about 1 m east-to-west, Fig. 1. At this time the volume transport within the subtropics was very close to that expected from the Sverdrup relation (Fig. 51, left), and of the expected sense in the tropics and subpolar regions. As we saw before with the
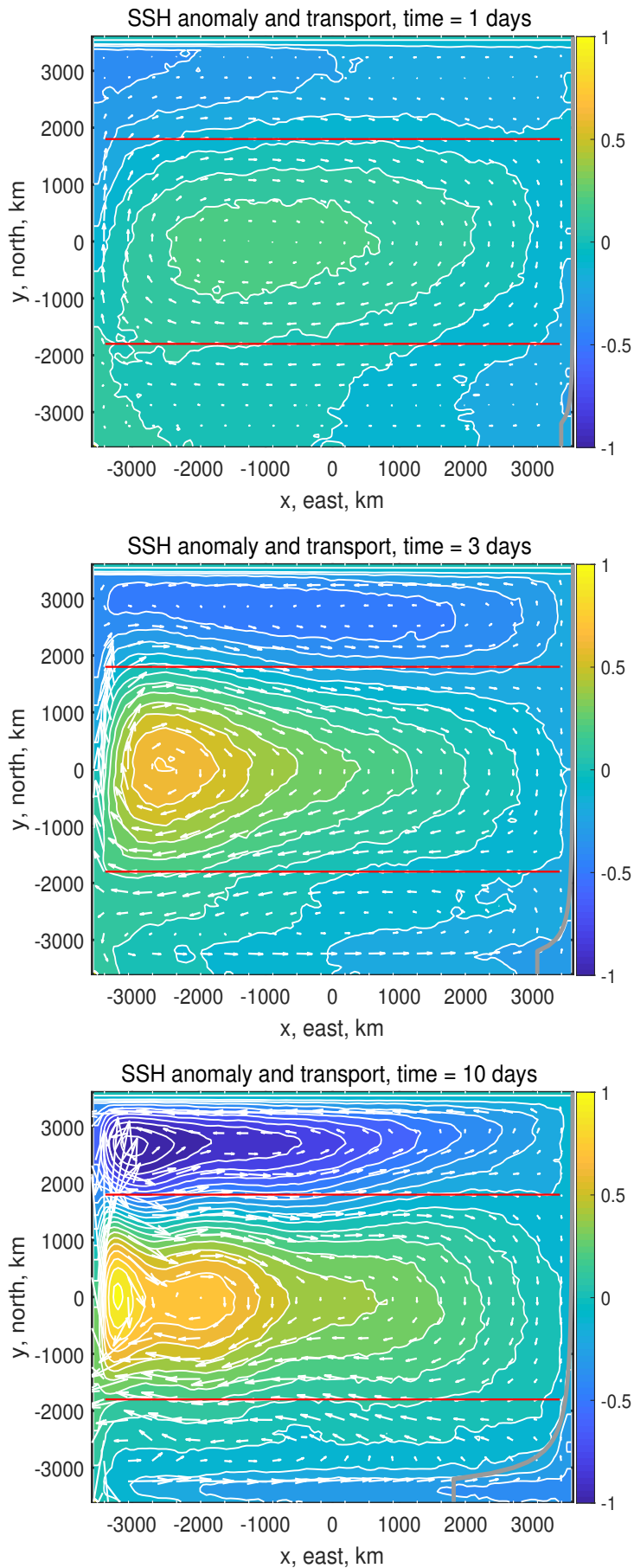
Figure 49: Three snapshots of SSH anomaly from a wind-driven, three-layer experiment at 1 day, 3 days and 10 days (top to bottom) after wind stress was switched on. The thin red horizontal lines are the axis of the westerly and easterly wind stress (Fig. 16). The small white arrows are the transport, though with the comparatively very large transports within the wbc omitted. The contours and colors are the SSH anomaly normalized with the barotropic Sverdrup SSH scale, Eqn. (87), evaluated at 30° N $\eta_{Sv-btr} = 0.06m$. The largest positive SSH anomaly at day 10 is (dimensional units) $\eta \approx 0.06$ m in the western central subtropical gyre, and the greatest negative value is ≈ -0.09 m in the western subpolar gyre. The basin scale pattern evident here, *viz*, three highly asymmetric gyres, persists with minor changes for hundreds of days.

sea surface height anomaly, y = 0
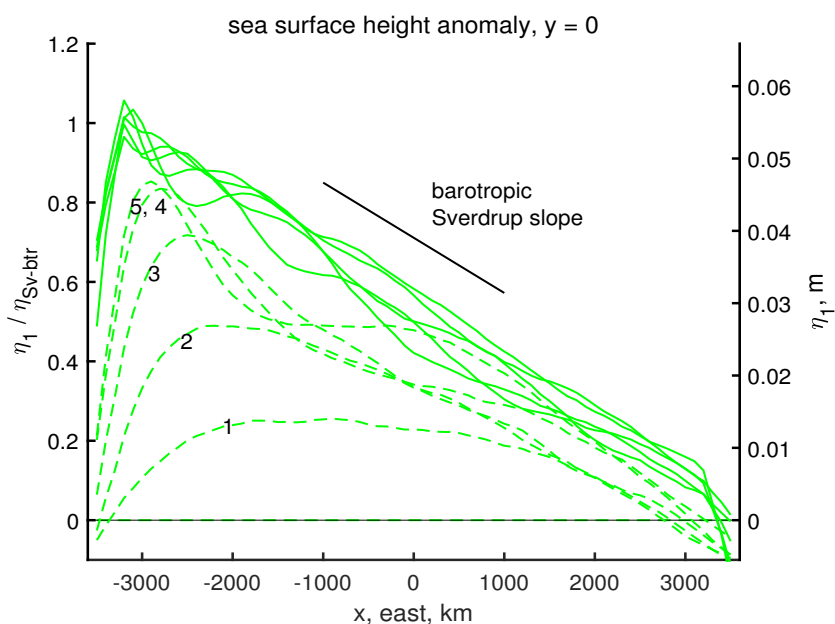
Figure 50: Successive across-basin profiles of SSH anomaly along $y = 0$. The first five days are the dashed green lines at 1 day intervals, and the next 25 days are solid green lines at 5 day intervals. The amplitude is scaled with the barotropic scale, Eqn. (86) which, for the parameters of this experiment, $\eta_{Sv-btr} = 0.05$ m. Note that on day 1 the SSH was a fairly symmetric mound. By day 3 this mound had shifted noticeably to the west, implying very rapid westward propagation, O(1000 km day^{-1}). After only about a week, the SSH slope over the interior region was close to the slope expected for a barotropic Sverdrup flow in geostrophic balance.

meridional interior volume transport, time =10 days
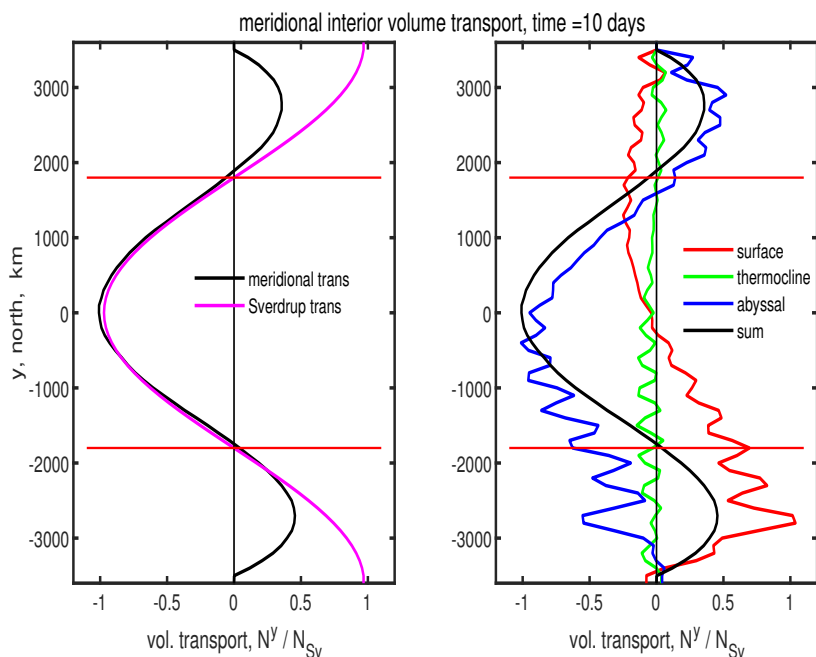
Figure 51: Meridional volume transport across the interior portion of the basin for all y and at time = 10 days. **(left)** Total transport (black line) and the expected Sverdrup transport (magenta). These are very similar over the subtropical gyre, but differ considerably near the northern and southern boundaries where the actual meridional transport must vanish. **(right)** Meridional transport in each of the layers of the three layer model, and summed to give the total transport, the black line, which is the same as at left.

reduced gravity model, there is a rather wide region adjacent to the northern and southern boundaries within which the meridional transport goes to zero as it must to satisfy the no normal flow condition on the solid boundaries. At this short time, the Sverdrup transport occurred throughout the water column, and in fact was mainly in the abyssal layer, Fig. (51, right).

8.4 Baroclinic adjustment to a surface intensified, steady state

After the first week, the SSH slope over the interior appeared to be quasi-steady. However, there was also evidence that SSH was continuing to evolve, albeit slowly. Sea level was rising very slowly over the entire subtropics, and, there was a region of much steeper SSH slope developing close to the eastern boundary and spreading slowly westward. This was the start of a baroclinic adjustment toward a surface-intensified, steady state.

The currents at $(x, y) = (0, -1000)$ km continued to evolve, albeit very slowly compared to the very rapid onset of the barotropic state. The abyssal layer transport, which early on made up most of the total Sverdrup transport, began to weaken at about 400 days, and then oscillated once and settled to nearly zero at about 1400 days, Fig. (47, middle). The total transport remained consistent with Sverdrup transport, but thereafter, the Sverdrup transport was contained within the thermocline and surface layers. At about 1500 days, the thermocline layer transport started a slow decrease and then nearly vanished by about 7000 days, Fig. (47, lower). Thereafter, the Sverdrup transport was contained almost entirely within the surface layer. These times, very roughly 1000 days and 5000 days, are very broadly consistent with the expected transit time of the first and second baroclinic modes from the eastern boundary to the basin center, about 700 days and 2700 days for the first and second baroclinic modes at this y which is equivalent to about latitude = 22° . Consistent with this, and perhaps more convincing of a modal description is that the change of the current profile over time looks a lot like the first and second baroclinic modes (Fig. 53), e.g., from 1500 days to 7000 days the change in the current is consistent with the arrival of a second mode (the abyssal layer remains at rest, while the thermocline and surface layers accelerate in opposite directions). If you look closely you can see that the change in the current profile is not exactly like a second mode in that the decrease of the thermocline layer is greater in amplitude than the is the evident increase of the surface layer. The size of the change is inversely proportional to the layer thicknesses, which at this time had changed quite a lot from the initial values; the surface layer was considerably thicker and the thermocline significantly thinner than in the initial state, Fig. (54).

The total transport — Sverdrup transport — is unchanged as these baroclinic waves pass by, but the distribution of the transport becomes increasingly surface intensified. In the final, steady state, the Sverdrup transport occurs entirely within the surface layer. At one level this is not surprising, as the surface layer absorbs all of the wind stress and stress curl. Thus, only the surface layer can sustain a steady meridional flow in the presence of a beta effect. The deeper layers can be set into motion during the transient stage of the response, since they are subject to pressure gradients, and hence can sustain geostrophic motion. They are also subject to being compressed and stretched, Fig. (55), and so can display some of the consequences of potential vorticity conservation, i.e., there can be a q-conserving flow in the deep and thermocline layers so long as they are being stretched. However, this can not continue into a steady state in which stretching (time changing thickness) vanishes.
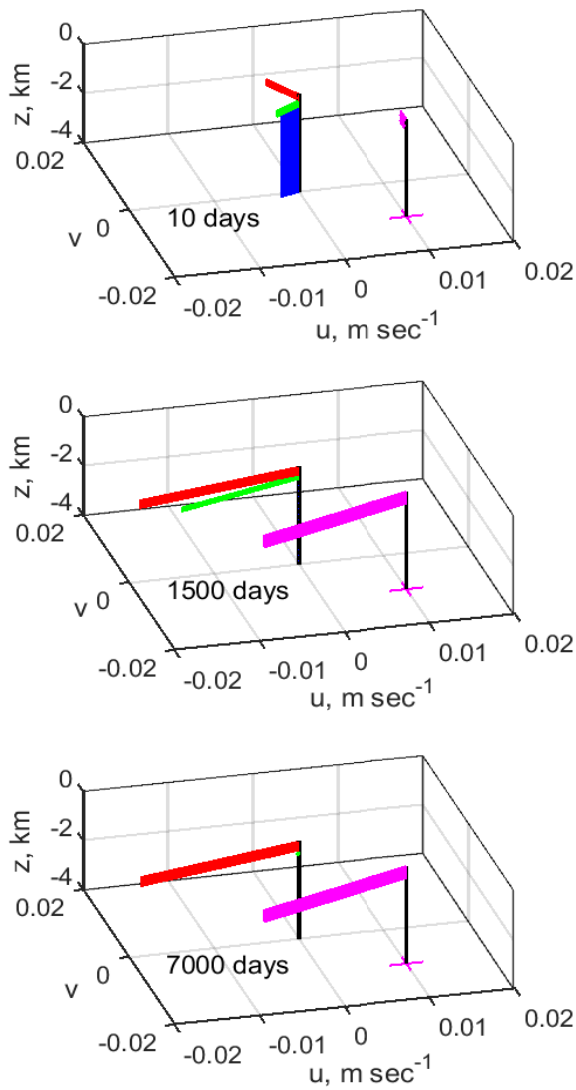
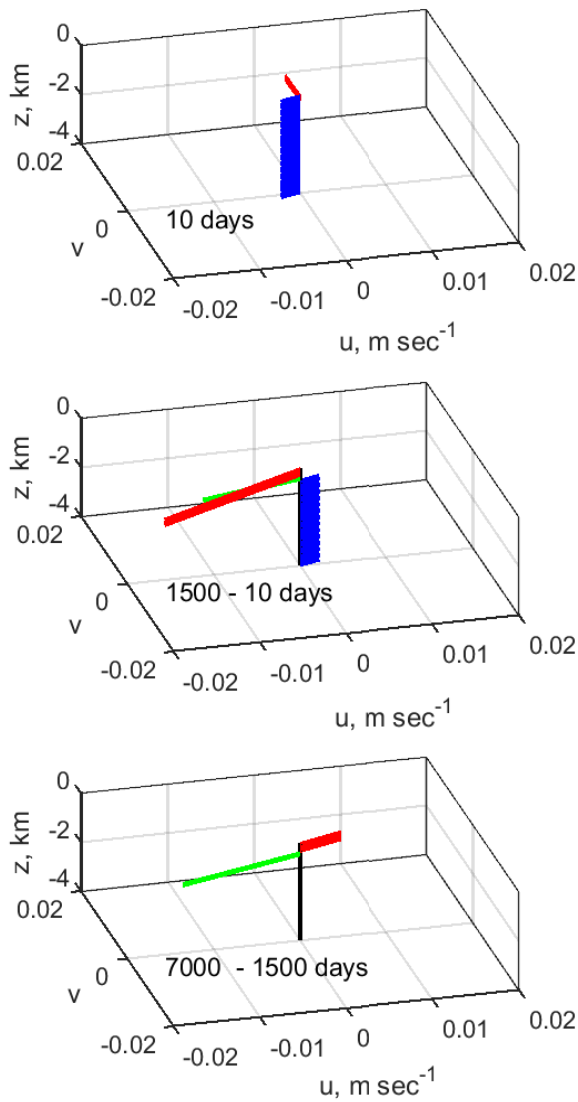Figure 52: Model-computed current profiles from the site $(x, y) = (0, -1000)$ km, shown at three times, **(top)** to **(bottom)**, 10 days, 1500 days and 7000 days. The three-color profile is from the three-layer model, and red, green and blue are the surface layer, thermocline and abyssal layers, respectively. The magenta only profile (offset from center) is from the single layer model. The view is towards the north-northeast. An abyssal layer flow is appreciable only at 10 days in the former. The three-layer profile goes from being barotropic with a small Ekman flow in the surface layer at 10 days, to entirely surface trapped at 7000 days. At this site the flow in the steady Sverdrup regime at 7000 days is somewhat stronger in the zonal direction than in the meridional direction, cf. Fig. (56). Notice that the current in the single layer model is quite similar to the three-layer profile, except at 10 days.

Figure 53: Current difference profiles from the site $(x, y) = (0, -1000)$ km, shown at three times, **(top)** to **(bottom)**, 10 days, 1500 days and 7000 days, as in the previous figure. In the top panel, the red arrows are mainly Ekman flow, and blue vectors are the abyssal layer, the depth-independent barotropic flow at 10 days. The middle panel is the velocity difference, 1500 days - 10 days. Notice that this velocity difference is qualitatively much like the first baroclinic mode; upper and middle layers are in roughly the same direction and opposite the abyssal layer. (Fig. 18). The bottom panel is the velocity difference 7500 days - 1500 days. There is only a very small current in the abyssal layer, while the surface and thermocline currents are in approximately opposite directions, much like the second baroclinic mode.
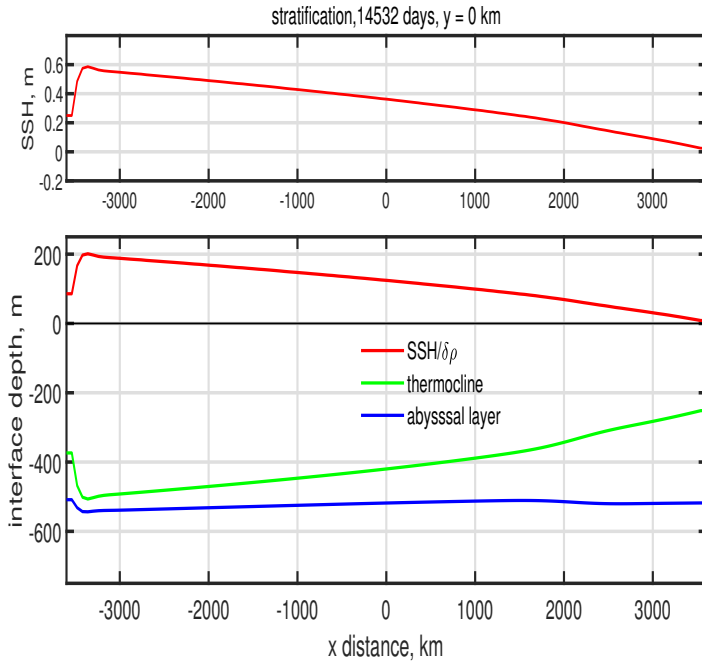
Figure 54: The SSH (upper panel, red line) and the interface between layers across the basin at y = -1000 km (red, green and blue; lower panel). Notice that the interface between the abyssal and thermocline layers (blue line) is essentially flat; there is almost no flow in the abyssal layer or the thermocline at this time. Also, note that the surface layer thickens markedly to the west and is generally much thicker than it was in the initial condition (250 m). The thermocline is generally much thinner.

9   Summary and closing remarks

9.1   O1: Upper ocean gyres seen in SSH are correlated with the wind stress curl

The large scale pattern of SSH anomaly, Figs. (1) and (4), correlates well visually with the large scale distribution of wind stress curl: SSH highs (the five subtropical gyres) are found beneath regions of negative stress curl, and SSH lows (the two subpolar gyres) are beneath positive stress curl. There is a simple mechanism behind this correlation, insofar as wind stress curl is approximately proportional to the divergence of the wind-driven Ekman transport (and negative stress curl yields a convergence of Ekman transport and thus a high of SSH and a thick upper ocean layer). This is the Stage 2 local response to wind and windstress curl discussed in Sec. 4.2. Model results suggest that a steady state, which is presumably what we see in the long-term mean of Fig. 1, follows from an adjustment to Sverdrup flow, in which the correlation is between meridional flow and wind stress curl.

9.2   O2: Upper ocean gyres are markedly asymmetric east to west

Sverdrup flow over most of the interior of a basin. The basin-scale, horizontal structure of the wind-driven ocean circulation, including western intensification and several of the qualitative differences between tropical, subtropical and subpolar gyres, have a plausible analog in solutions of the shallow
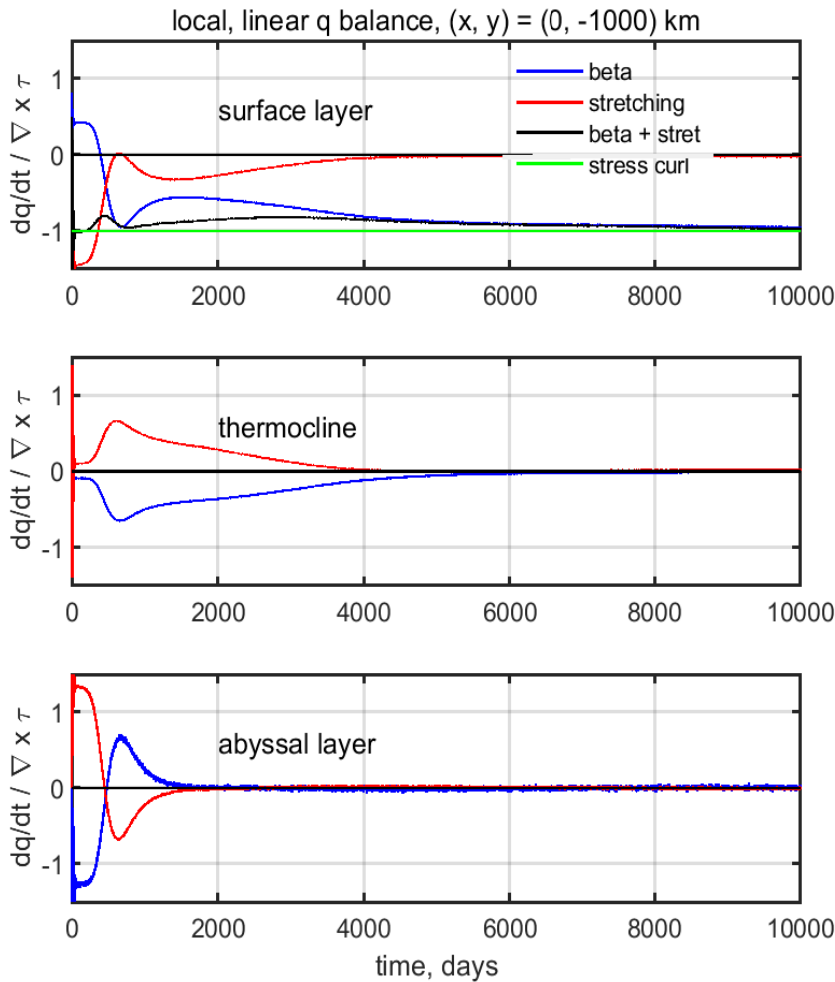
Figure 55: The linear balance of potential vorticity in, top to bottom, the surface layer, the thermocline and the abyssal layer.

water model. Over the subtropical North Atlantic, where the wind stress curl is negative, the interior meridional flow is southward as expected from the Sverdrup relation. Over the tropical and subpolar regions, the stress curl is positive and the meridional flow is northward, also as expected from the Sverdrup relation. This general result — that the Sverdrup relation provides a plausible and useful explanation of the major wind-driven gyres — has been accepted since at least the 1940s, and has been tested and validated quantitatively in modern, field data-based studies[10].

The Sverdrup relation is expected to be valid provided that the dominant processes of the potential vorticity balance are just two: the beta effect acting upon a very slow and thus linear meridional current, in balance with the curl (torque) of the wind stress. In practice, this holds in the majority of interior regions that are well away from zonal or meridional boundaries (hundreds of kilometers).

Departures from Sverdrup flow in zonal and meridional boundary regions. In a steady circulation, the meridional Sverdrup transport across every zonal, cross-basin section must be returned in
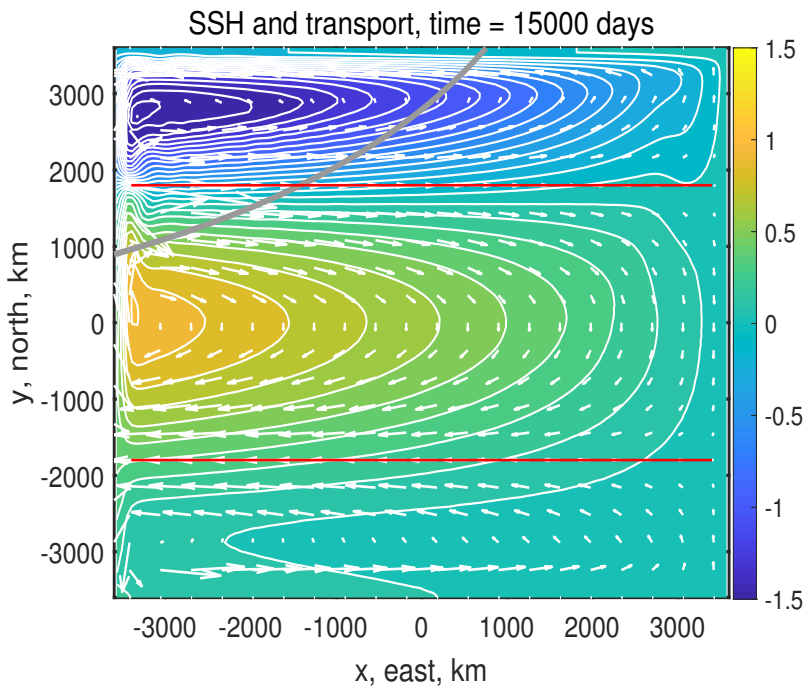
Figure 56: SSH anomaly from the three layer model experiment at time 15000 days. The thin red horizontal lines are the axis of the westerly and easterly wind stress (Fig. 16). The small white arrows are the transport, though with the comparatively very large transports within the wbc omitted. The SSH anomaly is nondimensionalized by the baroclinic scale, $\eta = 0.9$ m. The parabola at upper left is the second baroclinic eastern boundary wave, which notice, has still not swept the entire basin.
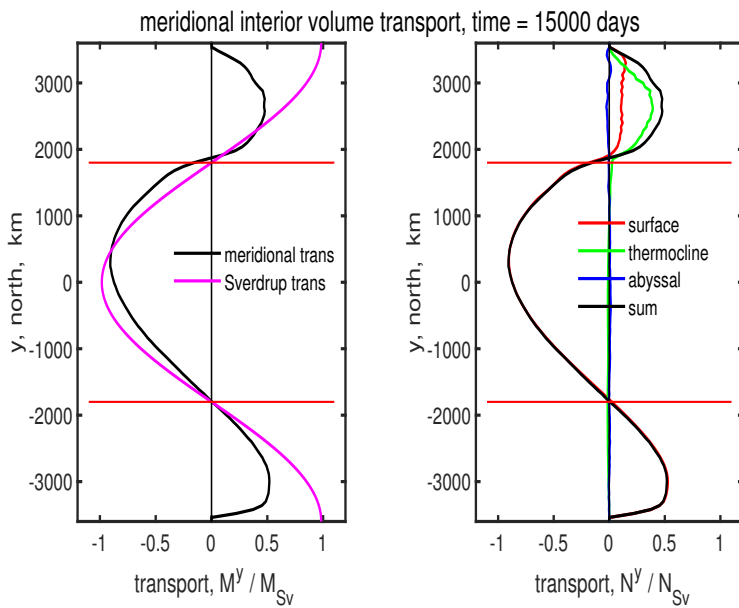

Figure 57: Meridional volume transport across the interior portion of the basin for all y and at time = 15000 days. **(left)** Total transport (black line) and the expected Sverdrup transport (magenta). These are similar over the subtropical gyre, but differ considerably near the northern and southern boundaries where the actual meridional transport must vanish. **(right)** Meridional transport in each of the layers of the three layer model, and summed to give the total transport, the black line, which is the same as at left. Notice that the total transport is mainly in the surface layer except in the subpolar gyre where there is still considerable transport in the thermocline, cf. Fig. (56).

103

the opposite direction by some other process. In the shallow water model and in the real ocean, this return flow occurs in a comparatively narrow and thus very intense western boundary current (wbc). The wbc is northward in the subtropical gyre where the Sverdrup transport is southward, and reversed in the subpolar and tropical gyres. The width of the western boundary region is observed to be very narrow, O(100 km). In the simple shallow water model used here, the width of the wbc is the baroclinic radius of deformation. The inviscid, linear Sverdrup interior fills the rest of the basin, 7000 km, and hence the westward intensification (east-west asymmetry) of the major ocean gyres is very pronounced, about 7000/100 in a North Atlantic-size basin.

The meridional flow must vanish on zonal boundaries. In the present model, the zonal boundary dynamics includes a significant contribution from linear friction, which is dubious as a model of dissipation in the real ocean. The width (north-south extent) of the affected zonal boundary region is rather wide, O(1000 km) and thus the meridional flow in the northern half of the subpolar region is less than would be expected from a Sverdrup balance and goes to zero on the boundary (which is expected, of course).

9.3   O3: Subtropical and subpolar gyres are quasi-steady while tropical circulation shows significant seasonal variation

Startup time of the baroclinic circulation. A wind-driven, start-up experiment in the 1l-rg (one layer, reduced gravity) model shows that the baroclinic circulation at a given point in the interior of a large ocean basin reaches an approximate, steady, Sverdrup flow some time after the passage of what amounts to a long, baroclinic Rossby wave starting from the eastern boundary. The long Rossby wave speed, $\beta C^2 / f^2$, which has a strong dependence upon latitude, is thus a crucial parameter in the time-dependent response of a wind-driven gyre. For a North Atlantic-sized basin, the elapsed time required to reach full steady state is about thirty years at a subpolar latitude, about five years in the subtropics, and much less, about a year, in the tropics.

Annually-varying winds. This marked latitudinal variation in the rise time of the baroclinic wind-driven circulation is relevant to understanding the observed response to an annually-varying wind stress. Model experiments that assumed a ±50% annual period variation of the wind stress find that the subpolar circulation varies almost not at all, the subtropical gyre varies only a little, while some aspects of the tropical circulation vary quite a lot. The transport of the tropical wbc varies by only about ±10%, but the zonal flow in the eastern half of the tropical gyre varies by ±50%. This latter variation is mainly a local a response to the annually-varying stress curl, and partly a Sverdrup flow. Thus a seasonally varying wind stress that will have almost no effect on the subpolar or subtropical circulation (interior or wbc) and yet will produce a fairly pronounced response of especially the zonal, open ocean SSH and currents within the eastern tropical ocean.

Barotropic circulation. This essay emphasizes the baroclinic circulation because that is what we can see in the kinds of observations that are most widely available — SSH from satellites and upper ocean density from a variety of *in situ* methods, e.g., Figs. (1) and (2). As well, baroclinic circulation contributes the majority of meridional heat transport by the oceans. However, we shouldn't dismiss out of hand the possibility and importance of a barotropic circulation (which is inaccessible to the 1l-rg model). To get a sense of the barotropic circulation requires a model with a free (moving) sea surface and that supports very fast barotropic waves (here, 3l-fs). Now let's ask the question — how long does it take to establish a quasi-steady Sverdrup regime after the onset of a wind field? The answer is about one week, if we acknowledge the barotropic response. The currents associated with the barotropic response are distributed throughout the water column, and hence the upper ocean current is very small. Similarly, the SSH signature is about 10% of that observed.

9.4   O4: The Sverdrup flow of the subtropical gyre is somewhat surface intensified

The vertical profile of the geostrophic current that makes up the Sverdrup transport of the North Atlantic subtropical gyre was observed to have a depth scale of about 300 - 600 m, with shallower values to the eastern side of the basin (Sec. 2.4). It is probably not coincidental that this is closely comparable to the thickness (depth) of the main thermocline. The zonal tilt of the main thermocline provides the thermal wind that leads to the somewhat surface intensified Sverdrup flow. A multi-layer model (Sec. 8) that was initialized with a plausible main thermocline thickness will develop Sverdrup flow within a surface layer that has about that same thickness and zonal tilt. That seems promising at first, but contains two difficulties. First, the approximate depth scale of the thermocline was initial data for the model, and so not truly predicted. Second, the Ekman layer and the Sverdrup layer of the present three-layer model are *per force* the surface layer of the model, and considerably thicker than is the actual Ekman layer of the ocean (400 m vs 100 m). A fully predictive model of the Ekman and Sverdrup layers will have to recognize vertical mixing associated with surface layer processes (wind mixing and air-sea heat flux, among others) in order to have a realistic Ekman layer thickness. As well, baroclinic instability will likely help redistribute horizontal momentum in the vertical, and increase the effective thickness of the Sverdrup layer well beyond that of the Ekman layer.[21]

---

[21]To follow up on this requires a depth-dependent model and some means to specify the depth of the Ekman layer, d_{Ek}. These are outside the present scope, but note that a landmark advance on the theory of wind-driven circulation was developed along this line by Jim Luyten, Joe Pedlosky and Hank Stommel, 'The ventilated thermocline', J. Phys. Oceanogr., Feb. 1983.

10 Supplemental material

10.1 Links to models and updated manuscripts

The code used to solve the wind-drive circulation problems discussed here is very similar to that used in the Parts 2 and 3 treatments of geostrophic adjustment and eddy propagation. However, the data required to specify the configuration of the wind-driven experiments is sufficiently different that a dedicated program was written:

>   **gyre.for** is a Fortran code that solves the shallow water equations for the wind-driven circulation in an enclosed ocean basin. A variety of wind stress forms and time histories may be specified. The numerical methods are not highly sophisticated or complex, and the code should be fairly amenable to modification. The longest integrations shown here will run in a few hours on a fairly capable, PC workstation. Output goes to a Matlab.mat file which may be read by a Matlab script,
>
>   **gyre_plot.m** makes several kinds of diagnostic plots from the data generated above.

These codes may be downloaded from https://www2.whoi.edu/staff/jprice/aCt-codes

10.2 Homework problems

1. At 30° N, $f = \Omega$, and the inertial period is $2\pi/\Omega = 23$ hrs, 56 min, or less than a day by $\approx 1/365$ days. Can you explain where this small difference with a day comes from?

2. Starting with Eqns. (8) and (7), eliminate v to derive the corresponding governing equation for h. Is it significant that this wave equation is first order vs. the more common second order equation, e.g., shallow water gravity waves? What is the consequence of the beta effect in the case that the zonal gradient of thickness is positive? Is it relevant that the momentum balance Eqn. (8) is geostrophic?

3. Can you relate the observed summer to winter change in SSH over the subtropical gyre (Fig. 10) to the change in steric height (change in upper ocean density)?

4. The steady solution Fig. (49) includes three gyres, tropical, subtropical and subpolar. Contrast the model-computed tropical and subpolar gyres with respect to the magnitude of their currents, layer thickness anomaly, and transports. Compare the solution Fig. (49, lower) with the observed SSH of Fig. (2). Why does the tropical gyre (or region) have a comparatively small SSH anomaly? The

subpolar and tropical gyres have roughly comparable anti-clockwise circulations, and yet the wind over the subpolar gyres is westerly, and the wind over the tropical gyre is easterly. But haven't we been saying all along that these gyres are wind-driven?

5. Explain the signs and the comparative magnitudes of the current components of Fig. (23). Notice that the Sverdrup meridional flow at the three sites is not identical. Why is there a small but systematic difference?

6. The overall pattern of SSH (Fig. 6, lower) and of the transport streamfunction (Fig. 11, left) are similar but not identical. Why is there a difference?

7. The potential vorticity derivation of the Sverdrup relation in Sec. 5.1 omitted some important details. 1) Can you show that the drag term in the q-balance equation for the interior is proportional to the Ekman number times L_{Earth}/L_{tau}, where L_{tau} is the horizontal scale of the wind stress field. 2) Given speed and space scales of the interior (Sverdrup) flow, show that the relative vorticity of the Sverdrup flow is indeed very, very small compared to planetary vorticity, f, and so to an excellent approximation the potential vorticity in the interior is given by $q \approx f/h$. 3) The advective term of Eqn.(42) may be approximated as Eqn. (18) because the geostrophic flow does not advect layer thickness. What evidence can you find in the steady solution, Fig. (49), that supports this (highly plausible) assertion?

8. The real ocean thermocline is continuously stratified in the vertical, and so the best one layer baroclinic model representation of the thermocline will likely have to compromise on something. The values used here, $H = 500$ m, and $\delta\rho = 2$ kg m^{-3} are round numbers that give an appropriate gravity wave speed. What thickness slope is consistent with the Rossby wave view of the subtropical gyre developed in Sec. 4.4, and where is that slope found in the water column of Fig. (1)?

9. Assuming that the boundary current will have a maximum current adjacent to the boundary (and so a single sign of relative vorticity), show that the mode $beta = drag$ can obtain also for the case of an equatorward western boundary current as occurs in the tropical and subpolar gyres. Can you envision this balance for an eastern boundary current of either sign?

10. In the discussion of the Stage 3 transient response we noted that the change in the current from Stage 2 zonal flow to meridional Sverdrup flow occurs at a time that is proportional to the transit time of a long Rossby wave starting from the eastern boundary. This suggests an interesting derivation of the Sverdrup relation (albeit for a slightly special wind field) that makes especially clear the crucial role of the eastern boundary in a problem in which there is no other imposed zonal scale. Assume that the wind stress is purely zonal, and is switched on at $t = 0$ and then held constant, as in the base case. The Stage 2 zonal flow u_{S2} then grows linearly with time until the arrival of the eastern boundary wave. How does the then extant zonal flow compare with Sverdrup zonal flow? In general, the $u_{S2}(x, y)$ current is not the same as the steady state Sverdrup zonal flow, since the former depends upon $\partial^2(\tau/f)/\partial y^2$ and not $f^{-1}\partial^2\tau/\partial y^2$ as does the Sverdrup zonal current (and see Figs. 21 and 24). To remedy this, suppose that the y scale of the wind stress field is

much less than R_E. This will result from setting $n = 6$ in the wind stress Eqn. (35), and thus $\tau^x(y) \propto \sin(6\pi y/L)$. Can you show that the zonal transport at $t = T_{ebw}$ is then approximated well by

$$hu_{S2}(t = T_{ebw}) \approx -\frac{(L-x)}{\rho_o \beta}\frac{\partial^2 \tau^x}{\partial y^2} = \frac{\partial \Psi_{Sv}}{\partial y},$$

where the last step used Eqn. (71). Why does the zonal transport increases in magnitude in proportion to distance from the eastern boundary, $L - x$?

11. Can you show that the vorticity balance form of the Ekman number appropriate to a western boundary current, Eqn. (76), is related to the usual, momentum balance form $E = r/f$, by

$$E_Q = E\frac{L_\tau}{R_d}.$$

12. Assume a steady, wind-driven circulation. What would you expect to follow if the wind stress suddenly vanished? Check your intuition against https://www2.whoi.edu/staff/jprice//wind-off Now Imagine an experiment in which the wind stress is spatially uniform over the entire basin, and northward. What would you expect for Stage 2 and Stage 3? (Major hint: consider the stress curl.) What is the steady response? Once you have formed your answer, take a look at the circulation computed from such an experiment shown in Fig. (43, lower).

Index

MIT OpenCourseWare
https://ocw.mit.edu

Resource: Topics in Fluid Dynamics
James Price

For information about citing these materials or our Terms of Use, visit: https://ocw.mit.edu/terms.